

FOR AUDIT PURPOSES ONLY

Calibration of the Site-Scale Saturated Zone Flow Model Draft 00B, 4/2000

DISCLAIMER

This contractor document was prepared for the U.S. Department of Energy (DOE), but has not undergone programmatic, policy, or publication review, and is provided for information only. The document provides preliminary information that may change based on new information or analysis, and represents a conservative treatment of parameters and assumptions to be used specifically for Total System Performance Assessment analyses. The document is a preliminary lower level contractor document and is not intended for publication or wide distribution.

Although this document may have undergone technical review at the contractor organization, it has not undergone a DOE policy review. Therefore, the views and opinions of authors expressed may not state or reflect those of the DOE. However, in the interest of the rapid transfer of information, we are providing this document for your information per your request.

WM-11
NMB507

**OFFICE OF CIVILIAN RADIOACTIVE WASTE MANAGEMENT
ANALYSIS/MODEL COVER SHEET**

1. QA: QA

Page: 1 of 104

Complete Only Applicable Items

<p>2. <input checked="" type="checkbox"/> Analysis Check all that apply</p> <table border="1" style="width:100%; border-collapse: collapse;"> <tr> <td style="width:20%;">Type of Analysis</td> <td><input type="checkbox"/> Engineering</td> </tr> <tr> <td></td> <td><input type="checkbox"/> Performance Assessment</td> </tr> <tr> <td></td> <td><input checked="" type="checkbox"/> Scientific</td> </tr> </table> <table border="1" style="width:100%; border-collapse: collapse;"> <tr> <td style="width:20%;">Intended Use of Analysis</td> <td><input type="checkbox"/> Input to Calculation</td> </tr> <tr> <td></td> <td><input checked="" type="checkbox"/> Input to another Analysis or Model</td> </tr> <tr> <td></td> <td><input checked="" type="checkbox"/> Input to Technical Document</td> </tr> </table> <p>Describe use: This analysis is used in the SZ PMR and the PA AMR.</p>	Type of Analysis	<input type="checkbox"/> Engineering		<input type="checkbox"/> Performance Assessment		<input checked="" type="checkbox"/> Scientific	Intended Use of Analysis	<input type="checkbox"/> Input to Calculation		<input checked="" type="checkbox"/> Input to another Analysis or Model		<input checked="" type="checkbox"/> Input to Technical Document	<p>3. <input checked="" type="checkbox"/> Model Check all that apply</p> <table border="1" style="width:100%; border-collapse: collapse;"> <tr> <td style="width:20%;">Type of Model</td> <td><input type="checkbox"/> Conceptual Model</td> <td><input type="checkbox"/> Abstraction Model</td> </tr> <tr> <td></td> <td><input type="checkbox"/> Mathematical Model</td> <td><input type="checkbox"/> System Model</td> </tr> <tr> <td></td> <td colspan="2"><input checked="" type="checkbox"/> Process Model</td> </tr> </table> <table border="1" style="width:100%; border-collapse: collapse;"> <tr> <td style="width:20%;">Intended Use of Model</td> <td><input type="checkbox"/> Input to Calculation</td> </tr> <tr> <td></td> <td><input checked="" type="checkbox"/> Input to another Model or Analysis</td> </tr> <tr> <td></td> <td><input checked="" type="checkbox"/> Input to Technical Document</td> </tr> </table> <p>Describe use: This calibrated model is used in the SZ PMR and the PA AMR.</p>	Type of Model	<input type="checkbox"/> Conceptual Model	<input type="checkbox"/> Abstraction Model		<input type="checkbox"/> Mathematical Model	<input type="checkbox"/> System Model		<input checked="" type="checkbox"/> Process Model		Intended Use of Model	<input type="checkbox"/> Input to Calculation		<input checked="" type="checkbox"/> Input to another Model or Analysis		<input checked="" type="checkbox"/> Input to Technical Document
Type of Analysis	<input type="checkbox"/> Engineering																											
	<input type="checkbox"/> Performance Assessment																											
	<input checked="" type="checkbox"/> Scientific																											
Intended Use of Analysis	<input type="checkbox"/> Input to Calculation																											
	<input checked="" type="checkbox"/> Input to another Analysis or Model																											
	<input checked="" type="checkbox"/> Input to Technical Document																											
Type of Model	<input type="checkbox"/> Conceptual Model	<input type="checkbox"/> Abstraction Model																										
	<input type="checkbox"/> Mathematical Model	<input type="checkbox"/> System Model																										
	<input checked="" type="checkbox"/> Process Model																											
Intended Use of Model	<input type="checkbox"/> Input to Calculation																											
	<input checked="" type="checkbox"/> Input to another Model or Analysis																											
	<input checked="" type="checkbox"/> Input to Technical Document																											

4. Title:
Calibration of the Site-Scale Saturated Zone Flow Model

5. Document Identifier (including Rev. No. and Change No., if applicable):
MDL-NBS-HS-000011, Rev. 00B

6. Total Attachments: 1	7. Attachment Numbers - No. of Pages in Each: 1: 2
----------------------------	---

	Printed Name	Signature	Date
8. Originator	George A. Zyvoloski		
9. Checker	Michael Wallace		
10. Lead/Supervisor	Al Eddebarh		
11. Responsible Manager	Dwight Hoxie		

12. Remarks:
Back Check copy

OFFICE OF CIVILIAN RADIOACTIVE WASTE MANAGEMENT
ANALYSIS/MODEL REVISION RECORD

Complete Only Applicable Items

1. Page: 2 of 104

2. Analysis or Model Title:

Calibration of the Site-Scale Saturated Zone Flow Model

3. Document Identifier (including Rev. No. and Change No., if applicable):

MDL-NBS-HS-000011, Rev. 00B

4. Revision/Change No.

5. Description of Revision/Change

00A

Initial issue of check copy

00B

Resolution of checker comments

TABLE OF CONTENTS

	Page
1. PURPOSE	13
2. QUALITY ASSURANCE	15
3. COMPUTER SOFTWARE AND MODEL USAGE.....	17
3.1 PARAMETER OPTIMIZATION	17
3.2 GRID GENERATION.....	17
3.3 FLOW MODELING.....	17
3.4 PARTICLE TRACKING.....	17
4. INPUTS	19
4.1 DATA AND PARAMETERS.....	19
4.2 CRITERIA.....	19
4.3 CODES AND STANDARS.....	20
5. ASSUMPTIONS.....	21
6. ANALYSIS	23
6.1 METHODOLOGY	24
6.1.1 Effective Continuum Representation	24
6.1.2 Boundary Conditions.....	25
6.1.3 Confined Aquifer Solutions.....	25
6.1.4 Recharge Redistribution	26
6.1.5 Groundwater Temperature.....	26
6.1.6 Anisotropy.....	27
6.2 INCORPORATION OF HYDROGEOLOGIC FRAMEWORK MODEL.....	27
6.2.1 Grid Generation and Checking	27
6.2.2 Gridding Procedure.....	28
6.2.3 Infiltration Map Translation to Boundary Conditions.....	29
6.2.4 Computational Grids.....	31
6.3 FEATURES	34
6.4 PARAMETER OPTIMIZATION	41
6.5 NUMERICAL FLOW MODEL.....	42
6.6 GROUNDWATER TEMPERATURE.....	45
6.7 CALIBRATION RESULTS	46
6.7.1 Calibration Criteria.....	46
6.7.2 Description of Base Case.....	47
6.7.3 Description of Transport Pathways Calculated from the Calibrated Model	53
6.7.4 Comparison of Observed and Calibrated Head measurements	53
6.7.5 Hydrochemical Data.....	53
6.7.5.1 Regional Flow Paths.....	53
6.7.5.2 Evaluation of Evidence for Local Recharge	56
6.7.5.3 Evaluation of Evidence for Timing of Recharge	56

6.7.5.4	Evaluation of Evidence for Mixing Relations Between Different Waters at Yucca Mountain.....	57
6.7.5.5	Evaluation of Evidence for the Magnitude of Recharge	57
6.7.5.6	Evaluation of Evidence for Downgradient Dilution	57
6.7.5.7	Likely Flow Paths from the Potential Repository Area.....	58
6.7.6	Comparing Hydrochemical Data Trends with Calculated Particle Pathways.....	59
6.7.7	Permeability Data from the Yucca Mountain Area	64
6.7.7.1	Single-Hole Tests	65
6.7.7.2	Cross-Hole Tests	68
6.7.7.3	Permeability Data from the Nevada Test Site.....	69
6.7.7.4	Lower Carbonate Aquifer (unit 4)	69
6.7.7.5	Valley-Fill Aquifer (unit 20)	70
6.7.7.6	Welded-Tuff Aquifer (unit 16)	71
6.7.7.7	Lava-Flow Aquifer (unit 17)	72
6.7.7.8	Inferences about Permeability from Regional Observations.....	73
6.7.7.9	Lower Clastic Aquitard (unit 3).....	73
6.7.7.10	Upper Clastic Aquitard (unit 5)	74
6.7.7.11	Faults.....	75
6.7.7.11.1	Orientation of faults relative to the minimum horizontal stress in the region	75
6.7.7.11.2	Amount and type of infilling material in the fault.....	75
6.7.7.11.3	Relative transmissivities of hydrogeologic units juxtaposed by offset across the fault	75
6.7.7.11.4	Recent seismic history	76
6.7.8	Comparing Permeability Data to Calibrated Permeability Values	76
6.7.9	Comparing Fluxes Derived from the Regional Model with Fluxes Calculated from the Calibrated Model	78
6.7.10	Comparing Permeabilities Used in the Regional Model to Permeabilities from the Calibrated Model.....	82
6.7.11	Comparing Measured Upward Hydraulic Gradient with the Estimated Upward Gradient from the SZ Model	82
6.7.12	Discussion of Hydrogeologic Features Used in Calibration.....	82
6.8	SPECIFIC DISCHARGE.....	82
6.9	MAJOR MODEL SENSITIVITIES AND TRENDS OBSERVED IN CALIBRATION.....	83
6.9.1	Sensitivity of Estimated Parameter Values	84
6.9.2	Analysis of Weighted Residuals	89
6.10	MODEL VALIDATION ISSUES AND RECOMMENDATIONS FOR THE SATURATED-ZONE FLOW	93
7.	CONCLUSIONS	95
8.	REFERENCES.....	97
8.1	DOCUMENTS CITED	97
8.2	CODES, STANDARDS, REGULATIONS, AND PROCEDURES	102
8.3	SOFTWARE	103

8.3 SOURCE DATA, LISTED BY DATA TRACKING NUMBER..... 103

ATTACHMENT I. CONVERT FEHM OUTPUT TO TECPLOT INPUT

INTENTIONALLY LEFT BLANK

FIGURES

	Page
1. Important Physiographic Features Near Yucca Mountain.....	24
2. Comparison of Recharge Data with FEHM Input Data.....	30
3. The 1000-m and 500-m Computational Grids.....	33
4. Geologic Features in the Area of the Site-Scale Flow and Transport Model.....	35
5. Map of Modeled Temperature at the Water Table for the Saturated Zone Site-Scale Flow Model Domain.....	46
6. Countour Plot of Water Level Data and Simulated Water Level Data with Residual Heads.....	52
7. Flow Paths from the Proposed Repository with Simulated Hydraulic Head Contours.....	54
8. Groundwater Flow Paths Near Yucca Mountain Estimated by Geochemical Data.....	55
9. Plot of Particle Movement at 600-Meters Elevation.....	60
10. Plot of Particle Movement at Zero-Meters Elevation.....	61
11. Plot of Particle Movement at -600-Meters Elevation.....	62
12. Plot of Particle Movement at -1200-Meters Elevation.....	63
13. Logarithms of Permeabilities Estimated during Model Calibration Compared to Mean Logarithms of Permeability Determined from Pump-Test Data from Yucca Mountain.....	77
14. Logarithms of Permeabilities Estimated during Model Calibration Compared to Mean Logarithms of Permeability Determined from Pump-Test Data from the Nevada Test Site.....	78
15. Flux Zones Used for Comparing Regional and Site-Scale Fluxes.....	80
16. Geology at the Water Table for the Site-Scale Model.....	81
17. Composite Scaled Sensitivities for the Estimated Parameters for the Final Calibrated Model Listed in Table 16.....	86
18. Largest Absolute Weighted Sensitivity and Corresponding Parameter Label for the Final Calibrated Model.....	87
19. Largest Absolute Weighted Sensitivity for Each Observation Location.....	88

20.	Weighted Residual as a Function of Weighted Simulated Value for the Final Calibrated Model	90
21.	Weighted Residual as a Function of Observation Location.....	91
22.	Normal Probability Plot of Weighted Residuals for the Final Calibrated Model.....	92
23.	Normal Probability Plot of Weighted Residuals (red circles) and Correlated Normal Random Deviates.....	92

TABLES

	Page
1. Computer Codes Used in the Saturated-Zone Model	18
2. Input Data Sources.....	19
3. Bounding Box.....	28
4. Vertical Grid Spacing Parameters	29
5. Geologic Units.....	32
6. Hydrological Features in the Saturated-Zone Flow Model.....	36–40
7. Observation Wells with Computed Head Data.....	48–50
8. Calibration Parameters Used in Saturated-Zone Site-Scale Model.	51
9. Statistical Summary of Permeabilities Calculated from Single-Hole and Cross-Hole Tests at Yucca Mountain	67
10. Permeabilities Calculated for the Lower Carbonate Aquifer.....	69
11. Permeability Estimates for the Valley-Fill Aquifer.....	71
12. Permeability Estimates for the Welded Tuff Aquifer.....	72
13. Permeabilities of the Lava-Flow Aquifer.....	73
14. Comparison of Regional and Site-Scale Fluxes	79
15. Parameter Values for Features Used in the Saturated-Zone Model.....	83
16. Estimated Values, Coefficients of Variation, and 95-Percent Confidence Intervals for the Parameters of the Final Calibrated Model.....	85

INTENTIONALLY LEFT BLANK

ACRONYMS

AMR	Analysis and Modeling Report
AVS	Advanced Visualization System
CRWMS M&O	Civilian Radioactive Waste Management System Management and Operating Contractor
CVFE	Control volume finite element
DOE	U.S. Department of Energy
DTN	Data tracking number
FEHM	A finite-element heat and mass transfer numerical analysis computer code
GFM	Geologic Framework Model
GMRES	Generalized minimum residual method
INEEL	Idaho National Engineering and Environmental Laboratory
LaGriT	Los Alamos grid generation software package
LM	Levenberg-Marquardt, the name of the optimization algorithm for PEST
MVA	Middle Volcanic Aquifer
NTS	Nevada Test Site
OCRWM	Office of Civilian Radioactive Waste Management
PA	Performance Assessment
PEBI	Perpendicular bisector
PEST	A code for parameter estimation
pmc	percent modern carbon
QARD	Quality assurance requirements and description
SSD	Sum-of-squares difference
STN	Software tracking number
SZ	Saturated zone
Tac	Calico Hills Formation
TBD	To be determined
TBV	To be verified
Tcb	Bullfrog Tuff of the Crater Flat Group
Tcp	Prow Pass Tuff of the Crater Flat Group
Tct	Tram Member at Crater Flat tuff
Tlr	Lithic Ridge Tuffs
USGS	U.S. Geological Service

UTM
UZ

Universal transverse Mercator
Unsaturated zone

1. PURPOSE

The purpose of the flow calibration analysis work is to provide Performance Assessment (PA) with a calibrated saturated-zone (SZ) flow model. This model will be a culmination of much of our knowledge of the SZ flow system

The objectives of this study are to provide a defensible SZ flow and transport model. To obtain a defensible model, all available data should be used (or at least considered) to obtain a calibrated model. A defensible model would include geologic and hydrologic data that are used to form the hydrogeologic framework model, hydrochemical information that is used to infer transport pathways, in-situ permeability measurements, and water level and head measurements. In addition, the model should include information on major model sensitivities. Especially important are those that affect calibration, the direction of transport pathways, and travel times. Finally, if warranted, alternative calibrations representing different conceptual models should be included.

This analysis is governed by the Office of Civilian Radioactive Waste Management (OCRWM) Analysis and Modeling Report (AMR) Development Plan *Calibrated Saturated Zone Flow and Transport Model Development Plan* (CRWMS M&O 1999a).

INTENTIONALLY LEFT BLANK

2. QUALITY ASSURANCE

The activities documented in this Analysis and Modeling Report (AMR) were evaluated in accordance with QAP-2-0, *Conduct of Activities*, and were determined to be quality affecting and subject to the requirements of the U.S. Department of Energy (DOE) Office of Civilian Radioactive Waste Management (OCRWM) *Quality Assurance Requirements and Description* (QARD) (DOE 2000). This evaluation is documented in *Activity Evaluation of M&O Site Investigations-(Q)* (CRWMS M&O 1999b; 1999c) and *Activity Evaluation for Work Package WP 1301213SM1* (Wemheuer 1999). Accordingly, the analysis activities documented in this AMR have been conducted in accordance with the CRWMS M&O quality assurance (QA) program, using approved procedures identified in CRWMS M&O (1999a). This AMR has been developed in accordance with procedure AP-3.10Q, *Analyses and Models*.

INTENTIONALLY LEFT BLANK

3. COMPUTER SOFTWARE AND MODEL USAGE

The following industry standard software was used in this analysis and documentation:

- EXCEL 98-SR-1: used for spreadsheet calculations and calculation of basic statistics using standard functions only
- SURFER for Windows, V6.03: used for plotting and visualization of analysis results in figures shown in this report
- TECPLOT, V7.5: used for plotting and visualization of analysis results in figures shown in this report
- MINITAB, releases 12.22 (MINITAB 1998)

In addition, the results of all calculations using SURFER and TECPLOT were visually checked for correctness, and the results of all calculations using EXCEL were checked with order-of-magnitude estimations.

The following public-domain geochemical software was used in this analysis:

NETPATH Version 2.0 (Plummer et al. 1994, pp. 1–30): used to correct carbon-14 ages for the effects of chemical reactions.

The results of all calculations using NETPATH were checked with order-of-magnitude estimations.

The computer codes used directly in the SZ Model are summarized in Table 1.

3.1 PARAMETER OPTIMIZATION

The parameter estimation (PEST) code (V2.0) from Watermark Computing was used to perform the parameter optimization for the hydrogeologic and feature permeabilities.

3.2 GRID GENERATION

Los Alamos Grid Generation software package (LaGriT), V2.0, is used for grid generation. LaGriT is a set of software macros that manipulate the Stratamodel Stratigraphic Framework data to create computational grids. The software macros translate the coordinate and attribute information into a form that is valid for finite-element heat and mass (FEHM) compilations and tied to the Stratamodel Stratigraphic Framework.

3.3 FLOW MODELING

The FEHM code, V2.0, software tracking number (STN) 10031-2.00-00, is used to solve for a steady-state flow solution. FEHM has been extensively verified (Dash et al. 1997).

3.4 PARTICLE TRACKING

FEHM is used to determine the streamlines (particle tracks) with the steady-state flow solution created in the previous step. FEHM has two different particle-tracking routines. This study uses the *sptr* macro for particle tracking. The particle-tracking portion of FEHM has been verified in a related AMR (CRWMS M&O 2000a).

Table 1. Computer Codes Used in the Saturated-Zone Model

Code Usage	Code	STN	Where Developed
Parameter Optimization	PEST (V2.0)	TBD	Watermark Computing (Australia)
Grid Generation	LaGriT (V2.0)	10212-1.0-00	LANL
Flow Modeling	FEHM	10031-2.00-00	LANL
Particle Tracking	FEHM	10031-2.00-00	LANL

4. INPUTS

4.1 DATA AND PARAMETERS

Input information used in this analysis comes from several sources, which are summarized in Table 2, along with their data tracking number (DTN).

Table 2. Input Data Sources

Data Set	Data Description	Data Tracking Number	Data Type
Water Level and Heads	Water Level and Head Distributions		Developed
Hydrochemistry	Major Ion Concentrations	GS000308312322.003 GS000308312322.004 GS920408312321.001 GS920408312321.003 GS920508312321.004 GS930108315213.002 GS930308312323.001 GS930508312322.001 GS930908312323.003 GS931100121347.007 GS940308312322.001 GS950808312322.001 GS971900012847.004 GS980908312322.008 GS991299992271.001 (data set 9902----2272.001) GS990608312133.001	Developed
Permeability	Permeability Distributions	SNT05082597001.003	Developed
Stratamodel Framework file	Surface Defining Hydrogeologic Units		Developed
Infiltration Map	Distribution of Recharge Flux	SN990870581999.001	Developed
Features	Feature and Fault Distributions		Developed
Temperature Profiles in Wells	Plots of Temperature Profiles in Wells (Sass et al. 1988)	GS930208318523.001	Acquired
Boundary Conditions	Boundary conditions inferred from regional-scale model	SN9908T0581999.001	Developed

4.2 CRITERIA

No criteria applicable to this analysis have been identified. This AMR complies with the U.S. Department of Energy (DOE) interim guidance (Dyer 1999). Subparts of the interim guidance that apply to this analysis are those pertaining to the characterization of the Yucca Mountain site (Subpart B, Section 15), the compilation of information regarding geochemistry and mineral stability of the site in support of the License Application (Subpart B, Section 21(c)(1)(ii)), and the definition of geochemical parameters and conceptual models used in PA (Subpart E, section 114(a)).

4.3 CODES AND STANDARDS

No codes or standards apply to this analysis, which involves no design or construction.

5. ASSUMPTIONS

The SZ Flow model is based on a number of simplifying assumptions explained below. Where appropriate, the details of applying these assumptions are given in Section 6.

1. A steady-state model is sufficient for calibration purposes and the intended uses of the SZ flow model. This assumption is justified by the slowly varying values of measured water levels and the fact that it is linked with a steady-state regional flow. Though issues remain regarding the transient drawdown of well in the Amargosa Valley, they can be addressed in future studies with sensitivity studies.
2. The Effective Continuum representation is an appropriate way to model the differing rock types in the SZ flow model. This assumption is justified in the model because the grid blocks are large enough to average the fracture effects and the model is steady state. The steady-state assumption insures that flow from the fractures to the surrounding intact rock, represented in a given gridblock, is unimportant.
3. A spatially varying but temporally constant temperature field is adequate for the SZ flow model. This assumption is justified by the fact that, of the parameters affecting flow, only viscosity varies significantly in the temperature range encountered with the SZ flow model.
4. The bottom of the SZ flow model can be simulated with a no-flow boundary. This assumption is justified because the SZ flow model is deep enough (3000 m) to include most of the regionally continuous carbonate aquifer. The rocks beneath the carbonate aquifer are very impermeable.
5. A vertical to horizontal anisotropy ratio of 0.1 is appropriate for most of the hydrogeologic units in the SZ flow model. This assumption is justified by common usage and by the Yucca Mountain Expert Elicitation Committee (CRWMS M&O 1998, Table 3-2).

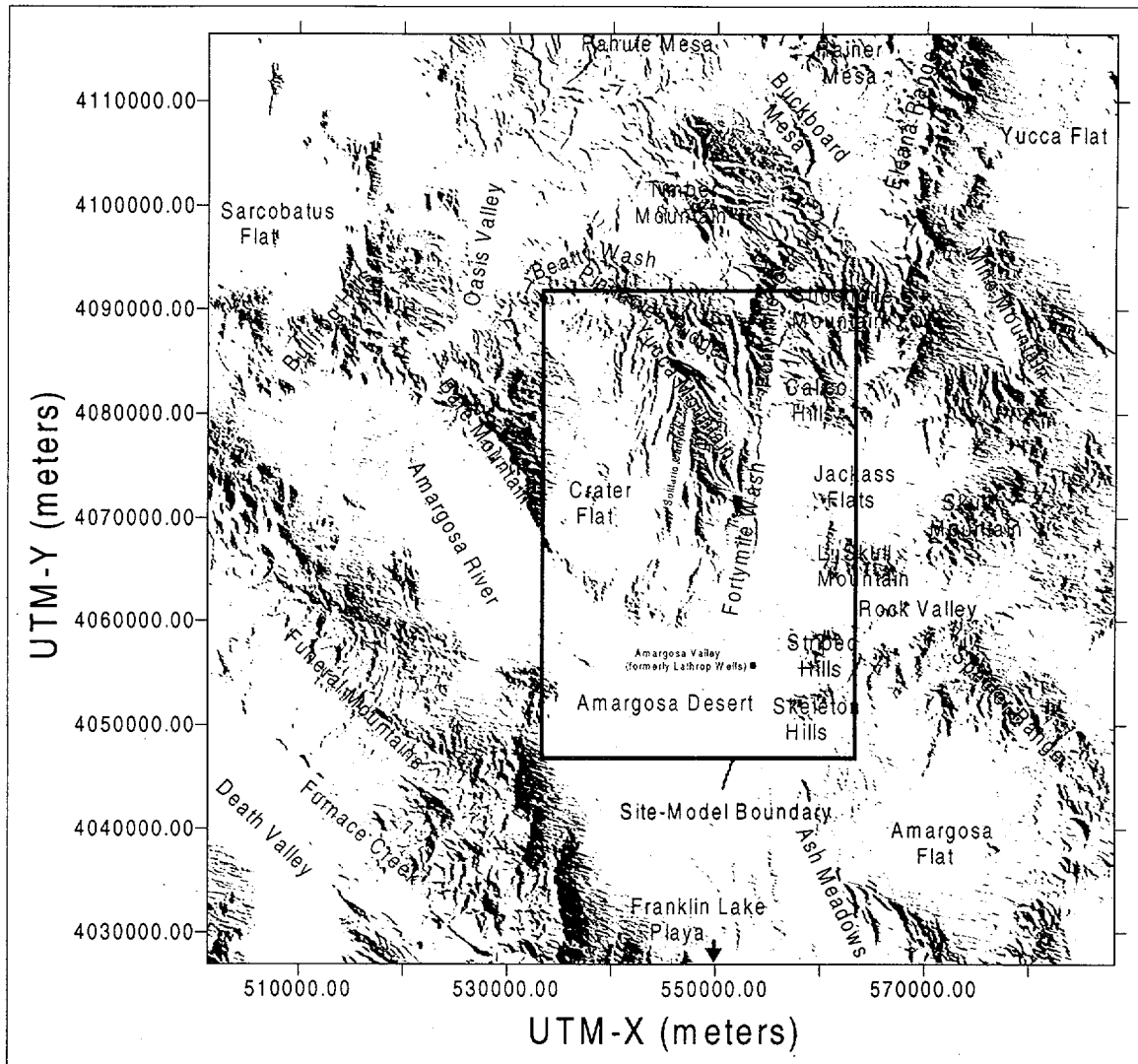
INTENTIONALLY LEFT BLANK

6. ANALYSIS

Yucca Mountain is located in the Great Basin about 150 km northwest of Las Vegas, Nevada. The mountain consists of a series of fault-bounded blocks of ash-flow and ash-fall tuffs and a smaller volume of lava deposited between 14 and 11 Ma (million years before present) from a series of calderas located a few to several tens of kilometers to the north (Sawyer et al. 1994). Yucca Mountain itself extends southward from the Pinnacles Ridge toward the Amargosa Desert, where the tuffs thin and pinch out beneath the alluvium (Figure 1). The tuffs dip 5 to 10 degrees to the east over most of Yucca Mountain. Crater Flat is west of Yucca Mountain and separated from it by Solitario Canyon, which is the surface expression of the Solitario Canyon Fault—a steeply dipping scissors fault with down-to-the-west displacement of as much as 500 m in southern Yucca Mountain (Day et al. 1998, pp. 6–7). Underlying Crater Flat is a thick sequence of alluvium, lavas, and tuffs that has been locally cut by faults and volcanic dikes. East of Yucca Mountain, and separated from it by Fortymile Wash, is Jackass Flats, which is underlain by a thick sequence of alluvium and volcanic rocks. Timber Mountain, approximately 25 km to the north of the potential repository area, is a resurgent dome within the larger caldera complex that erupted the tuffs at Yucca Mountain.

The central block of Yucca Mountain, into which waste would be emplaced if the site were licensed, is bounded by Drill Hole Wash on the north, the Solitario Canyon Fault on the west, the Bow Ridge Fault on the east, and is dissected by the Ghost Dance and Dune Wash Faults. Topography is pronounced and, north of the central block, is controlled by long, northwest-trending, fault-controlled washes. Within and south of the central block, washes are shorter and trend eastward. Topography in the southern part of Yucca Mountain is controlled by south-trending faults.

The boundaries of the numerical model for SZ flow and transport are shown in Figure 1, as well as on some subsequent figures. The hydrogeologic setting of the SZ flow system in the vicinity of Yucca Mountain was summarized by Luckey et al. (1996, p. 13). Yucca Mountain is part of the Alkali Flat-Furnace Creek subbasin of the Death Valley groundwater basin, as described by Waddell (1982, pp. 15–16). Discharge within the subbasin occurs at Alkali Flat (Franklin Lake Playa) and, possibly, Furnace Creek in Death Valley (Figure 1). Water inputs to the subbasin include groundwater inflow along the northern boundary of the subbasin, recharge from precipitation in high-elevation areas of the subbasin, and recharge from surface runoff in Fortymile Canyon and Fortymile Wash. North and northeast of Yucca Mountain, recharge from precipitation also probably occurs at Timber Mountain, Pahute Mesa, Rainier Mesa, and Shoshone Mountain (Luckey et al. 1996, p. 13).



DTN: N/A—reference only

NOTE: The blue rectangle is the boundary of the numerical model for saturated zone flow and transport.

Figure 1. Important Physiographic Features Near Yucca Mountain

6.1 METHODOLOGY

6.1.1 Effective Continuum Representation

Numerical modeling of fracture properties is done in one of two ways: (1) discrete fracture models or (2) effective continuum models. Discrete fracture models represent each fracture as a distinct object within the modeling domain. Although the discrete fracture approach retains the discrete nature of the fractures observed within the resulting model, the computational burden of calculating a flow solution on a discrete fracture model becomes extremely large for even a relatively simple fracture model. For this reason, and the fact that the Yucca Mountain Project does not have a qualified discrete fracture modeling software package, we use the effective continuum representation of fracture permeability in this study. The only exception in this study

is the use of a number of features that represent faults and/or fractures. These features are discussed in Section 6.2. The calibrated values of permeability represent average block permeabilities including the effect of fractures. This approach is appropriate because the field tests of permeability included the effects of fractures in the testing interval. Because the flow solution is steady state and the permeabilities represent block-averaged values, there is no difference between the solution described in this report and one obtained using discrete features. This argument assumes that the features would have the same averaged permeability at the block size of the continuum model. The issues of conservative versus nonconservative solutions arise in the transport solution. There the concept of effective porosity is used to bracket solutions ranging from fracture flow to porous media flow.

6.1.2 Boundary Conditions

The boundary conditions are derived from regional water level and head data (DTN: SN9908T0581999.001). The data are used to form fixed-head boundary conditions on the lateral sides of the model. By fixed heads, it is meant that the heads may vary in space along the boundary but not in the vertical direction or in time. Because of constant vertical head, this condition produces no vertical flow. This model contrasts with a known upward gradient in the area near well UE-25 p#1. This lack of vertical gradient would arise whether fixed-head or fixed-flux boundary conditions were used in the model. Nevertheless, some upward gradient can be obtained away from the boundaries with the present boundary conditions. This upward gradient, though smaller in magnitude than that measured in well UE-25 p#1, is sufficient to keep the modeled transport pathlines leaving the repository from reaching the deep carbonate aquifer. This situation will be discussed further in Section 6.7.11. Of special note is the southern boundary of the model, which coincides with a large number of wells in the Amargosa Valley. Here there are a variety of measurements over the time of usage. Some of the earlier measurements represent pre-development states, and the later measurements generally represent water levels with pumping. The boundary conditions represent current water levels and are described in CRWMS M&O (1999c).

6.1.3 Confined Aquifer Solution

The confined-aquifer solution approach is used in the SZ flow and transport model. The approach assumes no unsaturated zone (UZ) and, therefore, solves a simplified and computationally more efficient numerical model. In the numerical model, the top surface is represented with no-flow boundary conditions. This representation does not preclude the addition of spatially varying source terms to model infiltration and recharge. The confined aquifer solution was enforced in the FEHM code by adding a large artificial head to the numerical solution. This was later subtracted after the computer run to recover the true solution. Because none of the fluid or rock properties depend on head, no changes to the true solution occur other than forcing the bookkeeping coding in FEHM to assume fully saturated conditions. If we did not adopt this procedure, small variations in head around the water level value would result in FEHM testing for an air phase, thus decreasing the efficiency. The negative side of this approach is that the top surface of the numerical model corresponds to the measured water-table surface and may be inconsistent with the model-derived water-table surface. This discrepancy affects the flux through the model. The error is generally small because the flowing area is proportional to the depth of the model, and the errors between the calibrated and field data are

generally on an order of 10 m, compared to a model depth of approximately 3000 m. Furthermore, the discrepancy can be checked after the model is run. We note here that the numerical model averaged about 16 m discrepancy for the more than 100 head observations. If we assume that the water-table solution is in error by this amount, error for the “flow area” for the horizontal head gradient is small. It should be noted that care was taken to get the low head gradient area to the south and east of Yucca Mountain accurately modeled. Finally, it should be noted that the model allows for vertical flows that arise from recharge and heterogeneity. Thus, though there are similarities with the Dupuit-Forcheimer method, the numerical approach used is different.

6.1.4 Recharge Redistribution

The recharge map in CRWMS M&O (1999f) is mapped (with changes to be described later) to the top surface of the numerical grid described in this report. An important characteristic of the recharge data is that it was developed with the assumption that it is applied at land’s surface. The exception is the recharge in the area of the UZ model. Here the actual output of the UZ model is used. Thus, except for the area beneath the UZ model, redistribution of recharge in the UZ is likely to produce recharge at the water table that is different than that described in CRWMS M&O (1999f). The fact that most of the recharge occurs at higher elevations in rocks that are less permeable than in other regions has necessitated the increase in the permeability of the top layer in the SZ model. This change allows the flow to redistribute locally and avoid artificially high heads. This method conserved recharge mass flux and was deemed better than any procedure that modified the spatial distribution of the recharge. Sensitivity to this procedure on calibration and flow direction has been carried out qualitatively and is small.

6.1.5 Groundwater Temperature

In the analysis presented in this report, it is assumed that temperature is approximately proportional to the depth below the ground surface. This assumption of a uniform temperature gradient with depth is equivalent to assuming uniform geothermal heat flux through a medium of homogeneous thermal conductivity. In addition, the temperature at the ground surface is assumed to be equal to a uniform value. The data on temperature in boreholes presented in Sass et al. (1988) indicate that there is significant variability in the temperature gradient at different locations and within individual wells, presumably due to advective redistribution of heat from infiltration and vertical groundwater flow. However, these data also indicate that the temperature gradients generally become more linear with increasing depth below the water table. It is important to note that the goal of assigning temperature variations with depth in the SZ site-scale flow model is to account for resulting variations in fluid viscosity at different depths in the SZ. The viscosity of water changes by a factor of only about 3.3 over the temperature range of 20°C to 100°C (Streeter and Wylie 1985, p. 559) that is expected within the range of depths in the SZ site-scale model domain. Thus, the linear approximation of the temperature gradient is adequate to capture the general effects of variations in groundwater viscosity with depth in the SZ site-scale flow model. The density also varies with temperature, but the effect is much smaller than viscosity. Over the temperature range of 20°C to 100°C, water density varies only a few percent. Using a variable viscosity allows the calibration of intrinsic permeability to be made instead of transmissibility. The former is a rock property, whereas the latter is a rock and

fluid property. This approach, in turn, allows for more accurate flux calculations on the boundaries of the model.

6.1.6 Anisotropy

Anisotropy was included in the SZ model by applying a multiplicative factor of 0.1 to the z-direction of the permeability. This ratio of horizontal to vertical permeability is in the generally accepted range (CRWMS M&O 1998, Table 3-2). Some units were modeled with isotropic permeability. These units were the granites, the clastic units, the upper volcanic confining unit, the lava-flow aquifer, and the limestone aquifer. Faults and features were generally modeled with anisotropic permeability, though not with the same horizontal to vertical ratio as the hydrogeologic units. These features are explained in detail in Table 5. The FEHM data file in the Technical Data Management System associated with this AMR (DTN: LA9911GZ122135.001) contains the complete information on anisotropy.

6.2 INCORPORATION OF HYDROGEOLOGIC FRAMEWORK MODEL

6.2.1 Grid Generation and Checking

Previous models of Yucca Mountain SZ regional flow and transport have used both unstructured meshes and structured grids. The major reason structured grids have been used for this work is to allow for the use of the streamline particle tracking transport capability of FEHM. Although the structured meshes are not as flexible as unstructured meshes in fitting complex geometry, tests have shown that they provide accurate solutions as long as there is adequate resolution.

The resolution required for calculations must take into account two factors.

- The geometry of the different materials in each stratigraphic layer must be accounted for. The model has much larger dimensions in the horizontal directions than the vertical, so high-aspect-ratio cells are used.
- Any large gradients in the physics of the problem must be adequately resolved. This requirement, cannot always be determined before preliminary calculations have been done.

To address these issues, grids are created at different resolutions. The solutions to flow and transport can then be run at different resolutions and compared. The expectation is that there should be little difference in results between the highest resolution grids because there is sufficient resolution. If this does not occur, one must suspect that there is some dependence of the results on grid resolution.

A related aspect of the computational grid generation is that of providing information to facilitate the setting of boundary conditions and initial conditions. Standard procedures are used to assign and identify gridblocks by material type, boundary type (top, bottom, side, etc). The new procedure developed for this work is a flux-conserving method to interpolate from an infiltration map onto the top surface of the computational model. This procedure is used to interpolate the

Infiltration Map (DTN: SN9900870581999.001), which is at 125 m resolution (x and y), to the grid blocks of the numerical model, which are 500 m in the calibrated SZ model.

6.2.2 Gridding Procedure

The geometry of geologic units is defined by the U.S. Geological Service (USGS) in a Stratamodel Framework file (DTN: TBD), which forms the basis for defining the boundaries of each stratigraphic unit. The data in the Stratamodel Framework file conforms to the Geologic Framework Model (GFM) (DTN: MO9901MWDGFM031.000) in areas where the GFM is valid and comprises additional information for the other areas of the SZ model. The data that are used in the Stratamodel Framework file is described in CRWMS M&O (2000b). The grid generation software does not read data directly from a Stratamodel Framework file, so the Stratamodel Framework is converted to Advanced Visualization System (AVS) quadrilateral surfaces. This process is a reformatting of the data and is accomplished with a software macro program.

A structured computational grid with constant horizontal gridblock spacing and nonuniform vertical resolution is created at two different horizontal resolutions: 500 m and 1000 m (see Table 3 for the extents of the grid and Table 4 for vertical resolution).

The structured grid and the AVS surfaces that define the geology are imported into LaGriT, which is a grid-generation toolkit. The geometry defined by the Stratamodel framework is used to identify the stratigraphic layer designation for each gridblock and cell of the computational grid. The parts of the structured grid that are above the water table and below the surface defining the base of the geologic model are also identified. FEHM input files are created with LaGriT that include the mesh geometry, lists of gridblocks on external boundaries, and gridblock lists sorted by material property.

The accuracy of both the flow solution and the transport solution are of prime concern in the grid building process. An exhaustive study (Bower et al. 2000) was performed on ten grids to determine the appropriate resolution for flow and transport. Though the study was based on an earlier GFM, the results show that the 500-m grid is entirely adequate for the purposes described in this report. Quality checks are performed to assure that the final grid is correct. These include histograms of element volume and element aspect ratio. All gridblocks are automatically checked to ensure that they are assigned the correct material identification. Lists of the number of gridblocks associated with each material are compared to the volume of each material in the Stratamodel framework to confirm that the stratigraphic units are correctly identified.

Table 3. Bounding Box

Box Direction	Nevada State Plane Coordinates (m)
west to east	533,340 to 563,340
south to north	4,046,780 to 4,091,780
bottom to water table	-2,200 to 1,200

DTN: TBD (hydrogeologic framework model)

Table 4. Vertical Grid Spacing Parameters

Gridblock Elevation Zone Boundaries (m)		Grid	Zone	Grid Lines
Upper	Lower	Spacing (m)	Width (m)	per Zone
1200	1000	50	200	4
1000	840	40	160	4
840	760	20	80	4
760	700	10	60	6
700	640	20	60	3
640	600	40	40	1
600	300	50	300	6
300	0	100	300	3
0	-600	200	600	3
-600	-2200	400	1600	4
-2200	-2750	550	550	1
				Total: 39

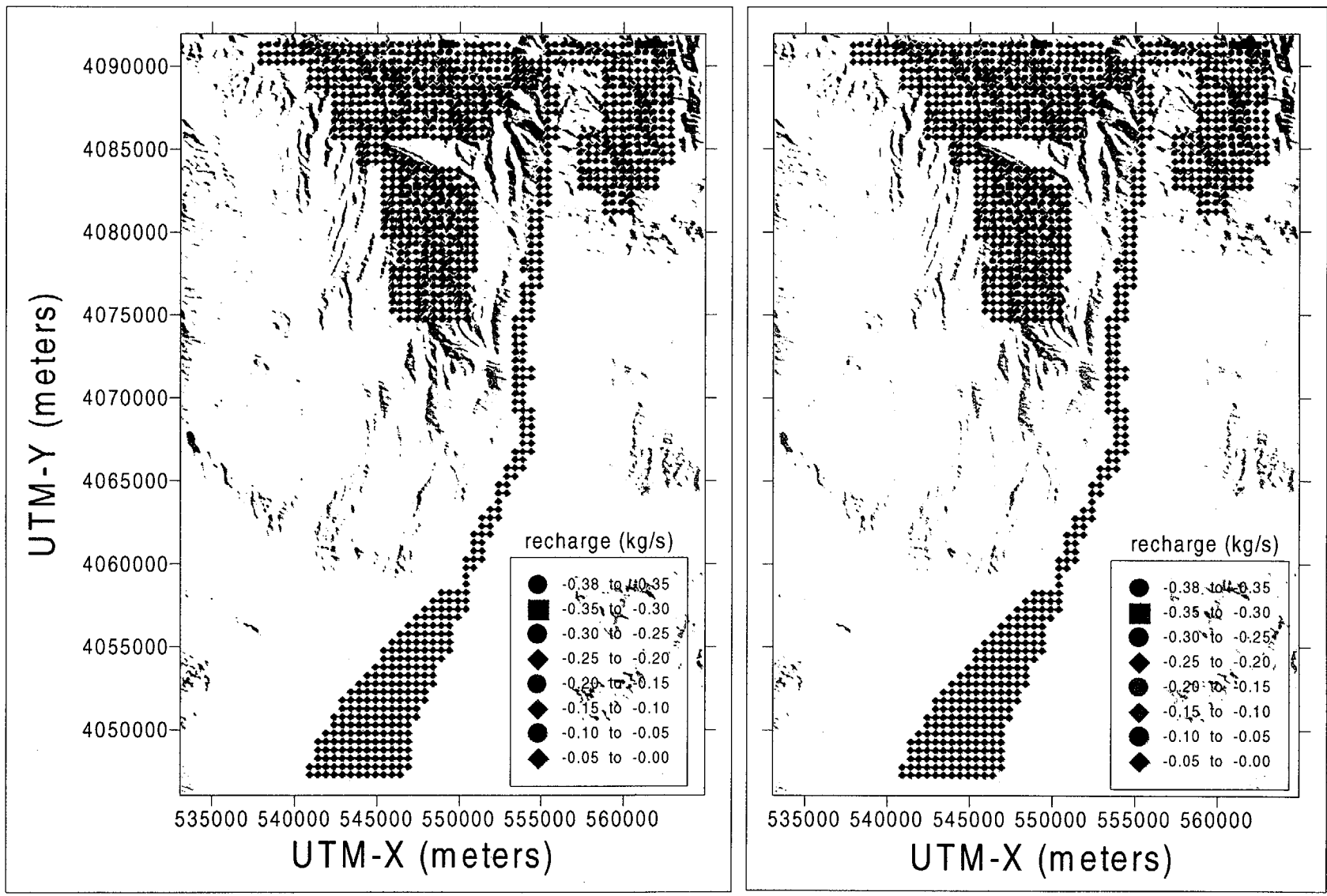
NOTE: Of the 39 grid lines, one defined the lower boundary of the model and, thus, was not considered in the model. Therefore, there were only 38 grid lines in the model.

6.2.3 Infiltration Map Translation to Boundary Conditions

An infiltration map (DTN: SN990870581999.001) is interpolated onto the computational mesh to provide the top surface flux boundary condition. The interpolation procedure is designed to ensure that the local small-scale features of the infiltration map are represented in the boundary conditions and that the total flux is preserved. The steps in that procedure are presented.

The infiltration map (DTN: SN990870581999.001) is provided as an ascii file with two coordinates, x and y , for each data point, the recharge area associated with that point, and the flux (mm/yr) for each point. The data points have an irregular spatial distribution. The computational mesh has a regular point distribution with points spaced at either 500-m or 1000-m horizontal intervals. A geometric sorting program is used to identify each point in the infiltration data with the closest gridblock in the computational mesh. This step is equivalent to computing the grid block for the regular 500-m mesh and determining which grid block each point of the irregularly spaced infiltration map belongs to. In areas of the infiltration map where points are closely spaced, there may be many infiltration map points associated with a single gridblock of the computational mesh. Figure 2 show a comparison of the data in the above-mentioned DTN and that recharge used in the FEHM input files for the SZ flow model. They are identical; thus proving the mapping used preserves the recharge distribution.

Next, for each gridblock, the sum of all the fluxes is calculated. This sum is then the total flux (kg H₂O/yr), which is provided as a FEHM boundary condition macro.



DTN: SN9908T0581999.001

Figure 2. Comparison of Recharge Data (left panel) with FEHM Input Data (right panel)

6.2.4 Computational Grids

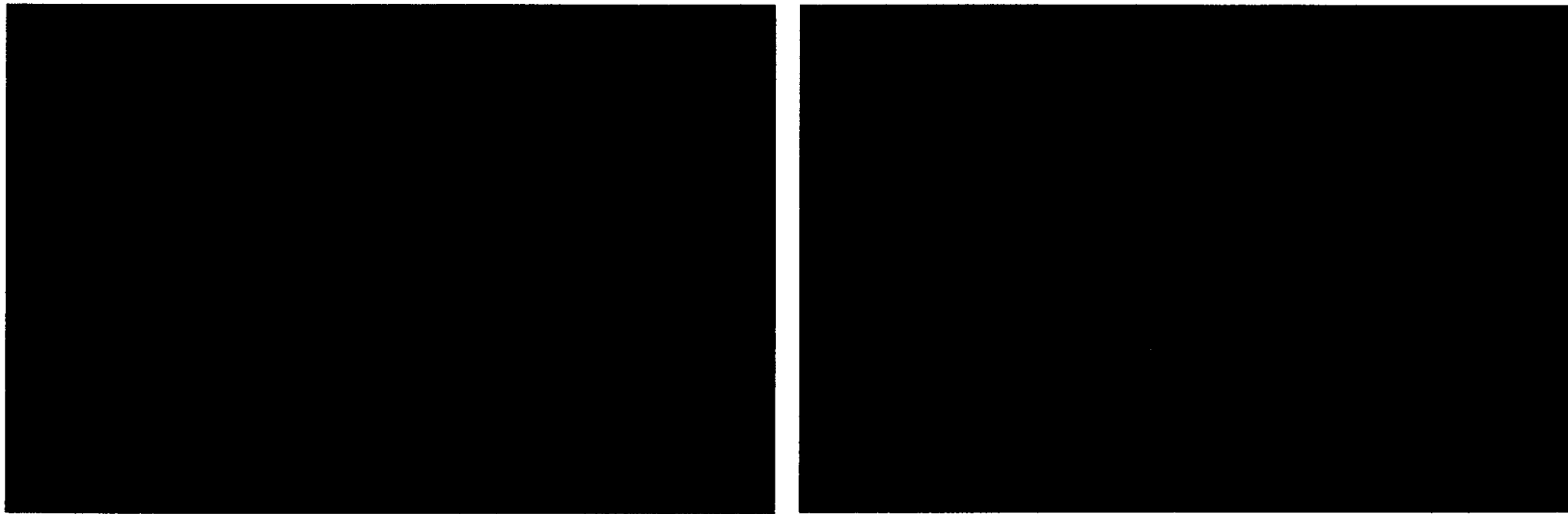
Gridding Procedure—For the SZ flow model, the Yucca Mountain area (Figure 3) was gridded so that the hydrogeologic properties and flow parameters in each individual grid cell could be given different values. Because grid resolution can affect the results of a model, two separate grids with different horizontal grid spacings were created so the results of each could be compared. The two grids used different horizontal grid spacing (500 m and 1,000 m) but the same vertical grid spacing. At a grid spacing of 500 m, there are four times as many cells as there are at a grid spacing of 1,000 m.

The computational grid included an area that ranged 45 km, from north of Yucca Mountain to south of Highway 95, and ranged 30 km, from east to west, approximately centered on Yucca Mountain (Figure 3). For both horizontal grids, a uniform grid spacing was used (i.e., 500 m and 1000 m), but in the vertical dimension, the grid spacing was nonuniform. The vertical grid spacing ranged from 10 m near the water table to 550 m deep within the SZ (Table 4). The vertical grid extended from an elevation of +1,200 m to -2,750 m (relative to sea level) and was divided into 11 groups (Table 4). Within each zone, the vertical grid spacing was uniform (e.g., in the +1,200 to +1,000 zone, the grid spacing was every 50 m). In total, there were 38 cells in the vertical dimension.

The geometry of geologic units was defined by the USGS in a Stratamodel Framework file (DTN: TBD), and these data formed the basis for defining the boundaries of each of the 19 stratigraphic units. The two grids were then overlaid on the stratigraphic units (Section 6.1.2), and the number of grid cell intersections per stratigraphic unit were calculated: 13 to 27,097 gridblocks per geologic unit for the 500-m horizontal gridblock spacing and 0 to 6,912 nodes per geologic unit for the 1000-m horizontal gridblock spacing (Table 5).

Table 5. Geologic Units

Surface Number	Hydrogeologic Units	Number of Gridblocks	
		1000 m	500 m
20	Alluvium (Valley-Fill Aquifer)	1,611	6,188
19	Valley-Fill Confining Unit	0	13
18	Limestones	60	227
17	Lava Flows	237	891
16	Upper Volcanic Aquifer	3,538	13,831
15	Upper Volcanic Confining Unit	1,986	7,845
14	Crater Flat - Prow Pass	1,428	5,666
13	Crater Flat - Bullfrog	1,618	6,472
12	Crater Flat - Tram	2,961	11,676
11	Lower Volcanic Confining Unit	2,298	9,142
10	Older Volcanic Aquifer	54	210
9	Older Volcanic Confining Unit	2,882	11,012
8	Undifferentiated Valley Fill	5,523	21,578
7	Upper Carbonate Aquifer	23	23
6	Lower Carbonate Aquifer Thrust	330	1,192
5	Upper Clastic Confining Unit	1,542	5,923
4	Lower Carbonate Aquifer	6,912	27,097
3	Lower Clastic Confining Unit	3,545	13,259
2	Granites	177	608
1	Base	0	0
	Total Number of Gridblocks	36,725	142,853
	Number of Elements	30 x 45 x 38	60 x 90 x 38



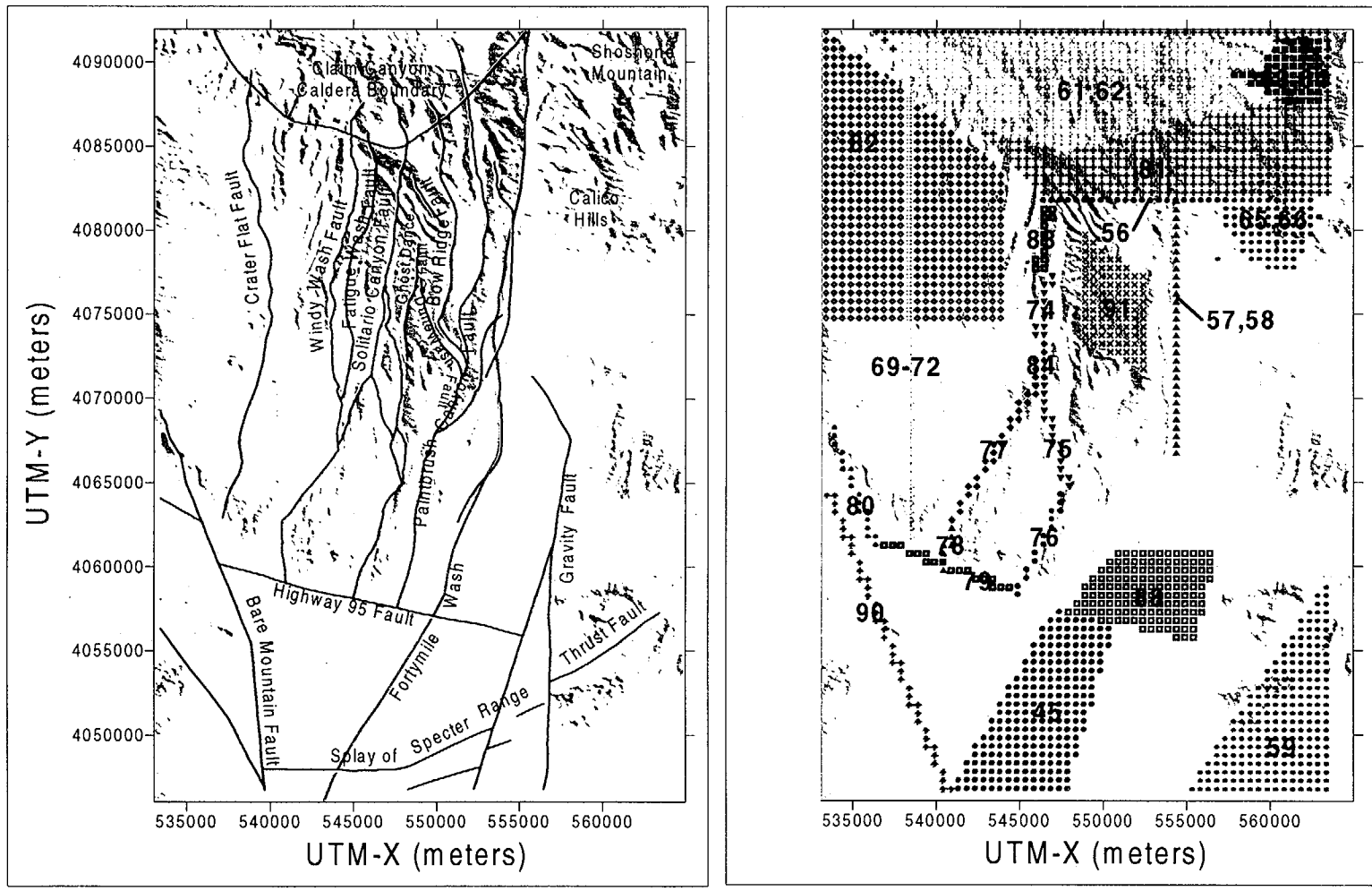
DTN: SN9908T0581999.001

NOTE: The computational grids are scaled by 5 vertically. Color in the grid is used only to distinguish units.

Figure 3. The 1000-m (left panel) and 500-m (right panel) Computational Grids

6.3 FEATURES

The hydrogeologic features included in the flow model primarily represent faults, fault zones, and areas of chemical alteration. The features described here are essentially vertical: some being linear in the horizontal extent, and some being of areal extent. These features are distinct from the subhorizontal geological formations, which form zones with distinct geometry and material properties and are described in the hydrogeological framework model section. Each of the features described in this report includes multiple geologic formations and represents zones of altered permeability within the individual formations: some features have enhanced permeability, some have reduced permeability, and some have anisotropic permeability. Each of them has a significant impact on the flow model. The geometric definition, description, nature of permeability alternation, and impact on the model for each of these features are described in Table 6. In the table, the numbers in the parentheses refer to zone numbers in the input file for FEHM. These features are shown in Figure 4, which is based on the Yucca Mountain area geologic map (Day et al. 1998) but which also shows their representation in the SZ flow model. Also shown in the figure are the zone numbers used in the input deck for FEHM. The permeability values associated with the features described in Table 6 are presented and discussed in Section 6.7.12. Because of their importance to PA, two proposed zones in the alluvium deserve special consideration. These zones are (1) the alluvial uncertainty zone and (2) the lower Fortymile Wash zone. The alluvial uncertainty zone was added to incorporate the new geology obtained with the recently drilled 2-D and Washburn wells (DTN: MO9909NYEEWDPO.000). The location of this zone is given in Table 6. The drilling records of these wells showed that Alluvium extended further north and east than the geologic model (created without benefit of the two wells) indicated. Because of the importance to PA, the alluvial zone was added to the model. The lower Fortymile Wash zone was added because of the distinct character of the Fortymile Wash in the southern part of the model. Field observations indicate possible channelization with attendant textural contrasts with surrounding alluvial material (Oatfield and Czarnecki 1991).



DTN: TBD

NOTE: Field data are on the left panel and the SZ model representation is the right panel. Numbers designate the following regions: 45 - Lower FortyMile Wash Zone; 56 - East-West Barrier Zone; 57 and 58 - Fortymile Wash Zones; 59 - Spotted Range-Mine Mountain Zone; 61 and 62 - Claim Canyon Caldera Zones; 63 and 64 - Shoshone Mountain Altered Zones; 65 and 66 - Calico Hills Altered Zones; 69, 70, 71, and 72 - Crater Flat Fault Zones; 74, 83, and 84 - Solitario Canyon Fault Zones; 75 and 76 - Solitario Canyon Fault Zones (East Branch); 77 and 78 - Solitario Canyon Fault Zones (West Branch); 79 - Highway 95 Fault Zone; 80 and 90 - Bare Mountain Fault Zones; 81 - Northern Zone; 82 - Northern Crater Flat Zone; 88 - Alluvial Uncertainty Zone (expected case); 91 - Imbricate Fault Zone

Figure 4. Geologic Features in the Area of the Site-Scale Flow and Transport Model

Table 6. Hydrological Features in the Saturated-Zone Flow Model

Feature Name and Description	Geometric Definition (UTM)	Hydrogeological Characteristics	Impact on Model
<p>1. Northern Zone (entire Claim Canyon, Calico Hills, and Shoshone Mt.; #81) This zone is wedge-shaped, spanning almost the entire northern boundary (except the western corner of the northern boundary) and approximately the upper fourth of the eastern boundary. Vertically, it extends from the top to the bottom of the model, and its areal extent is shown by the four points.</p>	<p>$x = 546436, y = 4.08211E+006,$ $x = 563657, y = 4.08211E+006,$ $x = 563549, y = 4.09208E+006,$ $x = 535832, y = 4.09202E+006,$ and $z = \text{top to bottom of model}$</p>	<p>It represents the general region of lowered permeability caused by hydrothermal alteration associated with the Claims Canyon Caldera.</p>	<p>Impact of the model on this zone is mainly to control the flow of water into the model from the north boundary.</p>
<p>2. Northern Crater Flat Zone (#82) This wedge-shaped zone is at the northern third of the western boundary of the model. Vertically, it extends from the top to the bottom of the model, and its areal extent is shown by the four points.</p>	<p>$x = 533077, y = 4.07458E+006,$ $x = 544206, y = 4.07453E+006,$ $x = 544103, y = 4.08349E+006,$ $x = 532974, y = 4.09223E+006,$ and $z = \text{top to bottom of model}$</p>	<p>It is a permeability reduction zone, representing a hydrothermally altered area associated with the Claims Canyon Caldera.</p>	<p>Impact of the model on this zone is to control influx from the northwest corner of the model.</p>
<p>3. Fortymile Wash Zones (#57 and #58) These two north-south linear features are located approximately halfway between Yucca Mountain and the eastern model boundary. Vertically, it extends from the top to the bottom of the model, and its areal extent is shown by the four points.</p>	<p>$x = 554330, y = 4066770,$ $x = 554350, y = 4066770,$ $x = 554350, y = 4081790,$ $x = 554330, y = 4081790,$ and $z = \text{top to bottom of model}$</p>	<p>It is an enhanced permeability zone representing the faulted area associated with the wash.</p>	<p>Impact on the model is to channel the flow of the east-central portion of the model in the Jackass Flat area in a southern direction, lower the hydraulic gradient in the area, and act as a regional drain.</p>
<p>4. Spotted Range-Mine Mountain Zone (#59) This triangular feature is in the southeast corner of the model. Vertically, it extends from top of the model down to the bottom. In the plan view, its corners are given by points.</p>	<p>$x = 555000, y = 4046770,$ $x = 563350, y = 4046770,$ $x = 563350, y = 4059000,$ $x = 563310, y = 4059000,$ and $z = \text{top to bottom of model}$</p>	<p>It is a zone of enhanced permeability associated with the Spotted Range Thrust Region</p>	<p>Impact on the model is to control the water flow into the model from the southern end of the east boundary and water flow out of the model of the eastern end of the southern boundary.</p>

Table 6. Hydrological Features in the SZ Flow Model (Continued)

Feature Name and Description	Geometric Definition	Hydrogeological Characteristics	Impact on Model
<p>5. Claim Canyon Caldera (east and west, #61 and #62) These zones span much of the northern boundary of the model, extending south as triangular shapes and terminating north of the Yucca Wash. Vertically, it extends from the top to the bottom of the model, and its areal extent is shown by the four points.</p>	<p>x = 536800, y = 4091760, x = 540000, y = 4086700, x = 547600, y = 4084700, and x = 547600, y = 4091760; and x = 547677, y = 4091760, x = 547631, y = 4084710, x = 560000, y = 4087660, x = 560000, y = 4091760, and z = top to bottom of model</p>	<p>These are zones of reduced permeability due to the hydrothermal alternation associated with the caldera; but the permeability reduction is somewhat less than the rest of the Northern zone, probably due to faulting associated with the vertical movement due to caldera collapse and the greater thickness of welded zones within the caldera.</p>	<p>Impact on the model of these zones is mainly to control the water flow into the model from the northern boundary.</p>
<p>6. Shoshone Mt. Altered Zone (north and south, #63 and #64) These two zones are in the northeastern corner of the model. They extend from the top of the carbonate aquifer up to the top of the model. Vertically, it extends from the top to the bottom of the model, and its areal extent is shown by the eight points.</p>	<p>x = 560634, y = 4.09153E+006, x = 559362, y = 4.08957E+006, x = 563090, y = 4.08962E+006, and x = 563044, y = 4.09148E+006; and x = 557045, y = 4.08962E+006, x = 560953, y = 4.08748E+006, x = 563137, y = 4.08775E+006, x = 563090, y = 4.08962E+006, and z = top to bottom of model</p>	<p>These are zones of permeability reduction due to hydrothermal alternation associated with the Claim Canyon Caldera.</p>	<p>Impact on the model of these zones is mainly to control the water flow into the model from the northern portion of the eastern boundary.</p>
<p>7. Calico Hills Altered Zone (north and south #65 and #66) These two zones are near the eastern end of the model, south of the Shoshone Mountain Zones, at approximately the same northing as the Yucca Wash. Vertically, it extends from the top to the bottom of the model, and its areal extent is shown by the eight points.</p>	<p>x = 556864, y = 4.08102E+006, x = 562957, y = 4.08102E+006, x = 561499, y = 4.08407E+006, and x = 558589, y = 4.08343E+006; and x = 556818, y = 4.08102E+006, x = 558821, y = 4.07807E+006, x = 561273, y = 4.07716E+006, x = 563142, y = 4.08098E+006, and z = top to bottom of model</p>	<p>These are zones of permeability reduction due to hydrothermal alternation associated with the Calico Hills</p>	<p>Impact on the model of these zones is mainly to control the water flow into the model from the northern portion of the eastern boundary.</p>

Table 6. Hydrological Features in the SZ Flow Model (Continued)

Feature Name and Description	Geometric Definition	Hydrogeological Characteristics	Impact on Model
<p>8. Crater Flat Fault (north-1, north-2, south-3, and south-4, #69, #70, #71, and #72) This is a linear feature running north-south in the western half of the model, starting to the south of the Claims Canyon and terminating near Highway 195, almost halfway between the western boundary and the Solitario Canyon. Vertically, it extends from the top to the bottom of the model, and its areal extent is shown by the sixteen points.</p>	<p>$x = 538330, y = 4.08380E+006,$ $x = 538350, y = 4.08380E+006,$ $x = 538350, y = 4.08943E+006,$ and $x = 538330, y = 4.08943E+006;$ and $x = 538330, y = 4.07475E+006,$ $x = 538350, y = 4.07475E+006,$ $x = 538350, y = 4.08380E+006,$ and $x = 538330, y = 4.08380E+006;$ and $x = 538330, y = 4.06650E+006,$ $x = 538350, y = 4.06650E+006,$ $x = 538350, y = 4.07475E+006,$ and $x = 538330, y = 4.07475E+006;$ and $x = 538330, y = 4.06140E+006,$ $x = 538350, y = 4.06140E+006,$ $x = 538350, y = 4.06650E+006,$ and $x = 538330, y = 4.06650E+006;$ and $z = \text{top to bottom of model}$</p>	<p>These are zones of permeability reduction normal to the fault orientation and permeability enhancement parallel to the fault orientation.</p>	<p>Impact on the model of these zones is to generate a somewhat high head gradient in the western half of the model and control the influx coming from the western boundary, and to restrict the flow towards the eastern half of the model.</p>
<p>9. Solitario Canyon Fault (#74, # 83 and #84) These are generally north-south trending linear features just to the west of Yucca Mountain. Vertically, it extends from the bottom of the model to the top of the model.</p>	<p>$x = 546451, y = 4.07754E+006,$ $x = 545632, y = 4.07355E+006,$ $x = 546384, y = 4.07355E+006,$ and $x = 547018, y = 4.07754E+006;$ and $x = 546451, y = 4.07754E+006,$ $x = 545632, y = 4.07752E+006,$ $x = 546384, y = 4.08158E+006,$ and $x = 547018, y = 4.08158E+006;$ and $x = 545638, y = 4.07111E+006,$ $x = 546379, y = 4.07108E+006,$ $x = 546647, y = 4.07355E+006,$ and $x = 546008, y = 4.07352E+006;$ and $z = \text{top to bottom of model}$</p>	<p>These are zones of permeability enhancement in the vertical and fault-parallel direction and permeability reduction normal to the fault.</p>	<p>Impact on the model of these features is to generate a higher head gradient to the west of Yucca Mt. and to impede flow from Crater Flat to Yucca Mountain.</p>

Table 6. Hydrological Features in the SZ Flow Model (Continued)

Feature Name and Description	Geometric Definition	Hydrogeological Characteristics	Impact on Model
<p>10. Solitario Canyon Fault, East Branch (#75, #76) These are generally north-northeast trending linear features just to the west of Yucca Mountain. Vertically, it extends from the bottom of the model to the top of the model.</p>	<p>x = 545632, y = 4.07111E+006, x = 547450, y = 4.06468E+006, x = 547996, y = 4.06468E+006, and x = 546384, y = 4.07109E+006; and x = 547450, y = 4.06468E+006, x = 544520, y = 4.05833E+006, x = 545040, y = 4.05815E+006, and x = 548022, y = 4.06468E+006; and z = top to bottom of model</p>	<p>These are zones of permeability enhancement in the vertical and fault-parallel direction and permeability reduction normal to the fault.</p>	<p>Impact on the model of these features is to generate a higher head gradient to the west of Yucca Mt. and to impede flow from Crater Flat to Yucca Mountain.</p>
<p>11. Solitario Canyon Fault, West Branch (#77, #78) These are generally north-northeast trending linear features just to the west of Yucca Mountain. Vertically, it extends from the bottom of the model to the top of the model.</p>	<p>x = 545632, y = 4.06109E+006, x = 540452, y = 4.06259E+006, x = 541018, y = 4.06261E+006, and x = 546384, y = 4.07106E+006; and x = 540426, y = 4.06259E+006, x = 540132, y = 4.05972E+006, x = 540699, y = 4.05947E+006, and x = 541018, y = 4.06259E+006; and z = top to bottom of model</p>	<p>These are zones of permeability enhancement in the vertical and fault-parallel direction and permeability reduction normal to the fault.</p>	<p>Impact on the model of these features is to generate a higher head gradient to the west of Yucca Mt. and to impede flow from Crater Flat to Yucca Mountain.</p>
<p>12. Highway 95 Fault (West, #79) This is a linear feature in the lower half of the western portion of the model. It is east-southeast trending. Vertically, it extends from the bottom of the model to the top of the model.</p>	<p>x = 536625, y = 4.06124E+006, x = 544355, y = 4.05838E+006, x = 544716, y = 4.05833E+006, x = 536486, y = 4.06184E+006, and z = top to bottom of model</p>	<p>This is a zone of permeability enhancement in the vertical and fault-parallel direction and permeability reduction normal to the fault.</p>	<p>Impact on this model is to restrict flow in the north-south direction and support high head gradients in that portion of the model.</p>

Table 6. Hydrological Features in the SZ Flow Model (Continued)

Feature Name and Description	Geometric Definition	Hydrogeological Characteristics	Impact on Model
<p>13. Bare Mountain Fault (#80 and #90) This is a northwest- to southeast-trending linear feature in the southwestern corner of the model. Vertically, it extends from the bottom of the model to the top of the model.</p>	<p>x = 533628, y = 4.06757E+006, x = 536126, y = 4.06102E+006, x = 536672, y = 4.06125E+006, x = 533628, y = 4.06898E+006, and and x = 540330, y = 4.04678E+006, x = 540850, y = 4.04678E+006, x = 533850, y = 4.06429E+006, and x = 533330, y = 4.06429E+006; and z = top to bottom of model</p>	<p>This is a zone of permeability enhancement representing the Bare Mountain fault.</p>	<p>Impact on the model is to drain the flow from Crater Flat to the Amargosa Desert.</p>
<p>14. Alluvial Uncertainty Zone (expected case, #88) This is a roughly rectangular region to the south of Yucca Mountain in the southern half of the model. Vertically, it extends from the top of the model down through the undifferentiated units.</p>	<p>x = 547622, y = 4.05731E+006, x = 555503, y = 4.05542E+006, x = 556740, y = 4.06206E+006, x = 550691, y = 4.06206E+006, and z = top of model to +400</p>	<p>This zone represents uncertainty in the border between the alluvium and tuff.</p>	<p>Although it does not strongly influence the flow model, it is expected to be important to PA calculations due to its effect on solute transport.</p>
<p>15. Imbricate Fault Zone (#91) This is a highly faulted area bounded in the west by the Ghost Dance fault, south by the Dune Wash, east by the Paintbrush Canyon fault, and to the north by the Drillhole Wash. Vertically, it extends from the top of the model down through the middle volcanics to the top of the undifferentiated units.</p>	<p>x = 548830, y = 4073270, x = 552350, y = 4071770, x = 552350, y = 4077290, x = 548830, y = 4079790, and z = top of model to +400</p>	<p>This is a region of permeability enhancement.</p>	<p>It allows the model to represent higher permeabilities due to faulting while retaining regional scale permeability values of the middle volcanic layers in the expected range.</p>
<p>16. East-West Barrier (#56) This linear feature runs east-west just to the north of Yucca Mountain, starting at the western edge of Yucca Mt. and extending eastwards but short of the Calico Hills. Vertically, it extends from the bottom of the model to the top of the model.</p>	<p>x = 546000, y = 4081440, x = 559000, y = 4081440, x = 559000, y = 4082000, x = 546000, y = 4082000, and z = top to bottom of model</p>	<p>This is a zone of permeability reduction.</p>	<p>The impact on the model of this barrier is mainly to create the steep hydraulic gradient to the north of Yucca Mountain between the wells G2, WT6 to the north and the wells WT18, H1 to the south.</p>
<p>17. Lower FortyMile Wash Zone (#45) This quadrilateral feature (plan view) encompasses the Lower FortyMile Wash part of the model. The depth of the zone includes the alluvium unit to the top of the model.</p>	<p>x = 546965, y = 4057460, x = 550691, y = 4056450, x = 547893, y = 4046760, x = 540833, y = 4046760, z = 400m to top</p>	<p>This is a zone of permeability enhancement.</p>	<p>The impact on the model of this barrier is mainly to create the low hydraulic gradient observed in the Fortymile wash area where it intersects the Southern Boundary.</p>

DTN: FEATURES DTN

6.4 PARAMETER OPTIMIZATION

The parameter estimation was accomplished with the PEST-FEHM computer code, which is a combination of FEHM (Zyvoloski et al. 1997a) and a commercial parameter estimation code named PEST. PEST is a Levenberg-Marquardt (LM)-based optimization algorithm. The LM package is a well-established algorithm (Press et al. 1992, pp. 678–683), very robust, and widely applicable. It will search for the minima of a multidimensional function. In this case, the “function” is the sum-of-squares difference (SSD) between a set of observations (the heads in the 100+ wells in the Yucca Mountain region plus side-boundary fluxes from the USGS regional flow model) and the solution to the partial differential equation that describes SZ flow at Yucca Mountain. PEST computes the derivatives of the SSD function with respect to the various parameters. In the case of the SZ flow model, the unknown parameters are the intrinsic permeability of each of the various geologic units (see Table 8) and some of the hydrogeologic features described in Sections 6.3 and 6.7.12. The method employed is as follows.

- An initial estimate or guess for each unknown parameter is specified at the beginning of the fitting process.
- FEHM computes the resulting heads for the initial estimate of parameters.
- The results are returned to the PEST code.
- Through a series of FEHM simulations with perturbations in the parameters, the LM package (PEST) computes the derivative of the SSD function with respect to each of the parameters.
- The LM package (PEST) then determines the amount to change each parameter’s current value to improve the fit to the data. It does this through a mathematical process that combines gradient information and second derivative (approximated) information.

This process is repeated until the fit to data is within a prescribed tolerance or until no further improvement is possible. This coupling between PEST and FEHM allows any variable in FEHM to be considered as a fitting parameter, if desired, whether it be a flow-related or a transport-related parameter. PEST will find local minima of the target function. To enable the PEST-FEHM code to search for the global minimum, a procedure is attached to the code that carries out a simulated annealing process, which allows the PEST-FEHM code to move from one local minimum to another, better, local minimum. This process is repeated until no further improvement occurs. The simulated annealing process (Press et al. 1992, pp. 436–448) is simple in principle. The approach is to occasionally reject an improved solution, move to a new location in parameter space, and continue the search. Theory indicates that this will eventually find the global or a near-global minimum. In the Yucca Mountain case, the procedure involves resetting the value of the LM step-size parameter after each local minimum is found.

In addition to the PEST optimization described above, several adjustments were made to the model. These were made to improve the model in ways that were not possible during the PEST

run. The most important of these adjustments were made to insure that the specific discharge within the 5-km compliance boundary was conservative with respect to the estimates given by the SZ expert elicitation (CRWMS M&O 1998). Because the specific discharge was calculated with the particle tracking feature of FEHM after the flow calculations were performed, this adjustment could not easily be incorporated in the PEST optimization. The specific discharge was adjusted by changing the permeability of the Bullfrog unit. Because of the large permeability of that unit, the specific discharge could be manipulated by changing the unit's permeability without adversely affecting the heads in the low-gradient area near Yucca Mountain (see Section 6.8 for additional details). Adjustments were also made to the permeability in the lower Fortymile Wash area so water levels in the 2-D and Washburn wells would be more consistent with those in the upper Fortymile Wash area, thus preserving the observed head gradient. Adjustments to the permeability of the alluvial uncertainty zone and the permeability of the valley-fill aquifer were also made to better match eastern boundary fluxes of the regional model.

Lastly, it is important to note that while the SZ model was calibrated with the application of the PEST code, the final product (a suite of FEHM files) does not include any PEST files. Thus, the SZ flow model may be used for PA or other purposes with the inclusion on the PEST executable code or related files.

6.5 NUMERICAL FLOW MODEL

The numerical model used in the flow and transport simulations in this report is fully described in Zylvoski et al. (1997b). Because the SZ modeling is a subset of the general multiphase, nonisothermal capability of the FEHM code, it is described herein.

The control-volume finite-element method is used to perform the groundwater modeling. The finite-element methods are based upon the assumption that a continuum may be modeled as a configuration of discrete elements. For each element, equations are written that describe the interaction of the element with its neighbors. These equations describe the hydrologic behavior of the elements. The finite-element method leads to a set of nonlinear equations that are then solved. The FEHM code is used to perform all groundwater flow calculations. For a complete description of the finite-element method, the reader is referred to Zeinkewicz (1977). FEHM is a nonisothermal, multiphase flow and transport code. It simulates the flow of water and air and the transport of heat and solutes in two- and three-dimensional saturated or partially saturated heterogeneous porous media. The code includes comprehensive reactive geochemistry and transport modules and a particle tracking capability. Fractured media can be simulated using an equivalent continuum, discrete fracture, dual porosity, or dual permeability approach. For a detailed description of FEHM, the reader is referred to Zylvoski et al. (1997b).

Only the conservation-of-mass equations are shown here, as the energy equations are not used for this study. The equations are for an isotropic, isothermal medium, though these restrictions do not exist in FEHM. The conservation of fluid mass is

$$\frac{A_{mass}}{t} + - \bar{f}_{mass} \bar{q}_{mass} = 0 \quad (\text{Eq.1})$$

where

A_{mass} is the fluid mass per unit volume given by

$$A_{mass} = \rho \bar{v} \quad (\text{Eq. 2})$$

\bar{f}_{mass} is the fluid mass flux given by

$$\bar{f}_{mass} = \rho \bar{v} \quad (\text{Eq. 3})$$

ϕ is the porosity in the system

ρ is the fluid density

\bar{v} is the fluid velocity

q_{mass} is the fluid mass source.

The velocity of the fluid can be expressed by Darcy's Law:

$$\bar{v} = -\frac{k}{\mu} \nabla(P - \rho g) \quad (\text{Eq. 4})$$

where

μ is the dynamic viscosity of the fluid

P is the fluid pressure

k is the permeability

g is the acceleration resulting from gravity.

The conservation-of-solute equation is described here for completeness because future revisions of this document will include detailed geochemical modeling, which will be based on the solution of the solute equation.

The conservation-of-solute equation is explicitly coupled to the pressure field and is given by

$$-\nabla \cdot C \frac{k\rho}{\mu} \nabla P - \nabla \cdot D_c \nabla C + \frac{\partial}{\partial x_3} g \frac{k\rho^2}{\mu} C + \rho_r \frac{\partial C_r}{\partial t} + \frac{\partial A_c}{\partial t} + q_c = 0 \quad (\text{Eq. 5})$$

where

C is the concentration of the solute

D_c is the dispersion coefficient

x_3 is the vertical coordinate

$\rho_r \frac{\partial C_r}{\partial t}$ is the adsorption term onto the porous medium and is not used for this study

A_c is the solute accumulation defined by

$$A_c = \phi \rho C \quad (\text{Eq. 6})$$

and q_c is the solute source or sink given by

$$q_c = Cq_{mass} \quad (\text{Eq. 7})$$

The reactive-transport module of FEHM also contains rock/solute interactions and aqueous speciation reactions. These features are not used in the present study, but for a complete description, the reader is referred to Viswanathan et al. (1998).

A control-volume finite-element (CVFE) approach is used in FEHM. The CVFE method has been used extensively in petroleum reservoir engineering (Forsyth 1989). The CVFE method treats the potentials in a finite-element approach while the control-volume aspect allows local mass conservation and upstream weighting (Verma and Aziz 1997). Quadrilaterals and triangles in two dimensions and hexahedra and tetrahedra in three dimensions are divided into volumes associated with gridblocks and areas associated with interblock distances (for the examples in this paper, structured tetrahedral elements are used). The gridblock volumes are the Voronoi volumes (Forsyth 1989) associated with each gridblock. Voronoi volumes are also called perpendicular bisector (PEBI) volumes. The Voronoi volume is formed by boundaries that are orthogonal to the lines joining adjacent gridblocks and that intersect the midpoints of the lines (Verma and Aziz 1997). Any point within a Voronoi volume is closer to its associated gridblock than to any other node in the grid. The CVFE representation of Equation 1 is

$$V_i \frac{(A_{mass}^{t+1} - A_{mass}^t)}{\Delta t} - \sum_{i \neq j} \frac{A_{ij}}{d_{ij}} \left(\frac{k\rho}{\mu} \right) \left[(P_j - P_i) - \left(\frac{\rho_i + \rho_j}{2} \right) g(x_{3,j} - x_{3,i}) \right] + q_{i, mass} = 0 \quad i = 1, N \quad (\text{Eq. 8})$$

where

A_{ij} and d_{ij} are the area and distance between connected nodes i and j

Δt is the timestep size

V_i is the Voronoi volume of node i

$x_{k,j}$ is the cartesian coordinate for node j in the k direction

N is the number of nodes.

The CVFE method can be shown on simple elements with constant properties to be equivalent to traditional finite-element methods.

The stiffness coefficients (e.g., elements of the stiffness matrix) of the traditional finite-element method can be interpreted as a linear function of the area through which the fluid passes traveling from one node to its neighbor. A stiffness coefficient uses the area of the boundary of the Voronoi volume that intersects the line joining adjacent nodes. LaGriT is designed to produce CVFE grids.

These terms are used to form control-volume difference equations for the conservation equations. This method is not traditional because equation parameters are defined by node, not element, but the method leads to an intuitive understanding of the numerical method.

In FEHM, the nodal definition of equation parameters leads naturally to a separation of the nonlinear and purely geometric parts. This separation is explained in detail in Zyvoloski (1983)

and is valid over lower-order elements. The nonlinear part uses average inverse kinematic viscosity,

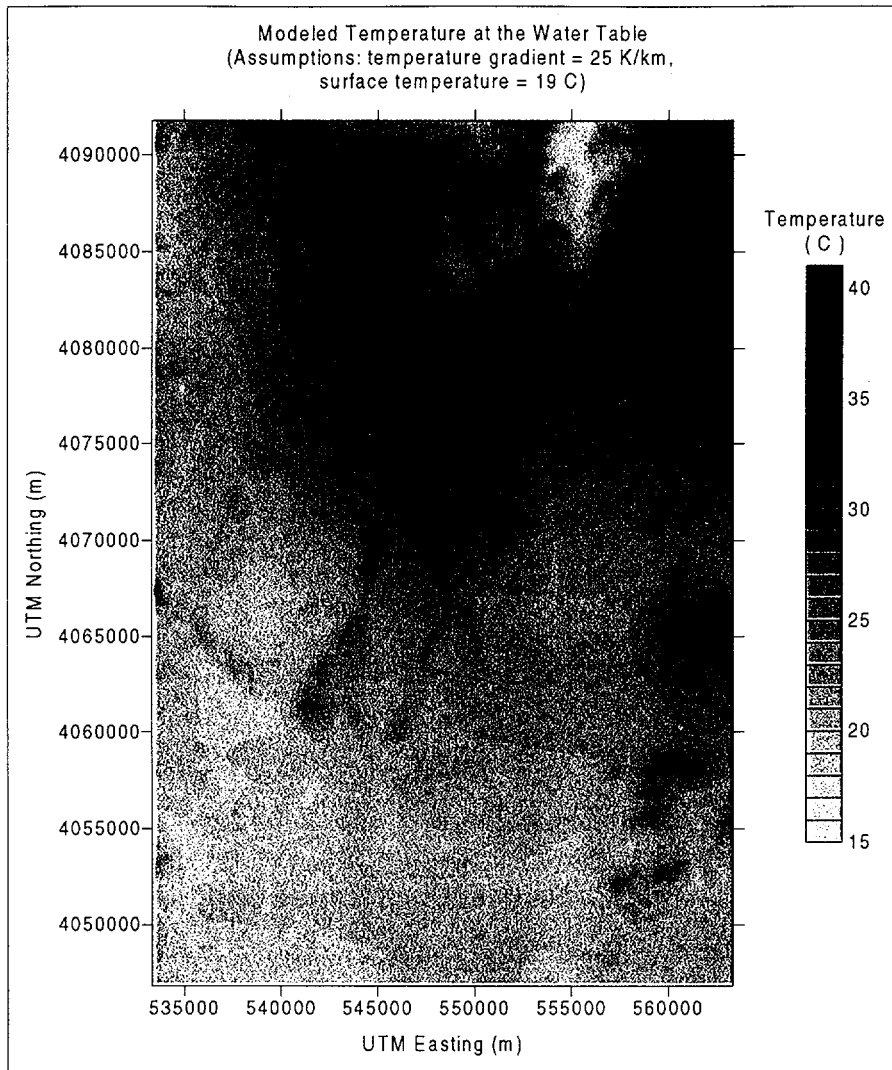
$$D = \frac{\rho}{\mu} \quad (\text{Eq. 9})$$

between two nodes—usually taken to be the upstream nodal value. The result is a much more stable code for solving nonlinear problems while still retaining much of the geometric flexibility of finite elements. This method has been used in FEHM since 1983 (Zyvoloski 1983) and has been extensively verified (Dash et al. 1997). A harmonic weighting of the intrinsic permeability is used. We note here that even though the SZ flow model is linear, the fact that it uses spatially varying viscosity terms (due to spatially varying temperatures), upwinding the viscosity terms is the standard way of modeling the interblock fluid fluxes. The Newton-Raphson iteration is applied to the system of equations, which is solved with a multidegree of freedom and preconditioned, conjugate gradient methods using Generalized Minimum Residual (GMRES) or biconjugate gradient-squared acceleration techniques.

6.6 GROUNDWATER TEMPERATURE

The approach taken to the incorporation of groundwater temperature in the SZ site-scale model is to evaluate the average temperature gradient using temperature measurements in boreholes and to use that temperature gradient to specify temperature at grid nodes in the SZ site-scale flow model. As implemented in the SZ site-scale flow and transport model, temperatures remain fixed at the specified value, and the heat-transport equations are not solved in the simulation. Thus, the specified values of temperatures are used to calculate the local groundwater viscosity, but temperature variations do not result in any variable-density flow processes.

Temperature profiles in a number of wells near Yucca Mountain are presented in Sass et al. (1988) (DTN: GS930208318523.001). The data in Figures 10, 4, 5, 6, 7, and 8 of Sass et al. (1988) were used to estimate an approximate average temperature gradient and representative surface temperature for the site. As noted by Sass et al. (1988), there is considerable variability (about 15°C/km to nearly 60°C/km) in the temperature gradients amount the wells (Sass et al. 1988, p. 2). However, the approximately average value of the temperature gradient in the wells is 25°C/km, and the average surface temperature is about 19°C. By using these values for the average temperature gradient and surface temperature, along with the water table and topographic surface evaluations, the estimated temperature at the water table is calculated as shown in Figure 5. The lower temperatures in Figure 5 correspond to areas of relatively small unsaturated thickness and the higher temperatures correspond to a thick UZ. The small computer routine used to form the temperature input for FEHM is given in the DTN associated with this AMR (DTN:LA9911GZ12213S.001).



DTN: TBD

Figure 5. Map of Modeled Temperature at the Water Table for the Saturated-Zone Site-Scale Flow Model Domain

6.7 CALIBRATION RESULTS

6.7.1 Calibration Criteria

The approach taken to calibrate the SZ site-scale model is similar to that described in Czarniecki et al.(1997) in which the combination of the computer codes PEST and FEHM was first used. The SZ site-scale model can only be calibrated if a variety of important data sources are considered: the field data for the water levels and hydraulic head, the permeability data from field and laboratory tests, known faults and other geologic data, hydrochemical data, and opinions expressed during the expert elicitation process. The goal is to deliver a realistic model for the case in which data exist and conservative model in other areas to PA. Thus, when field data and interpretations produce conflicting trends in calibration, the data that produce a more conservative model are used.

6.7.2 Description of Base Case

The base-case SZ flow and transport model uses 115 water level and head measurements and 10 flux values for calibration targets. These measurements (DTN: TBD) represent water levels and deeper head measurements. The deeper measurements represent average values over “open” or “packed-off” intervals and the coordinates of the observation represent mid-points of the interval. The calibration targets also represent steady-state values. Where pumping is taking place, as in the Amargosa Valley, current water levels are used (see Section 6.1.2 for additional details). The model results represent a linearly interpolated head at the observation coordinates based on the eight points surrounding it. The field data and the optimized model results are given in Table 7. The calibration procedure was described in Section 6.4; the calibration parameters are permeabilities and permeability multiplication factors. These parameters were constrained to a range of reasonable values based on available data. These data are described in Section 6.7.7. The calibration parameters are given in Table 8. Preferential weighting (20), used to multiply the square of the difference between model and field observations, was given to the 32 wells in the low-gradient region to the south and east of Yucca Mountain. This value contrasts with the default weighting of 1 given typical observations. These observation points were given high weighting because they are in the likely pathway of fluid leaving the potential repository site, and small changes in head in this area could have a large effect on the flow direction. High head and water-level observations north of Yucca Mountain were given a relatively low weighting (0.05). The five wells in this category were given low weights primarily because of the possibility of perching in this region and the attendant uncertainty in water-level measurements. The weights for each observation point are given in the last column of Table 7.

The base-case model used a grid with 500 m areal spacing. As discussed in Section 6.1.4, this resolution was sufficient for this application. The SZ flow model had a sum-squared weighted residual of about 27,600, which translates into about a 16-m (weighted) residual for each observation. Without weighting, the sum-squared residual was about 90,000, which corresponds to approximately 30-m average residual for each observation. The distribution of residuals is provided in Figure 6 along with the measured and simulated water level surfaces. It can be seen from the figure that the largest head residuals (~100 m) are in the northern part of the model in the high-head gradient area near the East-West barrier. These head values are largely the result of the low weighting (0.05) and the uncertainty in these measurements, possibly due to perched conditions. The next highest group of heads border the East-West barrier and Solitario Canyon Fault. These residuals (~50) are most likely the result of 500-m gridblocks not being able to resolve the 780-m to 730-m drop in head in the very short distance just east of the above-mentioned features.

Table 7. Observation Wells with Computed Head Data

Site Name	x (UTM) (m)	y (UTM) (m)	z (elevation) (m)	Head Data (m)	Model Data (m)	Weight
UE-29a 2 HTH	555753	4088350	990.8	1187.7	1165.96	0.05
GEXA Well 4	534069	4086110	859.2	1008	1017.9	0.05
UE-25 WT 6	549352	4083100	983.2	1034.6	945.34	0.05
USW G-2	548143	4082540	371.5	1020.2	933.87	0.05
UE-25 WT 16	551146	4081230	714.1	738.3	734.51	1
USW UZ-14	548032	4080260	793.4	779	734.89	1
UE-25 WT 18	549468	4080240	722.1	730.8	734.67	20
USW G-1	548306	4080020	125.7	754.2	735	1
UE-25a 3	561084	4079700	681.4	748.3	798.99	1
UE-25 WT 4	550439	4079410	709	730.8	734.46	20
UE-25 WT 15	554034	4078690	698.7	729.2	733.87	20
USW G-4	548933	4078600	542.2	730.1	734.5	20
UE-25a 1	549925	4078330	584	731	734.36	1
UE-25 WT 14	552630	4077330	703.6	729.7	733.79	20
USW WT-2	548595	4077030	702	730.7	734.18	20
UE-25c 1 HTH	550955	4075930	473.2	730.3	733.92	20
UE-25c 3	550930	4075900	474.3	730.3	733.92	20
UE-25c 2	550955	4075870	553.2	730.2	733.9	20
UE-25 WT 13	553730	4075830	703.8	729.1	733.35	20
USW WT-7	546151	4075470	740.9	775.8	768.09	1
USW WT-1	549152	4074970	708.4	730.4	733.86	20
USW G-3	547543	4074620	318.1	730.5	734.96	20
J-13 WW	554017	4073520	354.8	728.4	732.74	20
USW WT-10	545964	4073380	734.2	776	781.48	1
UE-25 WT 17	549905	4073310	705.4	729.7	733.58	20
USW VH-2	537738	4073210	282.8	810.5	794.35	1
UE-25 WT 3	552090	4072550	705.8	729.6	733.08	20
USW VH-1	539976	4071710	490.5	779.4	783.68	1
UE-25 WT 12	550168	4070660	702.6	729.5	732.92	20
USW WT-11	547542	4070430	691.9	730.7	733.71	20
J-12 WW	554444	4068770	659.6	727.9	731.44	20
JF-3 Well	554498	4067970	662.7	727.8	731.15	20
Cind-R-Lite Well	544027	4059810	710.2	729.8	737.49	20
Ben Bossingham	553704	4056230	697.4	718.4	715.41	1
Fred Cobb	553808	4055460	675.6	702.8	713.61	1
Bob Whellock	553883	4055400	682	704.1	713.61	1
Louise Pereidra	554131	4055400	698	705.6	714.16	1
Joe Richards	554008	4055340	679.3	701.7	713.61	1
NDOT Well	553685	4055240	682.1	705.3	713.61	1
James H. Shaw	549863	4054910	664.3	706.7	707.46	1
Airport Well	552818	4054930	636.5	705.5	711.65	1

Table 7 (Continued). Observation Wells with Computed Head Data

Site Name	x (UTM) (m)	y (UTM) (m)	z (elevation) (m)	Head Data (m)	Model Data (m)	Weight
TW-5	562604	4054690	688.7	725.1	726.67	1
Richard Washburn	549746	4053650	669.9	707.7	706	1
Richard Washburn	549679	4052320	675.3	704.4	703.92	1
Nye County Development Co	543481	4050070	638.6	694.4	696.65	1
Fred Wooldridge	536350	4050010	673.8	691.9	688.06	1
Fred J. Keefe	540673	4049990	676.7	694.3	696.14	1
Leslie Nickels	541518	4049940	654.7	694.4	696.35	1
L. Mason	553471	4049850	699.2	722.1	711.75	1
Unknown	545596	4049400	667.6	697.8	695.99	1
Davidson Well	536552	4049330	672	690.2	688.07	1
Eugene J. Mankinen	538889	4049000	678.6	707.4	691.83	1
Donald O. Heath	542194	4048890	651.6	698.1	694.5	1
Elvis Kelley	536903	4048620	685.1	691	688.16	1
Manuel Rodela	546718	4048670	686.7	693.6	695.3	1
Charles C. DeFir Jr.	538196	4048440	685.7	706.9	691.1	1
William R. Monroe	540035	4048450	669.5	699	694.8	1
DeFir Well	536655	4048400	671.1	691.3	688.21	1
Edwin H. Mankinen	540608	4048080	662.8	695.2	694.4	1
Bill Strickland	534967	4047970	677	689.2	687.22	1
M. Meese	547120	4047960	664.6	686.4	693.47	1
Theo E. Selbach	547941	4047780	673.3	696.2	693.99	1
C.L. Caldwell	537727	4047670	654.5	691.4	690.7	1
Leonard Siegel	552390	4047680	667.2	709	703.7	1
James K. Pierce	541778	4047600	664	690.4	693.41	1
James K. Pierce	541381	4047560	677.1	705.7	693.64	1
Cooks West Well	553609	4047630	690.2	717.2	712.24	1
Cooks East Well	554006	4047630	693.4	718.8	712.24	1
Nye County Land Company	548466	4047260	715.4	690.1	693.28	1
Amargosa Town Complex	548492	4047080	668.3	688.9	693.28	1
Nye County Development Co	550431	4047060	615.4	691.2	694.89	1
Lewis C. Cook	553612	4047080	702.5	717.4	714.02	1
Lewis C. Cook	553687	4047080	688.7	714.8	714.02	1
Amargosa Valley Water	548393	4046950	673.9	701.4	691.81	1
Earl N. Selbach	539147	4046840	672.1	696.5	694.05	1
Lewis N. Dansby	539968	4046820	664.7	694.2	695.22	1
Edwin H. Mankinen	540788	4046820	686.2	694	693.64	1
Willard Johns	552097	4046880	678.9	699.5	708.82	1
USW H-1 HTH tube 1	548727	4079930	-495.5	785.5	741.96	1
USW H-1 HTH tube 2	548727	4079930	193	736	734.68	1
USW H-1 HTH tube 3	548727	4079930	562.5	730.6	734.63	20
USW H-1 HTH tube 4	548727	4079930	680.5	730.9	734.65	20

Table 7 (Continued). Observation Wells with Computed Head Data

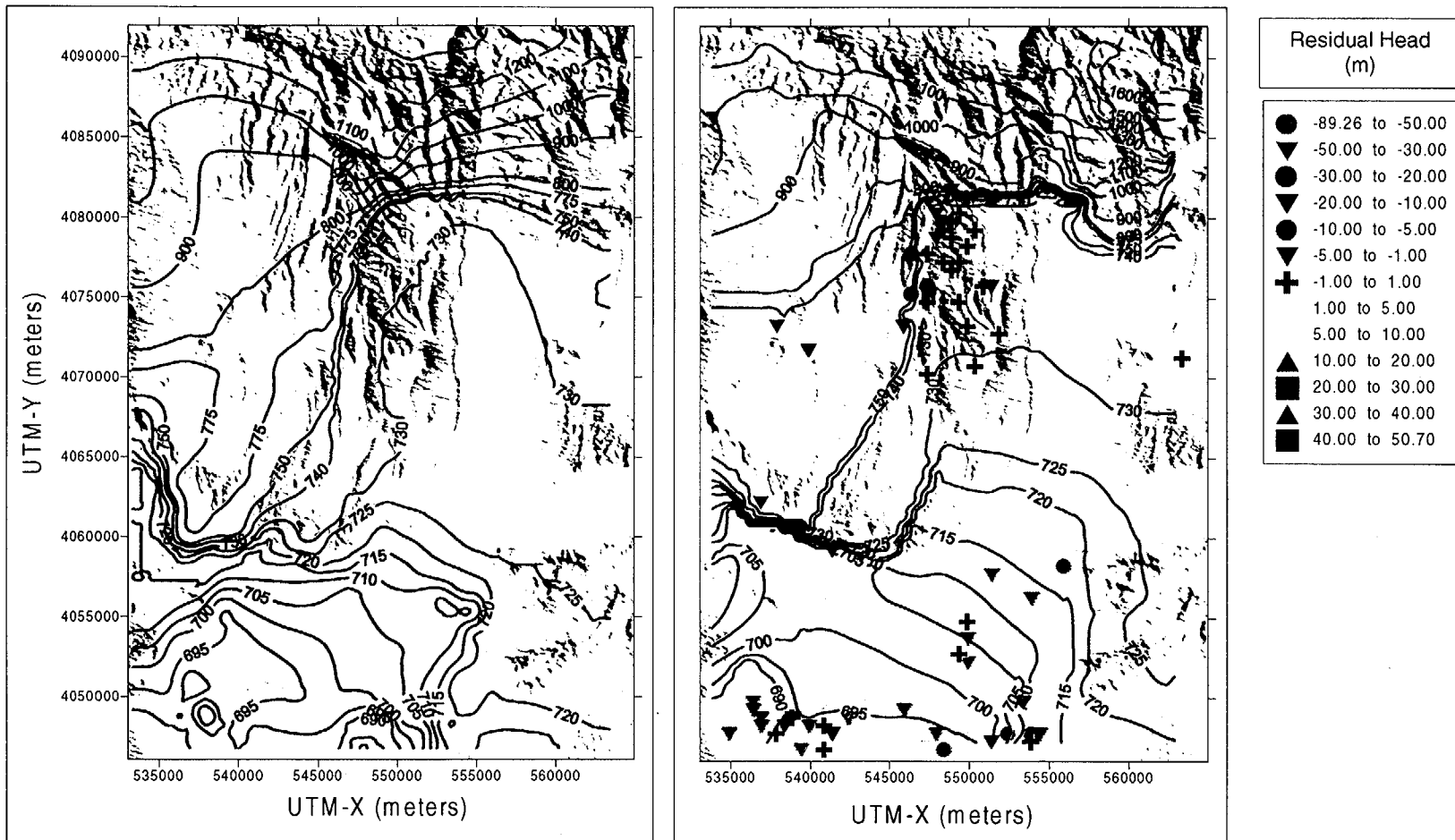
Site Name	x (UTM) (m)	y (UTM) (m)	z (elevation) (m)	Head Data (m)	Model Data (m)	Weight
USW H-5 HTH upper	547668	4078840	704.2	775.5	734.65	1
USW H-5 HTH lower	547668	4078840	446.4	775.6	734.66	1
UE-25b 1 HTH lower	549949	4078420	-8.8	729.7	735.53	20
UE-25b 1 HTH upper	549949	4078420	366.2	730.7	734.34	20
USW H-6 HTH upper	546188	4077820	662.9	776	764.08	1
USW H-6 HTH lower	546188	4077820	315.8	775.9	763.93	1
USW H-4 HTH upper	549188	4077310	395.5	730.4	734.25	20
USW H-4 HTH lower	549188	4077310	45	730.5	735.1	20
USW H-3 HTH upper	547562	4075760	576.9	731.5	734.48	20
USW H-3 HTH lower	547562	4075760	343.2	755.9	734.51	1
UE-25p 1 PTH (Lwr Intrvl)	551501	4075660	-410.3	752.4	739.69	1
USW SD-6	547578	4077550	725.9	731.2	734.84	20
USW SD-7	548384	4076500	637.7	727.6	734.13	20
USW SD-9	548550	4079260	678.3	731.1	734.64	20
USW SD-12	548492	4077420	696.7	730	734.31	20
WT-24	548697	4081910	734.8	839.8	830.76	1
NC-EWDP-1D	536768	4062500	413.5	785.8	763.9	1
NC-EWDP-1S	536771	4062500	747.8	786.7	773.29	1
NC-EWDP-2D	547744	4057160	507.2	706.3	709.26	1
NC-EWDP-3D	541273	4059440	376.7	717.1	703.88	1
NC-EWDP-3S	541269	4059440	719.1	718.7	702.54	1
NC-EWDP-5S	555676	4058230	603.9	724.1	717.98	1
NC-EWDP-9S	539039	4061000	721.2	766	732.49	1
NC-Washburn-1X	551465	4057560	668.8	714.6	714.55	1
J-11 WW	563799	4071060	687.2	732.2	731.57	20
BGMW-11	534386	4062600	673.4	715.9	724.56	1
Richard Washburn	549529	4052570	739.9	704.1	704.05	1
L. Cook	551348	4047430	704.1	713.3	699.01	1
Unknown	549532	4047670	691.8	689.5	695.05	1
Amargosa Water	547420	4047590	714.3	690.4	693.47	1
Lewis C. Cook	554329	4047670	735.5	715.7	713.71	1
Unknown	538989	4048880	710.1	690.8	691.83	1
USW UZ-N91	555680	4088200	1180.6	1186.8	1165.78	0.05

Table 8. Calibration Parameters Used in Saturated-Zone Site-Scale Model

Parameter Name	Geologic Unit or Feature	Calibrated Value	Parameter Type	Min Value	Max Value
gran	Granites	1.96×10^{-16}	Permeability	1.00×10^{-17}	1.00×10^{-14}
lcla	Lower Clastic Confining Unit	1.00×10^{-16}	Permeability	1.00×10^{-16}	1.00×10^{-14}
lca2	Lower Carbonate Aquifer	5.00×10^{-14}	Permeability	5.00×10^{-14}	1.00×10^{-12}
ucla	Upper Clastic Confining Unit	1.00×10^{-16}	Permeability	1.00×10^{-16}	1.00×10^{-14}
lca1	Lower Carbonate Aquifer Thrust	1.00×10^{-14}	Permeability	1.00×10^{-14}	1.00×10^{-12}
ucar	Upper Carbonate Aquifer	4.08×10^{-14}	Permeability (fixed)	4.08×10^{-14}	4.08×10^{-14}
udif	Undifferentiated Valley Fill	5.00×10^{-15}	Permeability	5.00×10^{-15}	1.00×10^{-12}
ovoc	Older Volcanic Confining Unit	2.00×10^{-16}	Permeability	2.00×10^{-16}	1.00×10^{-11}
ovoa	Older Volcanic Aquifer	5.00×10^{-16}	Permeability	3.00×10^{-16}	1.00×10^{-12}
lvoc	Lower Volcanic Confining Unit	2.00×10^{-15}	Permeability	1.00×10^{-15}	1.00×10^{-11}
tram	Crater Flat-Tram	2.36×10^{-13}	Permeability	1.00×10^{-13}	1.00×10^{-11}
bull	Crater Flat-Bullfrog	1.54×10^{-11}	Permeability	1.00×10^{-13}	8.00×10^{-11}
prow	Crater Flat-Prow Pass	8.00×10^{-12}	Permeability	1.00×10^{-13}	5.00×10^{-11}
uvoc	Upper Volcanic Confining Unit	5.00×10^{-14}	Permeability	4.00×10^{-14}	1.00×10^{-12}
uvoa	Upper Volcanic Aquifer	8.00×10^{-14}	Permeability	8.00×10^{-14}	1.00×10^{-11}
lava	Lava Flow Aquifer	1.00×10^{-12}	Permeability	1.00×10^{-16}	2.00×10^{-12}
lime	Limestone Aquifer	1.00×10^{-12}	Permeability	1.00×10^{-15}	1.00×10^{-11}
vala	Valley Fill Aquifer	5.00×10^{-12}	Permeability	1.00×10^{-13}	8.00×10^{-12}
ewba	East-West Barrier	1.05×10^{-18}	Permeability	1.00×10^{-18}	1.00×10^{-15}
nsba	Solitario Canyon Fault	1.00×10^{-18}	Permeability	1.00×10^{-18}	1.00×10^{-15}
fpb1	Fortymile Wash Fault	10	multiplier	2	100
fpb2	Spotted Range-Mine Mountain Zone	11.7789	Multiplier	1	70
fpb3	Northern Low Perm Zone	7.11×10^{-2}	Multiplier	1.00×10^{-5}	0.5
fpb4	Imbricate Fault Zone	1	Multiplier	1	100
cffz	Crater Flat Fault	5.00×10^{-14}	Permeability	1.00×10^{-15}	5.00×10^{-13}
allu	Alluvial Uncertainty Zone	3.20×10^{-12}	Permeability	1.00×10^{-13}	1.00×10^{-11}
wash	Lower Fortymile Wash Zone	5.00×10^{-12}	Permeability	1.00×10^{-14}	8.00×10^{-12}

DTN:

Note that both water-table surfaces are contoured and that the data distribution for both surfaces is not uniform. Evident in the comparison is the low-gradient region in the Fortymile Wash region, the high-gradient region north of Yucca Mountain, and the flow disruption caused by the Solitario Canyon fault. This indicates that the model at least qualitatively represents the current water table in the vicinity of Yucca Mountain. It should also be noted that transient pumping data does exist from tests performed in the C-Wells complex. The 500-m grid is not of sufficient resolution to adequately model these data. A refined grid is being developed currently and will be used to model the C-Well tests.



DTN: TBD

Figure 6. Contour Plot of Water Level Data (left panel) and Simulated Water Level Data with Residual Heads (right panel)

6.7.3 Description of Transport Pathways Calculated from the Calibrated Model

One-hundred transport pathways are shown in Figure 7. The particles were distributed uniformly over the area of the proposed repository. The pathways generally leave the repository in a south-southeasterly direction to the 20-km compliance boundary (the boundary is not shown on Figure 7). The 20-km compliance boundary is an important distance for PA calculations. From the 20-km boundary to the end of the model (which is approximately the 30-km compliance boundary), the flow paths trend to the south-southwest and generally follows the Fortymile Wash. This outcome is reasonably consistent with flow paths generated from hydrochemical data, which will be discussed in more detail in Section 6.7.5. The small computer routine used to convert FEHM output to a SURFER readable form is given in the text description accompanying the data associated with this AMR (DTN: LA9911GZ12213S.001).

6.7.4 Comparison of Observed and Calibrated Head Measurements

Data from 115 wells in the model area were used in calibrating this flow model. Table 7 shows the names and locations of these wells, along with the altitude of the measurement location within each well and the measured value of head used in this model. As previously discussed in sections 6.1.2 and 6.1.3, these measurements were assumed to represent steady-state values. They also represent, where appropriate, averages of measurement intervals, whether "open" or "packed off." The head values and weighting used in the calibration process for the base case are also given in the table.

6.7.5 Hydrochemical Data

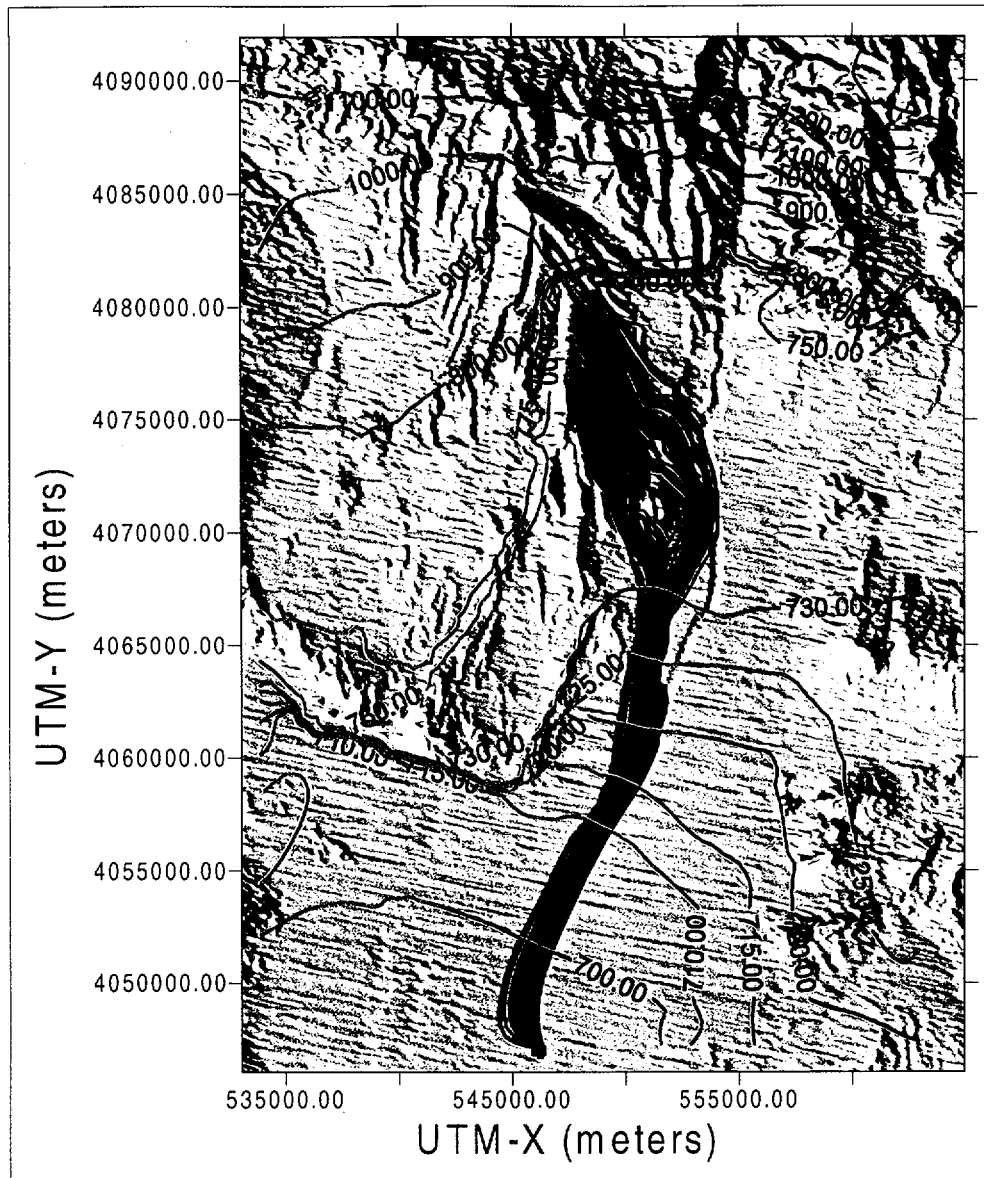
Hydrochemical data from the SZ in the Yucca Mountain area were compiled, documented, and analyzed in an associated AMR entitled "Geochemical and Isotopic Constraints on Groundwater Flow Directions, Mixing, and Recharge at Yucca Mountain" (CRWMS M&O 2000c). A summary of those interpretations is presented in this section along with figures that illustrate the main flow directions inferred from maps of chemical and isotopic concentrations.

6.7.5.1 Regional Flow Paths

Areal distributions of chemical and isotopic data were used to constrain flow paths in the region. The analysis traces flow paths by connecting upgradient areas with distinct chemical compositions to downgradient areas with similar chemical compositions. The map of the potentiometric surface was used to guide, but not determine, the selection of which downgradient areas could potentially be linked by a flow path to an upgradient area. Because the flow-path analysis presented assumes that groundwater can be traced in two dimensions, it does not consider the possible effects of local recharge and vertical mixing between aquifers.

Flow paths can be traced using chemistry and isotopes only where compositional differences exist that allow some directions to be eliminated as possible flow directions. Because no single chemical or isotopic species varies sufficiently to determine flow paths everywhere in the study area, multiple chemical and isotopic species were used to construct the flow paths. The flow-path analysis assumed that the $\delta^2\text{H}$, $\delta^{18}\text{O}$, Cl^- , SO_4^{2-} , Na^+ , and Ca^{2+} composition of groundwater

along a flow path did not change because of water/rock interaction, recharge of water with a



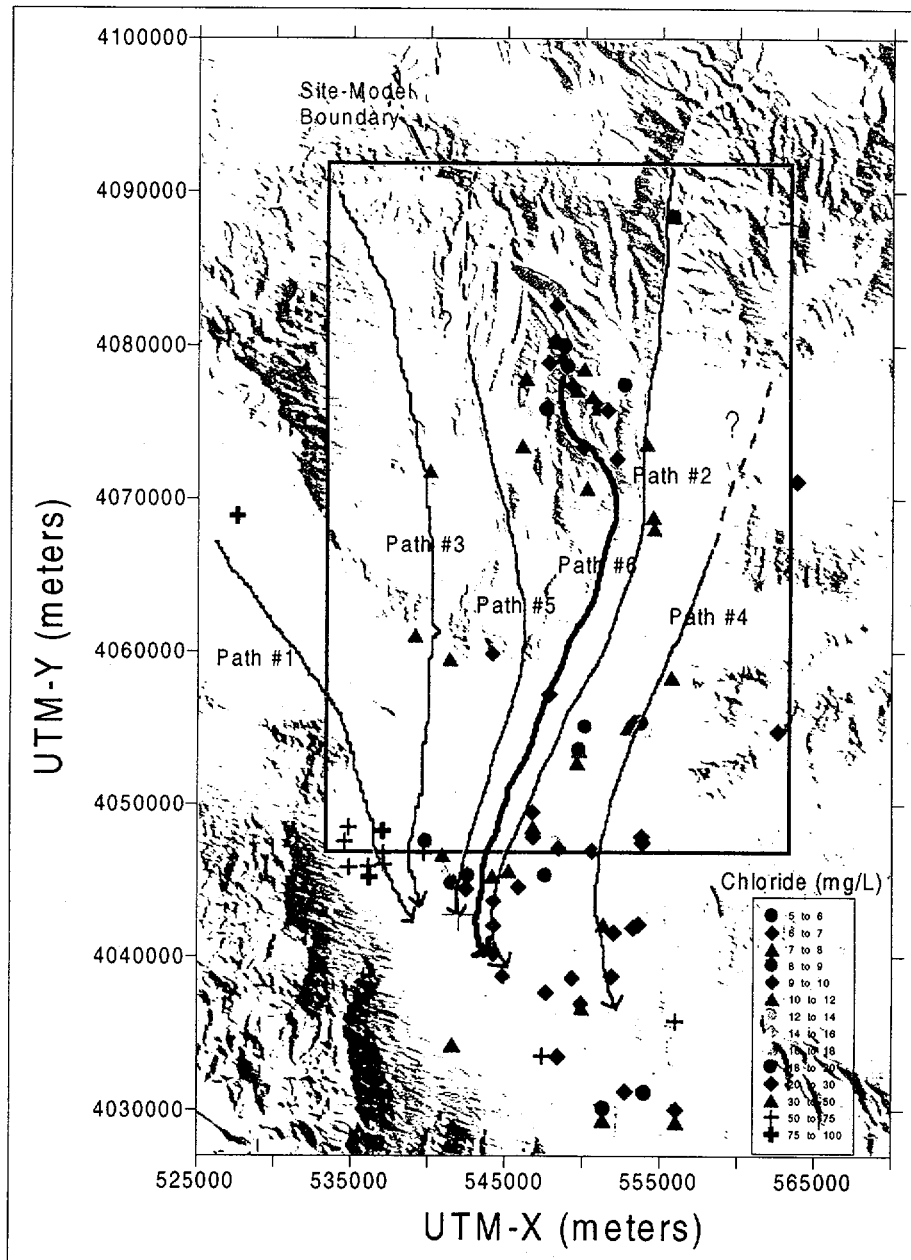
DTN: TBD

Figure 7. Flow Paths from the Proposed Repository with Simulated Hydraulic Head Contours

different composition, or vertical mixing between aquifers. The estimated flow paths are shown in Figure 8, superimposed on a plot of groundwater Cl^- concentrations in the Yucca Mountain area. Comparing the estimated flow paths in Figure 8 with the simulated SZ model flow paths in Figure 7 shows that the two results are consistent.

Flow Path #1 shows groundwater moving roughly parallel to the Amargosa River from an area west of Bare Mountain toward the southwest corner of the Site-Model Area (Figure 8). Flow Path #2 indicates that groundwater in the Fortymile Canyon area flows south/southwest along the axis of Fortymile Wash. Groundwater following Flow Path #3 flows from areas in the northwest corner of the Site Model, through central Crater Flat, and then southward to the

southern boundary of the Site Model. Groundwater in central Jackass Flats flows southwestward along Flow Path #4, roughly parallel to Fortymile Wash in the vicinity of Amargosa Valley, before turning south-southeast near the southern boundary of the Site-Model Area. Flow Path #5 shows groundwater moving predominantly south-southeast in eastern Crater Flat and then south-southwest after reaching the southern edge of Yucca Mountain. The flow path from beneath the potential repository to the Amargosa Desert (Flow Path #6) is constrained by Flow Path #5 to the west and by Flow Path #2 to the east. The development of Flow Path #6 is described in more detail in section 6.7.5.7.



DTN: TBD

Figure 8. Groundwater Flow Paths Near Yucca Mountain Estimated by Geochemical Data

The regional flow paths constructed on the basis of the hydrochemical and isotopic data are generally consistent with flow paths that could be inferred from the potentiometric surface but with a stronger north-south component" (CRWMS M&O 2000c, Figure 4). The stronger north-south component could be reflecting the general north-south structural fabric of the rock, the inability of the method to account for chemical mixing due to recharge or upwelling from the carbonate aquifer, or simply the sparseness of the data in certain regions of the model area.

6.7.5.2 Evaluation of Evidence for Local Recharge

Hydrochemical and isotopic data from perched water at Yucca Mountain were compared to similar data from the regional groundwater system at Yucca Mountain to verify whether local recharge is present in the groundwater. The data examined included uranium isotopes ($^{234}\text{U}/^{238}\text{U}$) and major anions and cations. Based on this comparison, local recharge, as represented by the perched water, was inferred to be a major component in the groundwater beneath Yucca Mountain. Realistic quantification of the percentage of local recharge in groundwater beneath Yucca Mountain is not possible with the currently available hydrochemical database. The conservative position on this issue would be to assume shallow groundwater is composed entirely of local recharge.

6.7.5.3 Evaluation of Evidence for Timing of Recharge

The timing of recharge at Yucca Mountain as determined by the uncorrected ^{14}C ages of the perched water is predominantly between 11,000 and 7,000 yr before present. However, the possibility exists that even younger recharge may be present in the groundwater beneath Yucca Mountain because of the presence of some perched water with a younger ^{14}C age and the absence of shallow groundwater samples from fault zones and other likely paths for rapid recharge.

Corrections to the ^{14}C ages of groundwater in the vicinity of Yucca Mountain were made using the geochemical code NETPATH, which considers the plausible chemical reactions that may have produced the observed chemistry of the groundwater samples. The corrected ^{14}C ages of the groundwater were approximately one ^{14}C half-life (5,730 yr) younger than the uncorrected ^{14}C ages. The uncorrected groundwater ^{14}C ages are about 22,000 to 18,000 yr in Crater Flat, 14,000 to 12,000 yr in northern Yucca Mountain, 18,000 to 15,000 yr in southern Yucca Mountain, and 13,000 to 9,000 yr beneath Fortymile Wash. Because of the assumption that all the carbon contributed by carbonate dissolution had a ^{14}C activity of 0 percent modern carbon (pmc) and because the model did not consider the increase in Ca^{2+} and Mg^{2+} in soil water due to evaporation in the soil zone, the corrected ^{14}C ages are considered lower limits for the true average age. The true ^{14}C ages probably are bounded by the corrected and uncorrected ^{14}C ages.

The ^{14}C activity of recently recharged groundwater in Fortymile Canyon was used to support an estimate for the initial ^{14}C activity of recharge ($^{14}\text{A}_0$) of approximately 65 pmc for this setting. Estimated groundwater ^{14}C ages calculated with a $^{14}\text{A}_0$ value of 65 pmc are approximately 3700 yr younger than the uncorrected ages and are considered to be the best estimate of groundwater ^{14}C ages in the Yucca Mountain area.

6.7.5.4 Evaluation of Evidence for Mixing Relations between Different Waters at Yucca Mountain

An evaluation of potential mixing relations among waters in the Yucca Mountain region is important because such mixing could lead to dilution of constituents that might be released to groundwater beneath the potential repository. Unfortunately, proving the occurrence of mixing between two or more groundwaters is a difficult problem. In fact, the available hydrochemical database is inadequate to prove the existence of mixing processes between groundwaters in the Yucca Mountain region beyond a reasonable doubt. Groundwater in the alluvial aquifer near the Skeleton Hills has chemical and isotopic characteristics that indicate it may have originated by upward leakage from the carbonate aquifer near the Gravity Fault, as originally proposed by Winograd and Thordarson (1975, p. C112). To the contrary, the available hydrochemical database can be used to argue that there is minimal mixing between groundwater in the carbonate and volcanic aquifers beneath Yucca Mountain itself.

6.7.5.5 Evaluation of Evidence for the Magnitude of Recharge

Estimates of the magnitude of recharge at Yucca Mountain were obtained using the chloride mass balance method. Based on the chloride concentrations of pore waters from the unsaturated zone, recharge ranges range from less than 0.5 mm/yr beneath washes with thick alluvial cover to a maximum of 20 mm/yr beneath ridge tops and side slopes. For groundwaters within the immediate vicinity of Yucca Mountain, chloride concentrations range from 5 to 9 mg/L, indicating local recharge rates between 7 and 14 mm/yr.

6.7.5.6 Evaluation of Evidence for Downgradient Dilution

If groundwater from Yucca Mountain flows toward Fortymile Wash, as suggested by the flow lines drawn on the basis of potentiometric and hydrochemical data, the potential exists for constituents in Yucca Mountain groundwater to be diluted by groundwaters below Fortymile Wash. Uranium concentration and isotope data were used to evaluate this potential dilution process. It was assumed that the uranium concentrations and activity ratios are conservative parameters in the flow systems involved.

The potential for mixing was evaluated using a two-component mixing equation involving the uranium concentration and $^{234}\text{U}/^{238}\text{U}$ activity ratio. Uranium concentration and isotopic data are available only for five wells in the area of interest, and these data do not allow a unique solution to this mixing equation. In effect, the range in uranium concentrations measured for multiple samples of the mixing end-member groundwaters is similar to the total range of uranium concentrations observed for the full set of groundwater analyses. If it is assumed that the uranium concentrations in the end-member groundwaters are the same in the mixing process, then the mixing proportions are only a function of the differences in the uranium activity ratios. Under this assumption, the estimated proportions of the Fortymile Wash component in the mixture range from 0.5 to 0.9, depending on which downgradient groundwater (from borehole J-12 or JF#3) is used to represent the mixed water.

The areal plot of chloride concentrations in groundwaters within the model boundary suggests that low chloride concentrations typical of groundwaters beneath Yucca Mountain and Fortymile

Wash extend to wells at the southern boundary of the model area. This observation, in turn, suggests there would be minimal dilution of constituents that may be present in upgradient groundwaters by mixing with groundwaters within alluvium of the Amargosa Valley.

An alternative interpretation is that the low chloride concentrations found in some Amargosa Valley wells reflect local recharge. In this case, dilution of constituents in upgradient waters by mixing with groundwaters in Amargosa Valley alluvium is a viable process. However, the viability of this interpretation is brought into question by data that suggest the groundwaters in Amargosa Valley alluvium are as old or older than groundwaters at Yucca Mountain. If these groundwaters had a large component of local recharge, they would be expected to have relatively young ages. On the other hand, the available age data would be consistent with the idea that these waters are largely composed of flow from upgradient sources north of Amargosa Desert (i.e., from Fortymile Wash) or with paleorecharge along Fortymile Wash in the Amargosa Desert itself.

6.7.5.7 Likely Flow Paths from the Potential Repository Area

General flow paths in the Yucca Mountain area were constructed by identifying areas that had similar concentrations of conservative chemical species, such as chloride or sulfate, and tracing a path through these chemically similar areas in a downgradient direction (see section 6.7.5.1). Of particular interest for this report are the paths leading from the potential repository area, such as the one constructed primarily on the basis of groundwater chloride concentrations (Figure 8). This pathway starts with groundwater from the repository area just east of Yucca Mountain Crest that has chloride concentrations of about 6 mg/L. The pathway follows wells along Dune Wash with similarly low chloride concentrations before turning south-southwest near Fortymile Wash. Well WT#12, located immediately south of Dune Wash, has a chloride concentration of 7.8 mg/L, indicating that the dilute water beneath Dune Wash probably flows southeast along the Dune Wash Fault towards Fortymile Wash before turning south-southwest, rather than flowing directly south under Dune Wash. From the intersection of Dune Wash and Fortymile Wash, the only downgradient borehole with a chloride concentration of approximately 6 mg/L is borehole NC-EWDP-2D. Groundwater at this borehole has a $\delta^{18}\text{O}$ value of -14.1 per mil, a value that indicates this water was probably not derived from the Fortymile Wash where $\delta^{18}\text{O}$ values are generally -13.2 to -12.8 per mil. Borehole NC-EWDP-2D provides the basis for extending the pathway south-southwest from the Dune Wash/Fortymile Wash area along the western margin of Fortymile Wash. South of borehole NC-EWDP-2D, the pathway is constrained by the presence of two areas of groundwater with much higher chloride concentrations: (1) a western zone, composed of groundwater flowing south from Crater Flat and, possibly, southeast from Oasis Valley; and (2) an eastern zone, composed of groundwater flowing southwest from Jackass Flats and from leakage upward from the carbonate aquifer near the Gravity Fault (Winograd and Thordarson 1975, p. C112). Groundwater in wells south of NC-EWDP-2D with chloride concentrations of approximately 6 mg/L have isotopic ($\delta^2\text{H}$ and $\delta^{18}\text{O}$) characteristics that indicate the water is associated with Fortymile Wash rather than Yucca Mountain. The hypothesized flow path was extended south from NC-EWDP-2D by keeping the path to the west of the axis of Fortymile Wash and east of the more highly concentrated water from Crater Flat and Oasis Valley. As mentioned earlier, this path is consistent with simulated fluid pathways starting from the repository area in the SZ flow model.

6.7.6 Comparing Hydrochemical Data Trends with Calculated Particle Pathways

Groundwater chemical and isotopic data were used to estimate groundwater flow paths near Yucca Mountain (Figure 8). The basis for constructing these flow paths and the assumptions associated with flow path construction were described in detail in an associated AMR (CRWMS M&O 2000c). The numerical flow model for Yucca Mountain was evaluated for consistency with the flow paths estimated from the hydrochemical data by placing particles along the western, northern, and eastern boundaries of the model and tracing their downgradient movement. Particles were placed at 5000-m intervals along the boundaries at elevations of 600 m, 0 m, -600 m and -1200 m, relative to sea level. Plots of particle movement for each of these starting elevations are shown along with the contour map of the simulated hydraulic heads at the top of the model in Figures 9 through 12.

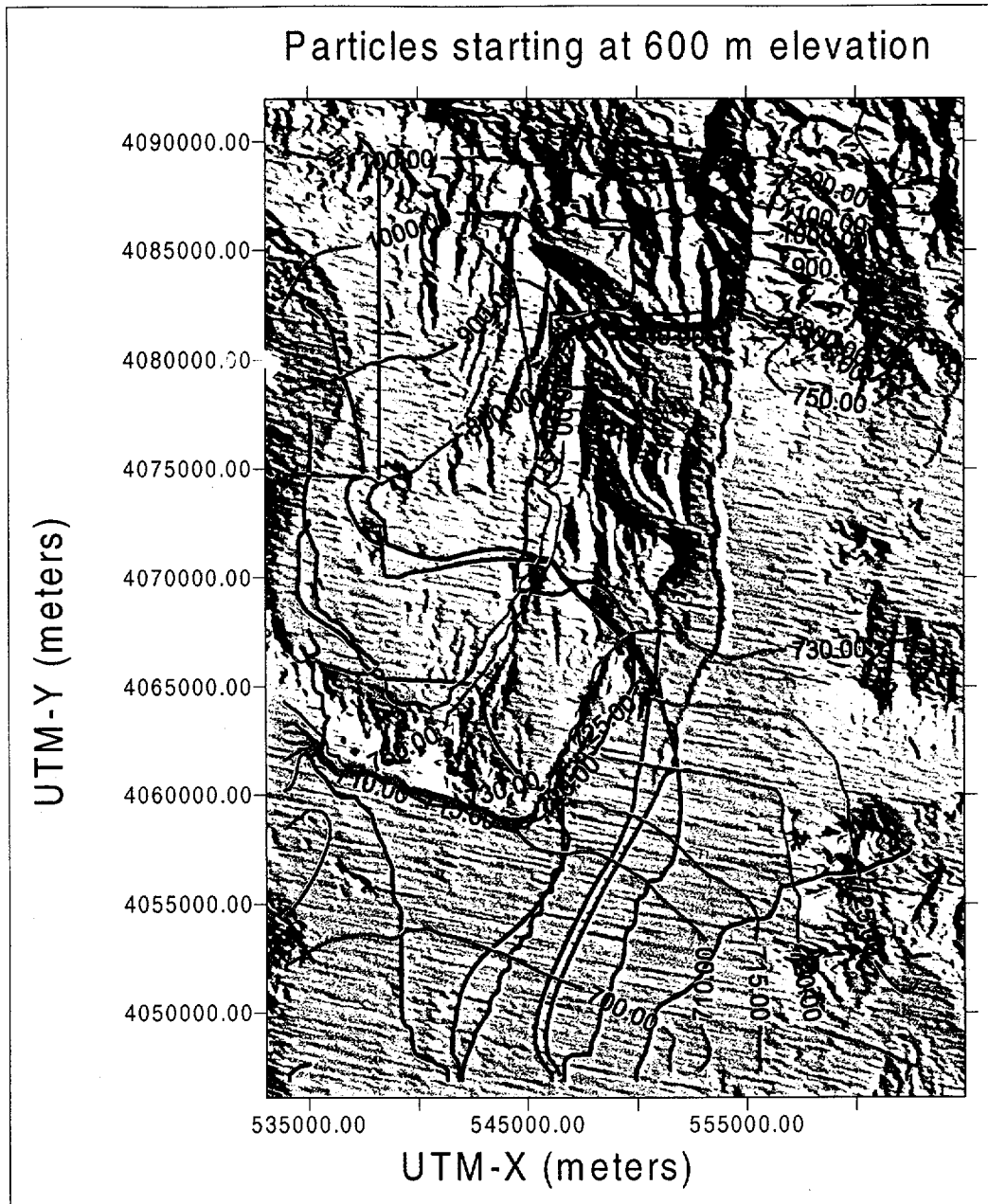
As indicated by these figures, many of the particles simply exit the flow system at the nearest boundary. Particles sometimes exited the boundary even at zones that had a net inflow because these zones also invariably included some cells that had outflow.

Some particle trajectories terminate within the flow system because these particles had not yet moved through the system within the one-million years over which the particle paths were traced. The failure of these particles to exit the flow system after one-million years suggests that very stagnant conditions exist locally within the modeled flow system.

In both map view and in three dimensions (not shown), the particles exhibit complex trajectories. An analysis of the particle paths in three dimensions indicated that the apparent crossing of flow paths in map view is a result of the different depths of the particle paths.

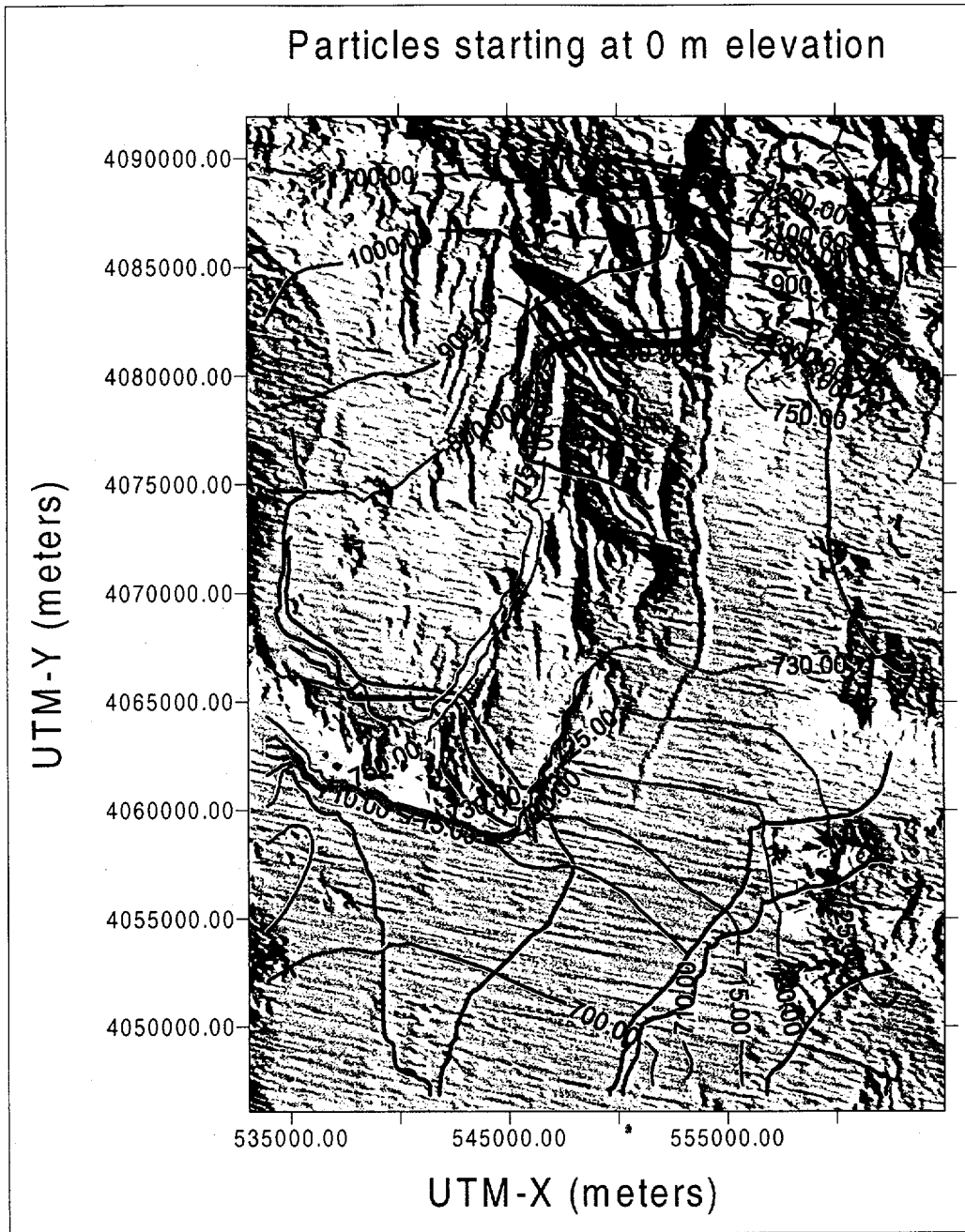
Most of the particles that originate along the boundaries in the northeastern part of the model domain exit through the eastern boundary. Only the particles that begin along the southern one-third of the eastern boundary near the Skeleton Hills exit the southern boundary. The flow model (Figures 9 through 11) indicates that the groundwater near the town of Amargosa Valley originates predominantly from flow entering from the east, rather than flow from the northeast as shown by Path #4 on Figure 8, although the particle originating east of Fortymile Canyon at a -1200-m elevation also passes beneath Amargosa Valley (Figure 12).

Particles along the northern boundary that do not immediately exit the flow system bifurcate around the east-west barrier in northern Yucca Mountain, which was used to simulate the large hydraulic gradient in that area. Particles originating immediately to the west of Fortymile Canyon flow around the western edge of the barrier and then eastward across Solitario Canyon and beneath Yucca Mountain before turning southwest in the Fortymile Wash area. Particles originating immediately to the east of Fortymile Canyon flow around the eastern edge of the barrier and, depending on the original elevation of the particle, either exit along the eastern boundary (Figure 10), terminate in southwestern Jackass Flats (Figure 11), or flow toward the southern boundary beneath Amargosa Valley (Figure 12). The particles originating toward the western end of the northern boundary flow beneath Crater Flat and southern Yucca Mountain along a somewhat more eastward trajectory than is indicated by Path #3 and Path #5 in Figure 8.



DTN: TBD

Figure 9. Plot of Particle Movement at 600-Meters Elevation



DTN: TBD

Figure 10. Plot of Particle Movement at Zero-Meters Elevation

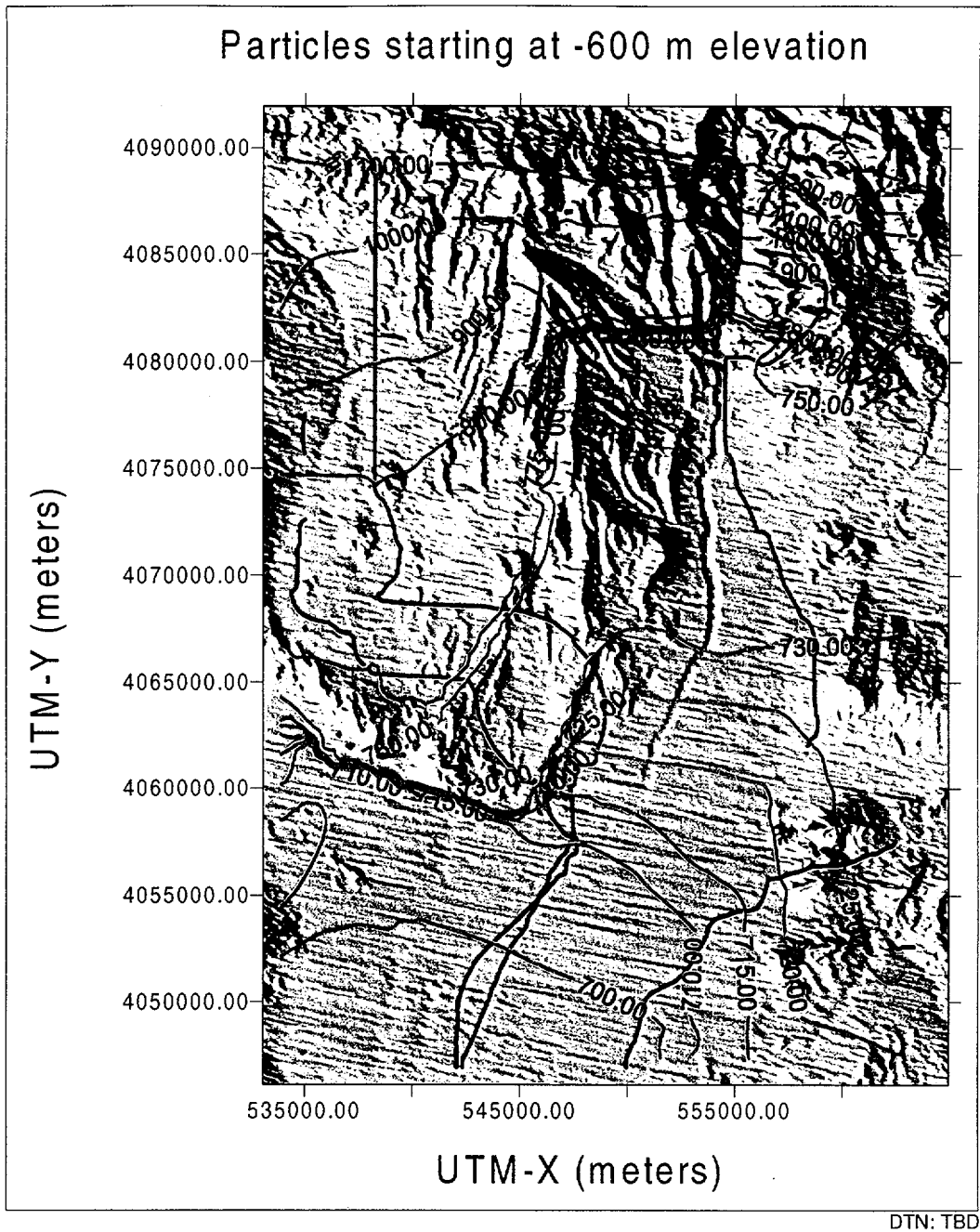
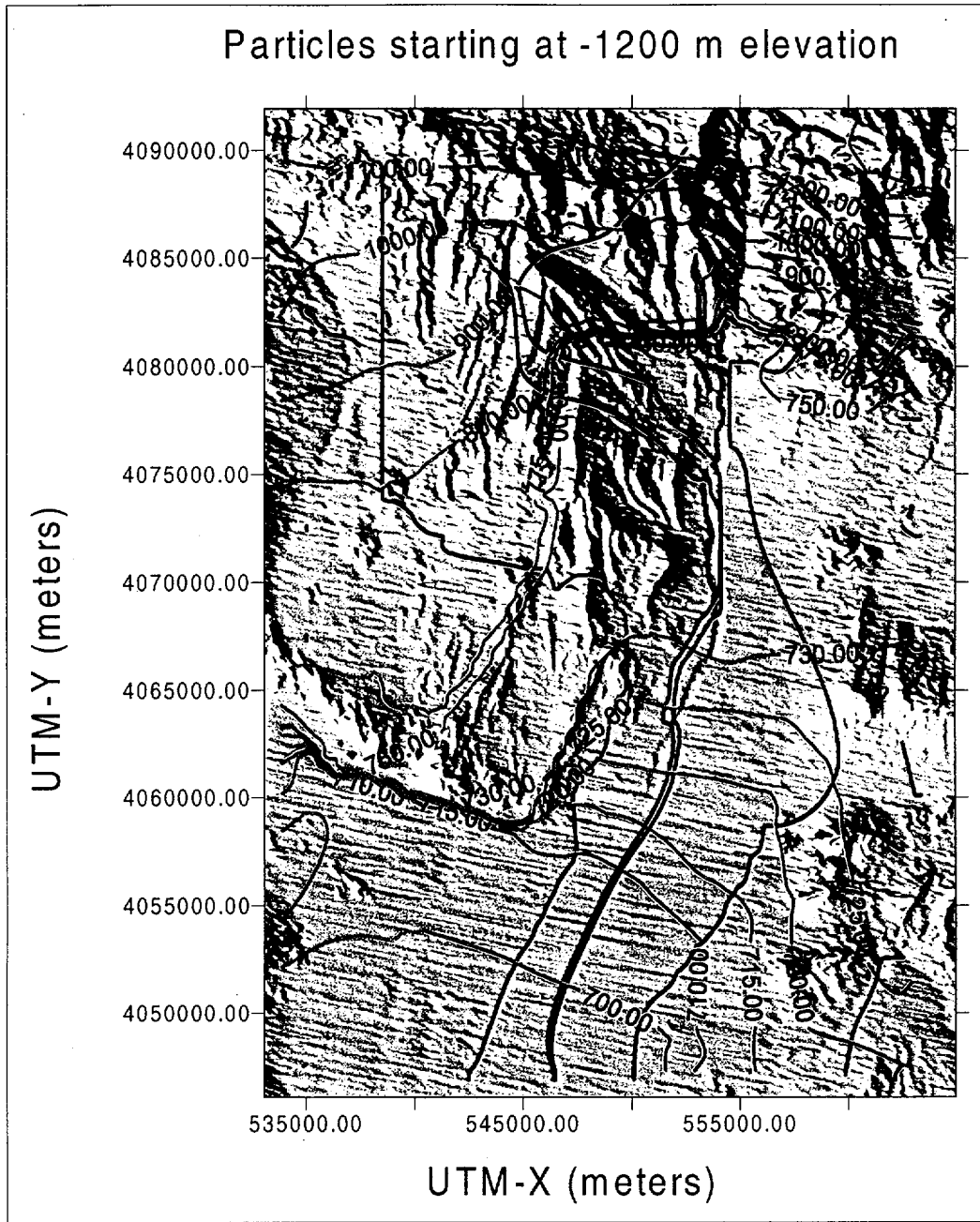


Figure 11. Plot of Particle Movement at -600-Meters Elevation



DTN: TBD

Figure 12. Plot of Particle Movement at -1200-Meters Elevation

Some of the particles originating along the western boundary of the model between UTM north coordinates 4,067,500 and 4,077,500 m flow east/southeast beneath southernmost Yucca Mountain before turning southwest. The trajectory of these particles is more strongly eastward than direction of flow indicated by Paths #3 and #5 in Figure 8. The movement of the particles originating at 600- and 0-m elevation along the western boundary at UTM north coordinate 4,062,500 m (Figures 9 and 10) agree with the direction of groundwater movement indicated by Path #1 in Figure 8.

The trajectories of particles originating at the potential repository shown in Figure 7 can be compared to Path #6 in Figure 8. Path #6 follows Dune Wash before turning southwestward near the intersection of Dune Wash and Fortymile Wash, whereas the particle trajectories shown in Figure 7 flow south across Dune Wash before turning southwestward. Nonetheless, the general direction of groundwater movement from the potential repository area predicted by the numerical model is in agreement with the flow direction estimated from the hydrochemical and isotopic data.

In summary, some differences exist between the flow directions estimated by the numerical model and flow directions estimated from an analysis of the hydrochemical and isotopic data. The most prominent difference is the much stronger eastward component of flow in Crater Flat in the numerical flow model compared to the flow directions determined in the hydrochemical analysis. The differences in the flow directions estimated for Crater Flat could be due to (1) the inability of the simple hydrochemical analysis to account for vertical mixing due to recharge or mixing between aquifers, (2) the assumption in the numerical model that the rock in Crater Flat is isotropic with respect to permeability, or (3) a combination of these factors. However, the most important flow paths determined by the numerical model, that is, the flow paths from the potential repository area, are very similar to those estimated from the hydrochemical data.

6.7.7 Permeability Data from the Yucca Mountain Area

Calibration of the numerical model was done by adjusting permeability values for individual hydrogeologic units in the model until the sum of the weighted-residuals squared (the objective function) was minimized. The residuals include the differences between the measured and simulated hydraulic heads and the differences between the groundwater fluxes simulated with the regional- and the site-scale models. Permeabilities estimated from hydraulic tests were not formally included in the calibration as prior information and were not considered in the calculation of the objective function. The field-derived permeabilities were instead used to guide the selection of bounds on the permissible range of permeabilities to be considered during the calibration and to check on the reasonableness of the final permeability estimates produced by the calibration.

Permeability data from single-hole and cross-hole tests were collected in the Yucca Mountain area from the early 1980s to the present day (1999). The test results published up to 1997 were recently compiled by Sandia National Laboratories (DTN: SNT05082597001.001). A statistical analysis of this data set is presented in this section.

6.7.7.1 Single-Hole Tests

The statistical analysis that follows required that the test results be grouped. This grouping was done by first compiling the permeability estimates for individual hydrogeologic units, where possible, and by considering progressively more general groupings for those cases in which the test interval spanned several hydrogeologic units. For instance, in cases in which the test interval was in the Prow Pass Tuff, with or without some portion of the adjacent bedded tuffs, the test results were grouped with other permeability estimates for the Prow Pass Tuff. If other units within the Middle Volcanic Aquifer (MVA), as defined by Luckey et al. (1996, Figure 7), were also present in the test interval along with the Prow Pass Tuff, the test results were considered to represent the MVA. If hydrogeologic units other than those in the MVA were present in the test interval along with the Prow Pass Tuff, the permeability estimate for the test was grouped with the most general category, which is the mixed tuffs. The mixed-tuff category includes data for all tests that would not fit into a more restrictive category. All tuffs older than the Lithic Ridge Tuff are listed as Pre-Lithic Ridge Tuffs ("Older Tuffs"). The other categories were named for the hydrogeologic unit to which they pertain and are believed to be self-explanatory.

There were several instances in which several kinds of hydraulic tests (injection, drawdown, or recovery) were conducted in the same depth interval in the same borehole. The results of these tests could have been treated in several different ways. For example, (1) the data for a particular depth interval could have been averaged and only the single average value considered in the statistical summary, in which case the statistical uncertainty could be interpreted as reflecting only the effects of spatial variability, or (2) all of the permeabilities that resulted from testing of the interval could have been used to calculate the summary statistics, which was done in this report. By considering multiple measurements from the same test interval, this statistical analysis attempts to reflect the effects of measurement uncertainty as well as the effects of spatial variability.

The base-10 logarithms of the permeabilities were calculated and the statistical analysis performed on the log-transformed values for each category using MINITAB (MINITAB 1998). The antilogarithms of the statistical parameters for each category were calculated and are listed in Table 9. The analysis indicates that the deepest tuffs, which are the Pre-Lithic Ridge Tuffs (Pre-Tlr), and the mixed tuff group have the lowest permeabilities, and the Topopah Spring Tuff and Prow Pass Tuff have the largest permeabilities. Where they could be calculated, the 95 percent confidence limits indicate that the mean permeability values are constrained within relatively narrow limits, except for the Pre-Lithic Ridge Tuffs.

The results also indicate that the Calico Hills Formation (Tac), which is a zeolitized tuff that functions as the Upper Volcanic Confining Unit (Luckey et al. 1996, Figure 7), has a higher permeability than the Bullfrog Tuff (Tcb) and the Carbonate Aquifer. This paradoxical result may reflect the fact that, because it is unsaturated in the western half of Yucca Mountain, the Calico Hills Formation could be hydraulically tested only in the highly faulted eastern half of Yucca Mountain, whereas the other units were also tested in less intensely faulted areas to the west.

Table 9. Statistical Summary of Permeabilities Calculated from Single-Hole and Cross-Hole Tests at Yucca Mountain

Single-Hole Tests

Unit	Topopah Spring Tuff	Calico Hills Formation	Prow Pass Tuff	Bullfrog Tuff	Tram Tuff	Lava Flows	Lithic Ridge Tuff	Pre-Lithic Ridge Tuff (Older tuff)	Middle Volcanic Aquifer	Mixed Tuffs	Carbonate Aquifer
Number of Tests	1	9	14	19	34	0	15	5	10	30	24
Mean	7.84×10^{-13}	9.38×10^{-14}	2.85×10^{-13}	3.07×10^{-14}	1.00×10^{-14}	—	1.09×10^{-14}	4.52×10^{-16}	5.59×10^{-14}	1.34×10^{-15}	7.17×10^{-14}
Lower 95% Confidence Interval for Mean	—	4.45×10^{-14}	8.13×10^{-14}	9.98×10^{-15}	4.03×10^{-15}	—	2.57×10^{-15}	1.87×10^{-18}	6.19×10^{-15}	4.56×10^{-16}	4.69×10^{-14}
Upper 95% Confidence Interval for Mean	—	1.97×10^{-13}	9.95×10^{-13}	9.45×10^{-14}	2.49×10^{-14}	—	4.60×10^{-14}	1.09×10^{-13}	5.05×10^{-13}	3.95×10^{-15}	1.10×10^{-13}
Minimum	—	2.72×10^{-14}	7.77×10^{-15}	2.28×10^{-16}	2.35×10^{-16}	—	8.35×10^{-17}	1.84×10^{-18}	1.85×10^{-16}	1.72×10^{-18}	1.69×10^{-14}
Maximum	—	4.19×10^{-13}	1.40×10^{-11}	1.67×10^{-12}	1.18×10^{-12}	—	1.22×10^{-12}	4.49×10^{-14}	1.40×10^{-12}	3.53×10^{-13}	1.40×10^{-12}

Cross-Hole Tests

	Calico Hills Formation	Prow Pass Tuff	Bullfrog Tuff	Tram Tuff	Middle Volcanic Aquifer
Number of Tests	6	8	13	1	6
Mean	1.68×10^{-13}	2.77×10^{-12}	1.37×10^{-11}	5.39×10^{-11}	1.78×10^{-11}
Lower 95% Confidence Interval for Mean	1.25×10^{-13}	1.78×10^{-12}	5.61×10^{-12}	—	8.33×10^{-12}
Upper 95% Confidence Interval for Mean	2.26×10^{-13}	4.31×10^{-12}	3.36×10^{-11}	—	3.81×10^{-11}
Minimum	1.08×10^{-13}	1.44×10^{-12}	1.08×10^{-12}	—	7.19×10^{-12}
Maximum	2.52×10^{-13}	7.19×10^{-12}	7.55×10^{-11}	—	5.75×10^{-11}

DTN: SNT05082597001.001.

NOTES: Permeabilities are in meters-squared. The Topopah Spring Tuff corresponds to the Upper Volcanic Aquifer (unit 16); the Calico Hills Formation corresponds to the Upper Volcanic Confining Unit (unit 15); and portions of the Lithic Ridge and Pre-Lithic Ridge Tuffs correspond to the Lower Volcanic Confining Unit (unit 11), the Older Volcanic Aquifer (unit 10), and the Older Volcanic Confining Unit (unit 9). The Middle Volcanic Aquifer includes the Prow Pass, Bullfrog, and Tram Tuffs and associated bedded units (Luckey et al., 1996, Fig. 7). Other units correspond to hydrogeologic units of the same name.

6.7.7.2 Cross-Hole Tests

Permeability data from cross-hole tests were compiled, grouped, and analyzed in a manner similar to the permeability data for the single-hole tests (see Table 9). The cross-hole data originate from tests conducted at the C-Wells complex. Whereas the permeabilities of the Calico Hills formation are similar for both the single- and cross-hole tests, the permeabilities of the Prow Pass Tuff (T_{cp}), Bullfrog Tuff, Tram Member of the Crater Flat Tuff (T_{ct}), and the Middle Volcanic Aquifer calculated from the cross-hole tests are one to several orders of magnitude greater than the mean permeabilities calculated from the single-hole tests. The differences in the mean permeability values between the single- and cross-hole tests generally have been attributed to the larger volume of rock affected by the cross-hole tests (Geldon et al. 1997), which allows a larger number of possible flow paths, including relatively rare, high-transmissivity flow paths, to be sampled during the test. However, some of the increase in permeability attributed to the effects of scale may also be due to the presence of a breccia zone associated with the Midway Valley Fault in the Bullfrog Tuff and Tram Member at boreholes UE-25 c#2 and UE-25 c#3 (Geldon et al. 1997, Figure 3). Thus, some of the difference in the mean permeabilities calculated for the single-hole and cross-hole tests may be due to local conditions in the vicinity of the C-Wells as well as to scale.

6.7.7.3 Permeability Data from the Nevada Test Site

Data from reports pertaining to the Nevada Test Site (NTS) were examined to help constrain permeability estimates for hydrogeologic units that were either not tested or that underwent minimal testing at Yucca Mountain. These permeability data, as well as more qualitative observations concerning the permeability of some of the hydrogeologic units in the site-model area, are summarized in the following sections. Additionally, these reports, including Blankennagel and Weir (1973), Winograd and Thordarson (1975), and Laczniaik et al. (1996), describe the hydrogeologic controls on groundwater movement at the NTS, thereby providing a regional perspective for groundwater flow at Yucca Mountain.

6.7.7.4 Lower Carbonate Aquifer (unit 4)

The results of hydraulic tests in the Lower Carbonate Aquifer were reported for eight boreholes by Winograd and Thordarson (1975, Table 3). For two of the boreholes, only transmissivity estimates based on specific capacity were made. At boreholes for which permeability estimates based on drawdown curves were also available, the estimates based on specific capacity were much lower than the estimates based on the drawdown curves. At five boreholes where both drawdown and recovery tests were conducted, the permeabilities estimated from recovery tests were several times higher than those estimated from drawdown tests. Both the drawdown and recovery data exhibited complex responses to pumping that were attributed to test conditions as well as to aquifer properties. These responses were manifested on log-linear plots of time versus drawdown as straight-line segments with distinct breaks in slope. Because they were unable to explain the differences in the results from the drawdown and recovery tests, Winograd and Thordarson (1975, p. c25) advised against the use of the transmissivities estimated from the recovery tests. The transmissivities estimated from drawdown tests in the lower carbonate aquifer are listed for six boreholes in Table 10 along with thicknesses of the test intervals and the

Table 10. Permeabilities Calculated for the Lower Carbonate Aquifer

Well	Thickness (ft)	Transmissivity ^a (gpd/ft) ^b	Hydraulic Conductivity (gpd/ft ²)	Permeability (m ²)
67-73	281	20,000	71.2	3.44 x 10 ⁻¹²
67-68	996	39,000	39.2	1.89 x 10 ⁻¹²
66-75	753	11,000	14.6	7.05 x 10 ⁻¹³
88-66	872	1,300	1.49	7.19 x 10 ⁻¹⁴
75-73	750	3,800	5.07	2.45 x 10 ⁻¹³
84-68	205	2,400	11.7	5.65 x 10 ⁻¹³

Source: Winograd and Thordarson (1975, Table 3)

NOTES: ^aThese transmissivities were estimated by Winograd and Thordarson (1975, Table 3) from drawdown curves.

^bgpd is gallons per day.

Statistics for the logarithm of permeability (log *k*) are

Mean = -12.224

Standard deviation = 0.605

Median = -12.999

Lower 95% confidence level for mean = -12.858

Upper 95% confidence level for mean = -11.5887.

calculated permeabilities. The permeabilities in m² were calculated from the hydraulic conductivity values using a viscosity of 0.001 Pascal seconds, a density of 1000 kg/m³, and a gravitation acceleration of 9.81 m/s². These viscosity and density values are appropriate for test temperatures of about 25°C. The actual test temperatures were not reported by Winograd and Thordarson (1975) but may have been substantially higher (greater than 50°C) than the temperatures assumed in this calculation, in which case the calculated permeabilities may overestimate the true permeabilities measured by the tests by a factor of 2 to 3. A statistical analysis of the base-10 logarithms of the permeabilities listed in Table 10 resulted in an estimated mean permeability for the carbonate aquifer of 6.0 x 10⁻¹³ m². The 95% lower and upper confidence limits for the mean permeability were 1.39 x 10⁻¹³ and 2.58 x 10⁻¹² m², respectively.

In addition to providing quantitative estimates of the permeability, Winograd and Thordarson (1975) made several qualitative observations regarding the distribution of permeability within the carbonate aquifers, which follow.

- The permeability data for the carbonate aquifer showed no systematic decrease either with depth beneath the top of the aquifer or depth beneath land surface (p. c20). The inference that groundwater may circulate freely within the entire thickness of the lower carbonate aquifer is not negated by chemical data, which indicate no significant increase in the dissolved-solids content to depths of several thousand feet (p. c103).
- No major caverns were detected during drilling in the lower carbonate aquifer, despite the fact that approximately 16,000 feet of the lower carbonate aquifer was penetrated in 26 holes drilled in 10 widely separated areas, including over 5,000 feet at 13 holes beneath

the Tertiary/pre-Tertiary unconformity, where caverns might be expected to exist (p. c19). Drill-stem tests in three holes in Rock Valley and Yucca Flat indicated negligible to moderate permeability immediately below the unconformity (p. c20).

- Outcrop evidence indicates that klippen, which are the upper plates of low-angle thrust faults and gravity slump faults, have a higher intensity of fracturing and brecciation than rock below the fault planes and may have above-average porosity and permeability (pp. c19–c20). Specific capacity data for five wells penetrating the upper plates of low angle faults in southern Yucca Flat and the northwestern Amargosa Desert indicated relatively high transmissibilities for these plates (p. c28).
- The presence of hydraulic barriers within the Lower Carbonate Aquifer is indicated in the hydraulic response in two-thirds of the wells pumped, indicating that zones of above-average transmissibility may often not be connected to each other (p. c116). However, this observation needs to be reconciled with hydraulic and chemical evidence supporting the existence of a “mega channel” extending over 40 miles between southern Frenchman Flat and the discharge area at Ash Meadows (Winograd and Pearson 1976).

6.7.7.5 Valley-Fill Aquifer (unit 20)

The Valley Fill Aquifer, as defined by Winograd and Thordarson (1975, Table 1; p. c37) is composed of alluvial fan, fluvial, fanglomerate, lakebed, and mudflow deposits in depressions created by post-Pliocene block faulting. Thus defined, the Valley Fill Aquifer of Winograd and Thordarson (1975) probably includes the Valley-Fill Aquifer (unit 20), the Valley-Fill Confining Unit (unit 19), and the Undifferentiated Valley Fill (unit 8) defined for the present study (Table 5).

Transmissivity estimates for the Valley-Fill Aquifer were made at six boreholes in Emigrant Valley, Yucca Flat, and Frenchmen Flat (Winograd and Thordarson 1975, Table 3). For two of the boreholes, only transmissivity estimates based on specific capacity data were available. However, these estimates are considered unreliable because of the lack of agreement with transmissivity estimates based on drawdown or recovery curves at boreholes in which both types of estimates were made. The transmissivity estimates made from drawdown and recovery curves were consistent with each other at wells where both types of tests were conducted, in which case the transmissivity values from the drawdown and recovery curves were averaged to produce the transmissivity estimates listed in Table 11. Values used for the viscosity, density, and gravity terms in the expression for permeability are the same as those used for the Lower Carbonate Aquifer. Based on a statistical analysis of the logarithm of the permeabilities listed in Table 9, the mean permeability of the valley fill is $1.57 \times 10^{-12} \text{ m}^2$, and the 95 percent lower and upper confidence limits for the mean permeability are 1.61×10^{-13} and $1.54 \times 10^{-11} \text{ m}^2$, respectively. The relatively high mean permeability calculated for the valley fill is probably more reflective of the permeability of the Valley-Fill Aquifer (unit 20) and, possibly, the Undifferentiated Valley Fill (unit 8) of this study, than of the Valley-Fill Confining Unit (unit 19).

In addition to providing the quantitative estimates of the permeability of the valley fill summarized in this section, Winograd and Thordarson (1975) also made numerous observations regarding the permeability of the valley fill at particular locations in the area of the NTS. Of

special interest to this report are those observations made for the valley fill in the Amargosa Desert. Winograd and Thordarson (1975) noted (pp. c84–c85) that hydraulic head contours south of Lathrop Wells (now Amargosa Valley) probably reflect the effects of upward leakage from the lower carbonate aquifer into poorly permeable valley fill along the Gravity Fault and associated faults and of the drainage of this water to more permeable sediments farther west. Immediately west of the Gravity Fault, gravity data indicate that downward displacement of the pre-Tertiary rocks west of the fault is 500 to 1,500 ft at a location one mile east of Lathrop Wells and 1,200 to 2,200 ft at a point one mile southeast of the inferred intersection of the Specter Range Thrust Fault and the Gravity Fault. The low permeability of the valley fill immediately west of the Gravity Fault was indicated by drillers' logs, which showed that the valley fill in this area was mainly clay, and also by analogy with the lakebed sediments southwest of the spring line at Ash Meadows, where groundwater discharging from the Lower Carbonate Aquifer into the sediments across the Gravity Fault is forced to the land surface by the low permeability of the sediments. Winograd and Thordarson (1975, p. c85) argued that the discharge across the Gravity Fault near Lathrop Wells was probably small because only the lowermost part of the Lower Carbonate Aquifer is present in the area and the Lower Clastic Aquitard, which underlies the carbonate aquifer at shallow depths, would probably not transmit much water.

Table 11. Permeability Estimates for the Valley-Fill Aquifer

Well	Thickness (ft)	Transmissivity (gpd/ft)	Hydraulic Conductivity (gpd/ft ²)	Permeability (m ²)
74-70 ^b	511	2,200 ^a	4.31	2.08 x 10 ⁻¹³
74-70 ^a	217	9,350 ^b	43.1	2.08 x 10 ⁻¹²
83-68	264	12,700 ^b	48.1	2.32 x 10 ⁻¹²
91-74	264	33,500 ^c	126.9	6.12 x 10 ⁻¹²

Source: Winograd and Thordarson (1975, Table 3)

NOTES: Permeability estimates based on transmissivity data from Winograd and Thordarson (1975, Table 3).
gpd is gallons per day.

^aAverage is the arithmetic sum of the results of one drawdown and two recovery tests.

^bAverage is the arithmetic sum of the results of one drawdown and one recovery test.

^cRepresentative Value is the result of one recovery test.

Statistics for the logarithm of permeability (log *k*) are

Mean = -11.803

Standard deviation = 0.623

Median = -11.658

Lower 95% confidence level for mean = -12.794

Upper 95% confidence level for mean = -10.812.

6.7.7.6 Welded-Tuff Aquifer (unit 16)

The welded tuff aquifer corresponds to the Upper Volcanic Aquifer (unit 16) of Table 5. Results of hydraulic tests conducted in the welded tuff aquifer were reported by Winograd and Thordarson (1975, Table 3) for four wells, but only two wells, both in Jackass Flats, had transmissivity estimates based on drawdown curves. Well 74-57 tested the Topopah Spring Tuff and well 74-61 tested both the Topopah Spring Tuff and the Basalt of Kiwi Mesa. Permeabilities

calculated from the drawdown curves at these wells are listed in Table 12. The geometric mean permeability based on the estimated permeabilities in Table 12 is $5.3 \times 10^{-12} \text{ m}^2$.

Table 12. Permeability Estimates for the Welded Tuff Aquifer

Well	Thickness (ft)	Transmissivity (gpd/ft)	Hydraulic Conductivity (gpd/ft ²)	Permeability (m ²)
74-61	290	28,000	96.6	4.7×10^{-12}
74-57	547	68,000	124.3	6.0×10^{-12}

Source: Winograd and Thordarson (1975, Table 3)

NOTES: Permeability estimates based on transmissivities determined from drawdown curves (Winograd and Thordarson 1975, Table 3).
gpd is gallons per day.

Statistics: The geometric mean permeability is $5.3 \times 10^{-12} \text{ m}^2$.

6.7.7.7 Lava-Flow Aquifer (unit 17)

Rhyolitic lavas and welded and nonwelded tuffs fill the Silent Canyon caldera complex, which now lies buried beneath Pahute Mesa by younger tuffs, erupted from the Timber Mountain caldera complex to the south (Blankennagel and Weir 1973, p. 6; Laczniak et al. 1996, p. 36). The permeabilities of the lava flows beneath Pahute Mesa are assumed to be an appropriate analog for the Lava Flows (unit 17) near Yucca Mountain.

A qualitative comparison of the water-producing attributes of the lavas and tuffs based on the concept of specific capacity (in gal/min/ft of drawdown) indicated that despite considerable overlap in their water-yield potential, the lavas generally were the most transmissive rocks tested, followed by the welded tuffs and, finally, the zeolitized nonwelded tuffs (Blankennagel and Weir 1973, Figure 4). Pumping tests were conducted in 16 boreholes at Pahute Mesa, including 14 in which the major water production came from the rhyolitic lava flows (Blankennagel and Weir 1973, Table 4-3). The borehole names, uncased saturated thickness, measured transmissivities, and calculated hydraulic conductivities and permeabilities associated with these 14 tests are given in Table 13. The mean permeability of the rhyolitic lava is estimated to be $2.67 \times 10^{-13} \text{ m}^2$, with 95 percent lower and upper confidence limits of 9.18×10^{-14} and $7.76 \times 10^{-13} \text{ m}^2$, respectively. However, these estimates should be viewed as approximate lower bounds because other, less permeable rocks (welded and nonwelded tuffs) are present in the test interval, and these less permeable rocks would cause the transmissivity to be lower than the transmissivity that would be expected if only lava had been present. Resistivity logs indicated that nonwelded tuffs could constitute as much as 73 percent of the upper 2000 ft of saturated rock at the boreholes listed in Table 7 (Blankennagel and Weir 1973, Table 2). Because most of the water pumped from the lava enters the wells from zones that constitute only 3 to 10 percent of the total saturated thickness (Blankennagel and Weir 1973, p. 11), permeabilities in the lava may be locally much higher than the calculated mean value.

Table 13. Permeabilities of the Lava-Flow Aquifer

Well	Uncased, Saturated Thickness (ft) ^a	Transmissivity (gpd/ft) ^b	Hydraulic Conductivity (gpd/ft ²)	Permeability (m ²)
UE-18r	3,375	23,000	6.82	3.28 x 10 ⁻¹³
TW-8	4,422	185,000	41.8	2.01 x 10 ⁻¹²
UE19b-1	2,310	56,000	24.2	1.17 x 10 ⁻¹²
UE19c	2,099	12,000	5.72	2.75 x 10 ⁻¹³
UE-19d	5,129	20,000	3.90	1.88 x 10 ⁻¹³
UE-19fs	2,214	11,000	4.97	2.39 x 10 ⁻¹³
UE-19gs	1,658	30,000	16.1	7.77 x 10 ⁻¹³
UE-19h	1,383	140,000	101.0	4.87 x 10 ⁻¹²
UE-19l	5,104	1,400	0.274	1.32 x 10 ⁻¹⁴
U-20a-2	2,434	18,000	7.40	3.56 x 10 ⁻¹³
UE-20d	2,047	44,000	21.5	1.03 x 10 ⁻¹²
UE-20e-1	4,573	8,300	1.82	8.73 x 10 ⁻¹⁴
UE-20f	9,230	1,000	0.108	5.21 x 10 ⁻¹⁵
UE-20h	4,701	11,000	2.34	1.13 x 10 ⁻¹³

Source: Blankennagel and Weir (1973, Table 3)

NOTES: ^aUncased, saturated thickness was calculated as the depth to water or depth of casing, whichever was greater, minus the depth of the well. The depth to water was used for TW-8, where the casing was perforated.

^bgpd is gallons per day

Statistics for the logarithm of permeability (log *k*) are:

Mean = -12.574

Standard deviation = 0.803

Median = -12.521

Lower 95% confidence level for mean = -13.037

Upper 95% confidence level for mean = -12.110

6.7.7.8 Inferences about Permeability from Regional Observations

In addition to the permeability values from the NTS summarized in the previous section, Winograd and Thordarson (1975) made numerous qualitative evaluations of the relative magnitude of permeability of different hydrogeologic units. These evaluations were based on examination of core for fractures and mineral infilling, the geologic setting and the magnitude of discharge of springs in the region, and the correspondence between changes in hydraulic gradients and the underlying hydrogeologic unit. Sections 6.7.7.9 through 6.7.7.11 will focus on qualitative assessments of hydrogeologic units that have little actual test data and for which the qualitative evaluations thus assume relatively more importance.

6.7.7.9 Lower Clastic Aquitard (unit 3)

The lower clastic aquitard of Winograd and Thordarson (1975, Table 1) corresponds to the Lower Clastic Confining Unit (unit 3) of Table 5. According to Winograd and Thordarson (1975, p. c43), the large-scale transmissivity of the lower clastic aquitard is probably controlled by its interstitial permeability, which, based on the hydraulic conductivity of 18 cores (Winograd

and Thordarson 1975, Table 4), ranges from 3.4×10^{-20} to $4.8 \times 10^{-18} \text{ m}^2$ and has a median value of $9.7 \times 10^{-20} \text{ m}^2$. Although the lower clastic aquitard is highly fractured, Winograd and Thordarson (1975, p. c43) argued that fractures probably do not augment the interstitial permeability of the unit on a regional scale to the same degree as in the Lower Carbonate Aquifer for the following reasons:

- The argillaceous formations within the unit have a tendency to deform plastically, that is, by folding, rather than by fracturing. Thus, fracture continuity across the Lower Clastic Aquitard is disrupted by the argillaceous layers.
- Micaceous partings and argillaceous laminae tend to seal the fractures in the brittle quartzite parts of the unit, reducing or eliminating the ability of the fractures to transmit water.
- The clastic rocks that constitute the unit have a low solubility; therefore, solution channels, which can further enhance permeability along fractures in carbonate rocks, are not likely to be present in this unit.

The low permeability of the Lower Clastic Aquitard compared to the carbonate rocks also was indicated by the observation that, in the Spring Mountains, the total discharge issuing from the Lower Clastic Aquitard is only a small fraction of the total discharge of the springs in the Lower Carbonate Aquifer (Winograd and Thordarson, 1975, pp. c42–c43, c53). The comparatively low permeability of the Clastic Aquitard also is indicated by a head drop across the Lower Clastic Aquitard of 2000 ft over a distance of less than eight miles (an apparent hydraulic gradient of 250 ft/mile) in the hills northeast of Yucca Flat (Winograd and Thordarson 1975, Plate 1). In contrast, the hydraulic gradient in the carbonate aquifer ranges from 5.9 ft/mile or less along the axis of the potentiometric trough in Yucca Flat to 20 ft/mile along the flanks of the trough (Winograd and Thordarson 1975, p. c71).

6.7.7.10 Upper Clastic Aquitard (unit 5)

The Upper Clastic Aquitard is equivalent to Upper Clastic Confining Unit (unit 5) of Table 5. The Upper Clastic Aquitard corresponds to the Eleana Formation, which consists of argillite, quartzite, conglomerate, and limestone (Winograd and Thordarson 1975, Table 1). The upper two-thirds of the unit consists mainly of argillite whereas the lower one-third of the unit is principally quartzite (Winograd and Thordarson 1975, p. c118). Winograd and Thordarson (1975, p. c43) argued that fractures were unlikely to remain open in the rock at depth because of the plastic deformation behavior of the rock, which is evidenced by tight folds, and the fact that the formation serves as a glide plane for several thrust faults at the NTS. No core-scale permeability measurements exist, but based on analogy with the Lower Clastic Aquitard, its interstitial permeability probably is less than $1 \times 10^{-4} \text{ gpd/ft}^2$ (Winograd and Thordarson 1975, p. c43). In the hills northwest of Yucca Flat, an approximately 2,000-ft. drop in hydraulic head in the pre-Tertiary rocks over a distance of less than 10 miles (an apparent hydraulic gradient of 200 ft/mile) suggests a comparatively low regional permeability for the Upper Clastic Aquitard. However, because land-surface elevation changes abruptly over this same distance and because water-table elevations often mimic ground-surface elevations, it is not possible to isolate the effects of permeability from the effects of topography on the head gradient in this area.

6.7.7.11 Faults

A summary of the possible effects of faults on groundwater movement in the Death Valley region was recently presented by Faunt (1997). The transmissivity of faults was described by Faunt (1997, p. 30) to be a function of many factors:

- The orientation of the fault relative to the minimum horizontal stress in the region
- The amount and type of fill material in the fault
- The relative transmissivities of hydrogeologic units juxtaposed by offset across the fault
- The solubility and deformation behavior of the rock adjacent to the fault
- Recent seismic history.

6.7.7.11.1 Orientation of faults relative to the minimum horizontal stress in the region

In the vicinity of Yucca Mountain, the mean orientation of the minimum horizontal stress is 306 ± 11 degrees (Faunt 1997, Table 4-4), so that faults with traces oriented north-northeast are expected to be more open and permeable than faults with traces oriented in directions that place them in either a shear or a compressive state. Faults oriented northwest, or perpendicular to the maximum horizontal stress direction, would be expected to be least transmissive, all other factors being equal. One example cited by Faunt (1997, pp. 34–35) to illustrate that northeast-southwest trending structures that may have relatively high transmissivity is the “megachannel” formed in the Spotted Range-Mine Mountain shear zone between Frenchman Flat and Ash Meadows. The presence of a highly transmissive zone in the carbonate aquifer was indicated by a potentiometric trough in this area and relatively young carbon-14 ages of groundwater discharging from springs at the distal end of the trough (Winograd and Pearson 1976).

6.7.7.11.2 Amount and type of infilling material in the fault

Fine-grained gouge or clayey infilling material can cause faults to become poorly transmissive, even if their orientation relative to the stress field indicates they have the potential to be highly transmissive. The effects of deformation behavior, solubility, and infilling material in the clastic aquitards and carbonate aquifer were discussed in the sections “Lower Clastic Aquitard” and “Upper Clastic Aquitard.” Solution channels along faults in the carbonate rock have the potential to further enhance the transmissivity of faults in this unit.

6.7.7.11.3 Relative transmissivities of hydrogeologic units juxtaposed by offset across the fault

Where faults juxtapose hydrogeologic units with contrasting permeabilities, the hydrologic effects caused by juxtaposition may be difficult to isolate from the effects of the fault properties themselves. As indicated in Faunt (1997, Figure 16), an increase in the local head gradient compared to the regional gradient can occur across a fault if:

- The fault is closed, thereby blocking flow

- The fault is open, thereby redirecting flow
- The permeability of the material downgradient of the fault is low compared to the upgradient material so that flow across the fault is blocked
- The permeability of the material downgradient of the fault is high compared to the upgradient material so that flow can drain away from the fault faster than it can be delivered by the upgradient material.

Evidence that springs in Ash Meadows are caused by the juxtaposition of poorly permeable sediments and rocks downgradient of the carbonate aquifer across the Gravity Fault was presented in Winograd and Thordarson (1975, p. c82). Hydraulic data in southern Indian Springs Valley were interpreted by Winograd and Thordarson (1975, p. c67–c68) to indicate the presence of two hydraulic barriers related to the Las Vegas shear zone: (1) a northern barrier caused by the juxtaposition of the lower clastic aquitard and lower carbonate aquifer; and (2) a southern barrier, that was attributed to the presence of gouge along a major fault zone.

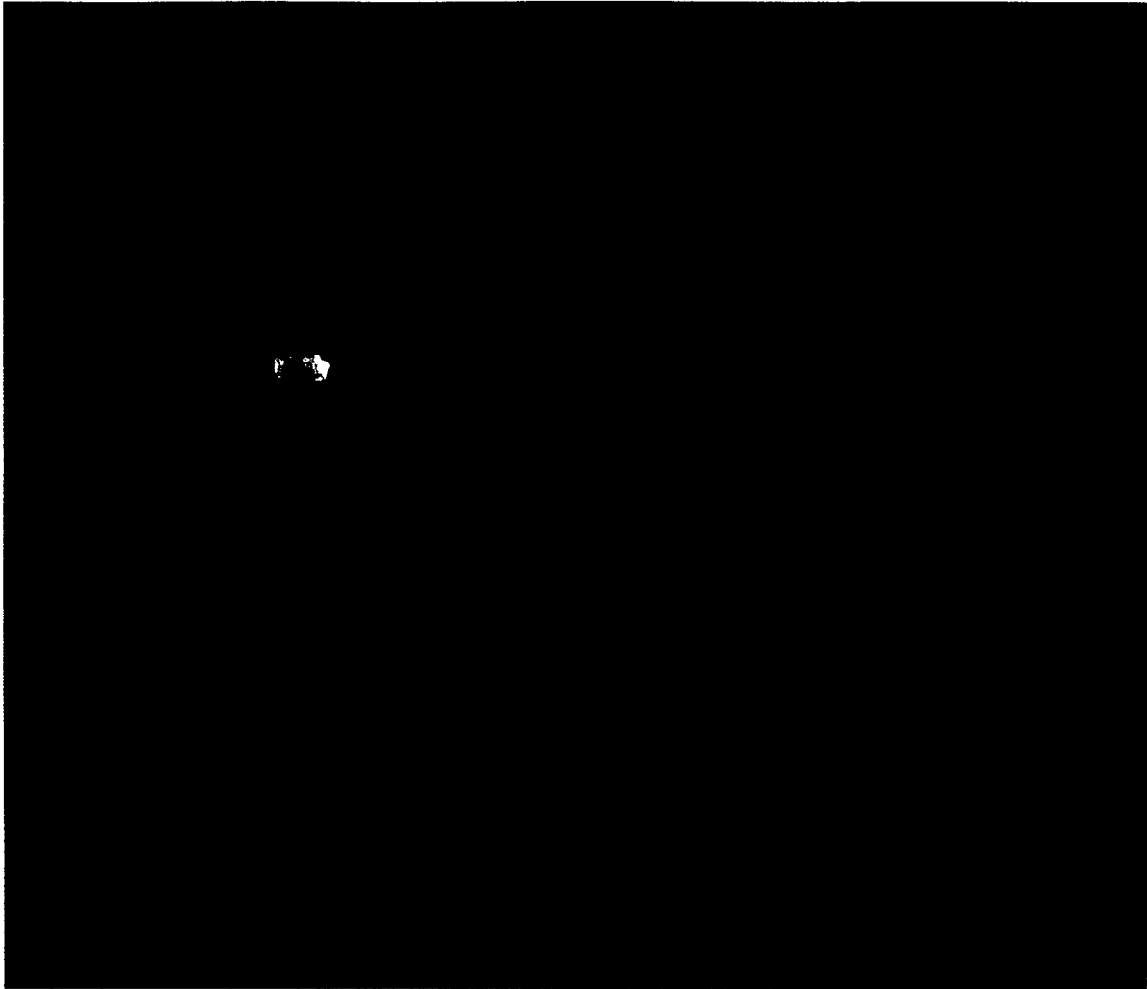
6.7.7.11.4 Recent seismic history

The seismic history of the faults may indicate which faults have undergone recent movement. Recent movement on a fault may serve to break calcite or silica cement or other material that may have closed the fault. A map showing which faults or fault segments near Yucca Mountain have undergone recent movement was developed by Simonds et al. (1995). Of the faults that have been mapped near the potential repository area, only the Solitario Canyon Fault and short segments of the Bow Ridge Fault near Exile Hill show evidence of late Quaternary (or more recent) movement.

6.7.8 Comparing Permeability Data to Calibrated Permeability Values

To check if the permeabilities estimated by PEST during the calibration of the site-scale model are reasonable, the logarithms of permeabilities estimated during calibration of the model are compared to the mean logarithms of permeability estimated from pump-test data from Yucca Mountain in Figure 13 and to data from elsewhere at the NTS in Figure 14. Where they could be estimated, the 95% percent confidence limits for the mean logarithm of the permeability data also are shown in Figures 13 and 14. For the Calico Hills Formation, the Prow Pass Tuff, the Bullfrog Tuff, the Tram Tuff, and the MVA, permeabilities are shown for both the single-hole and for the cross-hole tests at the C-well complex.

The calibrated permeabilities for the Calico Hills Formation, the Pre-Lithic Ridge Tuffs, and the carbonate aquifer are within the 95 percent confidence limits of the mean permeabilities estimated from single-hole pump test analyses at Yucca Mountain (Figure 13). The calibrated permeability for the Bullfrog Tuff is within the 95 percent confidence limits of the mean-measured permeability determined from the cross-hole tests. The calibrated permeability of the Prow Pass Tuff is slightly higher than the mean permeability estimated from the cross-hole tests, whereas the calibrated permeability of the Tram Tuff is between the mean permeabilities estimated for the unit from the single-hole and cross-hole tests (Figure 13).

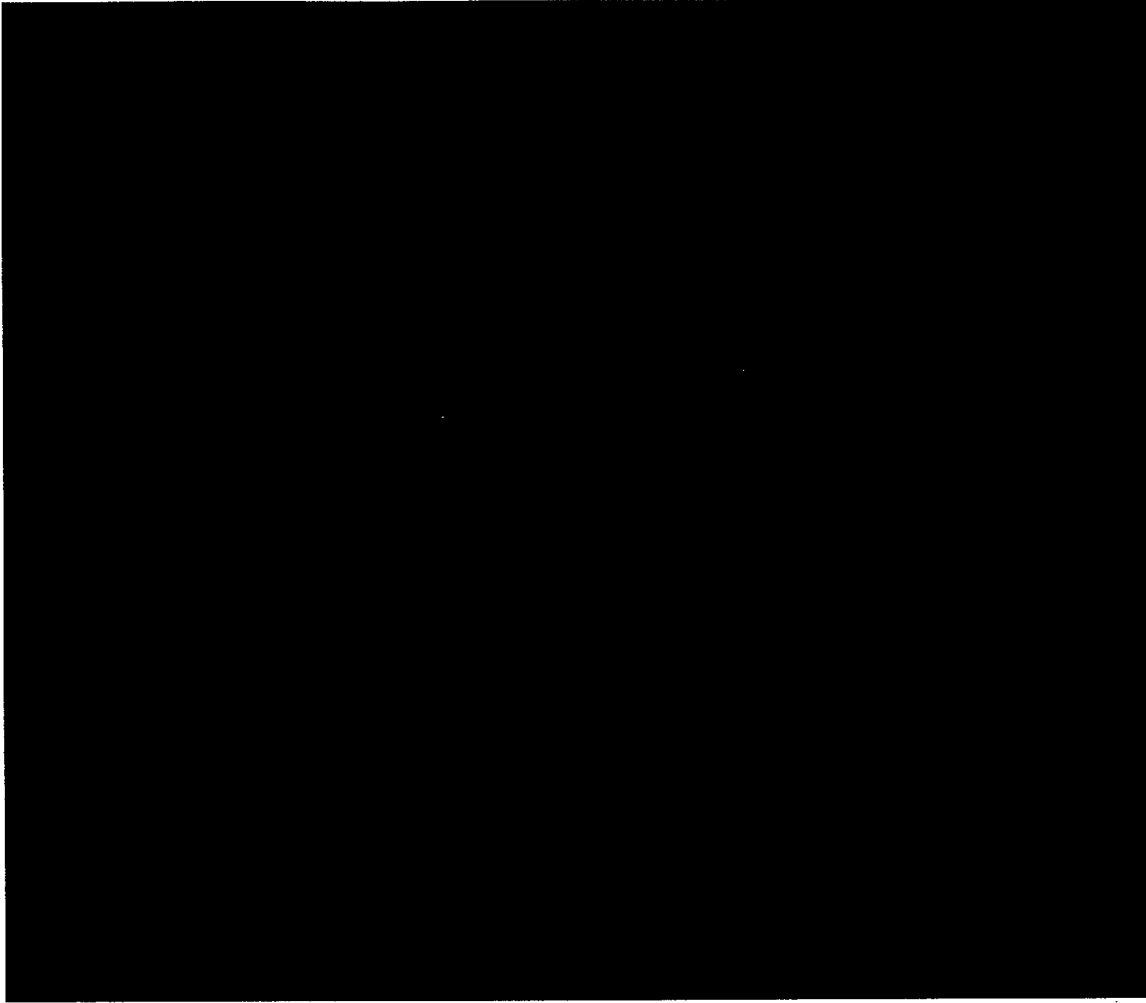


DTN: TBD

Figure 13. Logarithms of Permeabilities Estimated during Model Calibration Compared to Mean Logarithms of Permeability Determined from Pump-Test Data from Yucca Mountain

The mean measured permeability of the Carbonate Aquifer is higher elsewhere at the NTS than either the mean-measured permeability at Yucca Mountain or the calibrated permeability for the Carbonate Aquifer (Figures 13 and 14). The calibrated permeabilities for the Alluvial Aquifer and the Lava-Flow Aquifer are within or very close to the 95 percent confidence limits for the mean permeabilities of these units. The calibrated permeability for the Upper Volcanic Aquifer is about two orders of magnitude less than the mean-measured permeability of this unit.

Overall, the calibrated permeabilities are consistent with most of the permeability data from Yucca Mountain and elsewhere at NTS, except for the Upper Volcanic Aquifer. The calibrated permeability of the Tram Tuff is lower than the mean permeability derived from the cross-hole tests but higher than the permeability estimated from the single-hole tests. The relatively high permeability estimated for the Tram Tuff from the cross-hole tests may be at least partially attributable to local conditions at the site of these tests. A breccia zone is present in the Tram Tuff at boreholes UE-25 c#2 and UE-25 c#3 (Geldon et al. 1997, Figure 3), a factor that may have caused a local enhancement in the permeability of the Tram Tuff.



DTN: TBD

Figure 14. Logarithms of Permeabilities Estimated during Model Calibration Compared to Mean Logarithms of Permeability Determined from Pump-Test Data from the Nevada Test Site

6.7.9 Comparing Fluxes Derived from the Regional Model with Fluxes Calculated from the Calibrated Model

The SZ flow model describes a small part of the Death Valley regional groundwater flow system. By comparing the SZ flow model with the numerical model of the larger regional system, additional constraints can be applied to the model. The comparison between the two models was also suggested by the expert elicitation committee (CRWMS 1998). The numerical model of regional flow system models a closed system and contains data from spring discharges to help fix the water flux through the system (D'Agnese et al. 1997). Thus, it is appropriate to compare the fluxes in the two models. A fact that diminishes the value of this comparison is the use of different hydrogeologic models. The regional model uses an older hydrogeologic model described in D'Agnese et al. (1997). The SZ flow model uses a newer hydrogeologic model described in CRWMS M&O (2000b). In Section 6.1.2, the methodology for applying fixed-head boundary conditions on the sides of the SZ flow model was described. With fixed-head boundary conditions, the flux through the boundary is a function of the permeabilities. A

comparison of fluxes derived from the regional model and fluxes derived from the calibrated site-scale model are shown in Table 14. In Table 14, the zones with “N” in the label refer to the northern boundary, those with an “E,” the eastern boundary, and so on. The zones are depicted graphically in Figure 15. The comparison is reasonable on the northern and eastern boundaries. The northern boundary, for instance, has a total flux of 189 kg/s across it in the regional model and 169 kg/s across it in the SZ calibrated model. As can be seen in Table 14 and Figure 15, the distribution is different, which is not unexpected because the regional and SZ calibrated models are based on different hydrogeologic models. The match was good on the east side of the model with the lower thrust area, E1. The other zones showed small flows in both models. The match between the two models was poor on the western boundary. The southern boundary flux, which is simply a sum of the other boundary fluxes plus the recharge, is also a good match. The difference in southern fluxes (shown as zone S in Table 14) is about 21 percent.

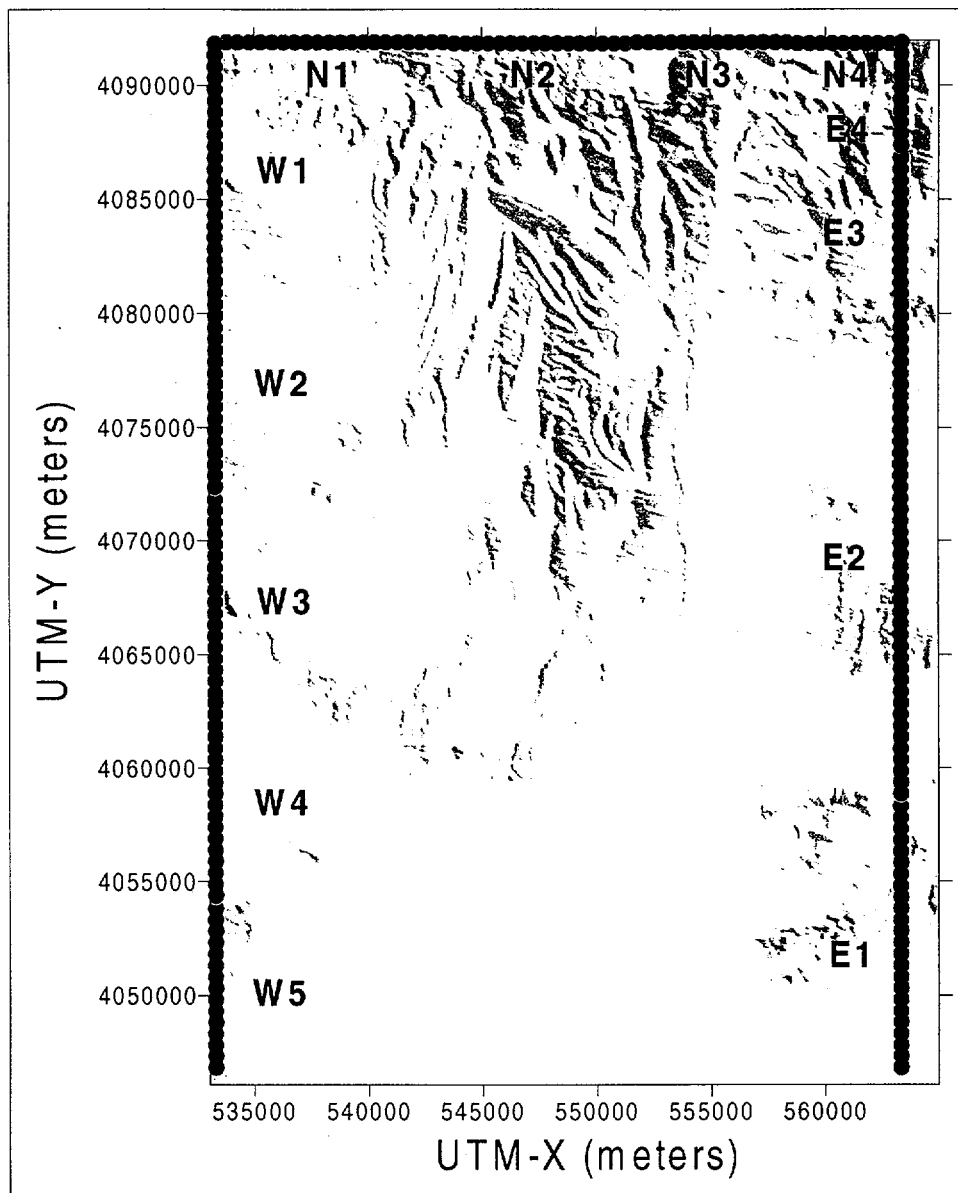
Table 14. Comparison of Regional and Site-Scale Fluxes

Boundary Zone	Regional Flux (kg/s)	Site-Scale Flux (kg/s)	Calibration Target ?
N1	-101.24	-60.009275	Yes
N2	-16.48	-33.442643	Yes
N3	-53.05282	-30.557419	Yes
N4	-18.41	-44.807523	Yes
W1	3.45	4.1663	No
W2	-71	-0.0071871	No
W3	-6.9	-0.0000078	No
W4	2.73	-0.0000223	No
W5	-46.99	-6.8542863	No
E1	-555.45	-553.85002	Yes
E2	-5.46	3.5334027	Yes
E3	2.65	16.4956192	Yes
E4	-3.07	16.8224586	Yes
S	918	724	No

DTN: TBD

NOTE: A negative value indicates flow into the model.

Several factors affect the flux match between the two models: the vertical resolution, the hydrologic framework model, and the permeability distribution. The vertical resolution of the site-scale SZ model is an order of magnitude finer than the regional model (39 layers versus 3 layers), which means that fluxes calculated by the site-scale model may depend more strongly on a few units than on the regional-scale model. This fact is important when we consider that many of the unit permeabilities in the site-scale SZ model are constrained by field data. The hydrologic framework model used in the regional-scale model is older than that used in the site-scale model. The newer framework model differs considerably (as shown in Figure 16), which is why the matching requirements for the fluxes were relaxed for the western boundary and the flux



DTN: TBD

Figure 15. Flux Zones Used for Comparing Regional and Site-Scale Fluxes

distribution is different on the northern boundary. The last factor affecting the flux distribution in the regional model is the use of permeability classes. In this method, permeabilities associated with specific units are not defined (D'Agnese et al. 1997). Rather, the permeabilities are grouped into classes and gridblocks assigned to classes, which makes it difficult to reproduce the distribution of fluxes on the side of the site-scale model (if done on a unit-by-unit basis). In turn, this discrepancy makes it difficult to reproduce vertical flow near the lateral boundaries, because this would require a flux distribution by hydrogeologic unit.



- 21 Valley-fill Aquifer
- 20 Valley-fill Confining Unit
- 19 Limestone Aquifer
- 18 Lava-flow Aquifer
- 17 Upper Volcanic Aquifer (TSw and TCw)
- 16 Upper Volcanic Confining Unit (Calico Hills Tuff)
- 15 Undifferentiated Units
- 14 Lower Volcanic Aquifer - Prow Pass
- 13 Lower Volcanic Aquifer - Bullfrog
- 12 Lower Volcanic Aquifer - Tram
- 11 Undifferentiated Units (northwest)
- 10 Lower Volcanic Confining Unit
- 9 Older Volcanic Aquifer
- 8 Older Volcanic Confining Unit
- 7 Upper Carbonate Aquifer
- 6 Lower Carbonate Aquifer (thrust)
- 5 Upper Clastic Confining Unit
- 4 Lower Carbonate Aquifer
- 3 Lower Clastic Confining Unit
- 2 Lower Carbonate Aquifer (thrust)
- 1 Granites
- 0

DTN : TBD

NOTES: The Old Geologic Framework Model Refers to that used in the regional SZ model (D'Agnese et al. 1997).
 The New Model refers to the Geologic Framework Model used in the Site-Scale SZ Flow model (CRWMS 1999c)

Figure 16. Geology at the Water Table for the Site-Scale Model.

6.7.10 Comparing Permeabilities Used in the Regional Model to Permeabilities from the Calibrated Model

The volcanic units, clastic confining units, and the carbonate aquifer, play a major role in the performance of the regional SZ model (D'Agnese et al. 1997) as well as that of the SZ model. It would therefore be of interest to compare the calibrated values of these in both models. The regional model, due to its lack of resolution in the vertical direction, used permeability classes rather than individual permeability values for individual hydrogeologic units. This fact made comparing the models difficult. In the next version of the regional model, individual hydrogeologic unit permeabilities will be used. It should be noted that, in general, good agreement with published permeability values was achieved with the SZ model.

6.7.11 Comparing Measured Upward Hydraulic Gradient with the Estimated Upward Gradient from the SZ Model

The upward gradient is represented in this model. Evidence for the upward gradient is given by Bredehoeft (1997). A measure of that gradient in the vicinity of Yucca Mountain is obtained from the head measurement in well UE-25 p#1, the only well completed in the carbonate aquifer. The measured head in the carbonate aquifer is 752 m, which compares to heads in the volcanic aquifers of about 730 m in the same area. The SZ model value for the head at well UE-25 p#1 was 740 m. Some of the lack of upward gradient can be attributed to the fixed-head boundary conditions, which produce no vertical flow (the boundary conditions are discussed in Section 6.1.2). This simulated head, though smaller than the field measurement, is still sufficient to force the path lines leaving Yucca mountain to remain shallow. The shallow pathlines are consistent with geochemical evidence.

6.7.12 Discussion of Hydrogeologic Features Used in Calibration

Features such as individual faults and fault zones played an important role in the calibration process. The values of some features were modified during the calibration process. Features not changed during the calibration process were given one value and held constant. The features, their geometric location, hydrologic characteristics, and impact on the model are described in Table 6. Features were given either permeability values or multipliers, where the multipliers were used as multiplying factors for existing permeability values. In Table 15, each model feature is identified, its permeability or multiplying factor listed, and indication given as to whether the value was fixed or calibrated.

6.8 SPECIFIC DISCHARGE

The specific discharge was estimated for a nominal fluid path leaving the repository area and traveling to the compliance boundaries at 5 km, 20 km, and 30 km (the boundaries are shown in Figure 15). The specific discharge was calculated by setting the porosities of all gridblocks equal to 1.0 and simulating 100 distributed particles leaving the repository area. The value of specific discharge was calculated from the distance of the boundary and the arrival time of the fiftieth particle. (It is assumed that the fiftieth particle gives a representative value of specific discharge.) Values for specific discharge of 1 m/yr, 2 m/yr, and 2 m/yr were obtained, respectively, for the three compliance points. The expert elicitation committee estimated

(CRWMS M&O 1998, Fig. 3-2e) a specific discharge of 0.71 m/yr for the 5-km compliance boundary. Thus, agreement is good (and conservative). The expert elicitation committee did not consider other compliance boundaries

Table 15. Parameter Values for Features Used in the Saturated-Zone Model

	Feature	Parameter	Value	Calibration Use
1.	Northern	Mult	0.071	Calibrated
2.	Northern Crater Flat	Mult	0.004	Fixed
3.	Fortymile Wash	Mult	10.0	Fixed
4.	Spotted Range-Mine Mountain	Mult	11.78	Calibrated
5.	Claim Canyon	Mult	0.071	Calibrated
6.	Shoshone Mtn.	Mult	0.071	Calibrated
7.	Calico Hills	Mult	0.071	Calibrated
8.	Crater Flat Fault	Perm	5×10^{-14}	Fixed
9.	Solitario Canyon Fault	Perm	1×10^{-18}	Calibrated
10.	Highway 95 Fault	Perm	1×10^{-15}	Fixed
11.	Bare Mountain Fault	Perm	1×10^{-15}	Fixed
12.	Alluvial Uncertainty	Perm	5×10^{-12}	Calibrated
13.	Imbricate Fault Zone	Mult	1.00	Calibrated
14.	East-West Barrier	Perm	1.05×10^{-18}	Calibrated

DTN: TBD

NOTES: The number in the first column refers to the feature number given in Table 6. The terms "Mult" and "Perm" refer to using the features with a multiplying factor or a permeability factor, respectively.

6.9 MAJOR MODEL SENSITIVITIES AND TRENDS OBSERVED IN CALIBRATION

In terms of impact on the PA calculations and the simulated performance on Yucca Mountain, the length of the flow path of particles leaving the repository area and the type of rock (and retardation characteristics) are all very important. The fluid velocities along the pathway are also important. There are three calibration targets that affect most strongly the PA issues. These are the lateral fluxes on the eastern boundary, the low-gradient area water level, and the upward gradient (that is, the match to well UE-25 p#1). The lateral fluxes on the eastern side of the model are important because they exert a major influence of the partial pathways leaving the potential repository region. The regional model fluxes indicate small fluid fluxes in the north and central parts of the eastern boundary and a large flux into the SZ model in the southern part. Reproducing these fluxes produced flow paths that were in agreement with flow paths inferred from geochemical data. The low-gradient area to the south-southeast of Yucca Mountain is important to model accurately because that gradient and the rock type in the area are responsible for the specific discharge to the 5-km compliance boundary, an important PA performance measure. The upward head gradient from the carbonate aquifer to the volcanic aquifer is important because it tends to keep the particle pathlines shallow and out of the regional Carbonate aquifer.

It is important to note here that the sensitivity analysis presented in Sections 6.9.1 and 6.9.2 is dependent on the calibrated parameter values. This dependence is manifested in parameters

which have low sensitivity such as the Older tuffs and the Clastic unit. These units would have higher sensitivities if their values were greater; past a certain threshold, any low value produces essentially the same result. The Carbonate aquifer shows a high sensitivity despite the fact that it contains relatively few observations. This can be attributed to its large volume and high permeability. This gives rise to a large flow which can effect many of the units which do contain observations. If the Carbonate aquifer permeability were smaller, it would not have a large effect.

6.9.1 Sensitivity of Estimated Parameter Values

The composite scaled sensitivities and the linear confidence intervals on the estimated parameter values provide a measure of the amount of information provided by the data for any parameter. Composite scaled sensitivities are calculated as follows. First, the sensitivities are scaled by multiplying by the parameter value and the square root of the weight to obtain dimensionless values. The scaled sensitivities for each parameter are then summed and these values are taken directly from the PEST output. These numbers are then divided by the number of observations to be comparable to values produced by MODFLOWP (Hill 1992). The composite scaled sensitivities equal the square root of these values. If the composite scaled sensitivity values for each of the parameters vary by more than two orders of magnitude from each other, the optimization procedure has difficulty estimating values for the less sensitive parameters. Because, for nonlinear parameter-estimation models, the sensitivities depend on the parameter values, the sensitivities can only be truly gauged at the optimal parameter values.

The composite scaled sensitivities for the site-scale SZ flow model are shown in Table 16 along with the final estimated values, the coefficients of variation, and the 95-percent linear confidence intervals. The composite scaled sensitivities are also shown in Figure 17 for the 26 parameters described in Table 16. There is a wide range in composite scaled sensitivities, with the model being most sensitive to the permeability multipliers associated with the Claim Canyon, Calico Hills, and Shoshone Mountain fault zones (fpb3), and decreasingly sensitive to the Lower-Carbonate Aquifer (lca2), Bullfrog Unit (bull), Lower Fortymile-Wash Channel (wash), and Tram unit (tram) permeabilities, respectively. The model is relatively insensitive to the remaining parameters, as reflected in their unreasonable confidence intervals. This large range in parameter sensitivities indicates that the most-sensitive parameters can be divided into multiple parameter zones and the least-sensitive parameters could be grouped into fewer parameters.

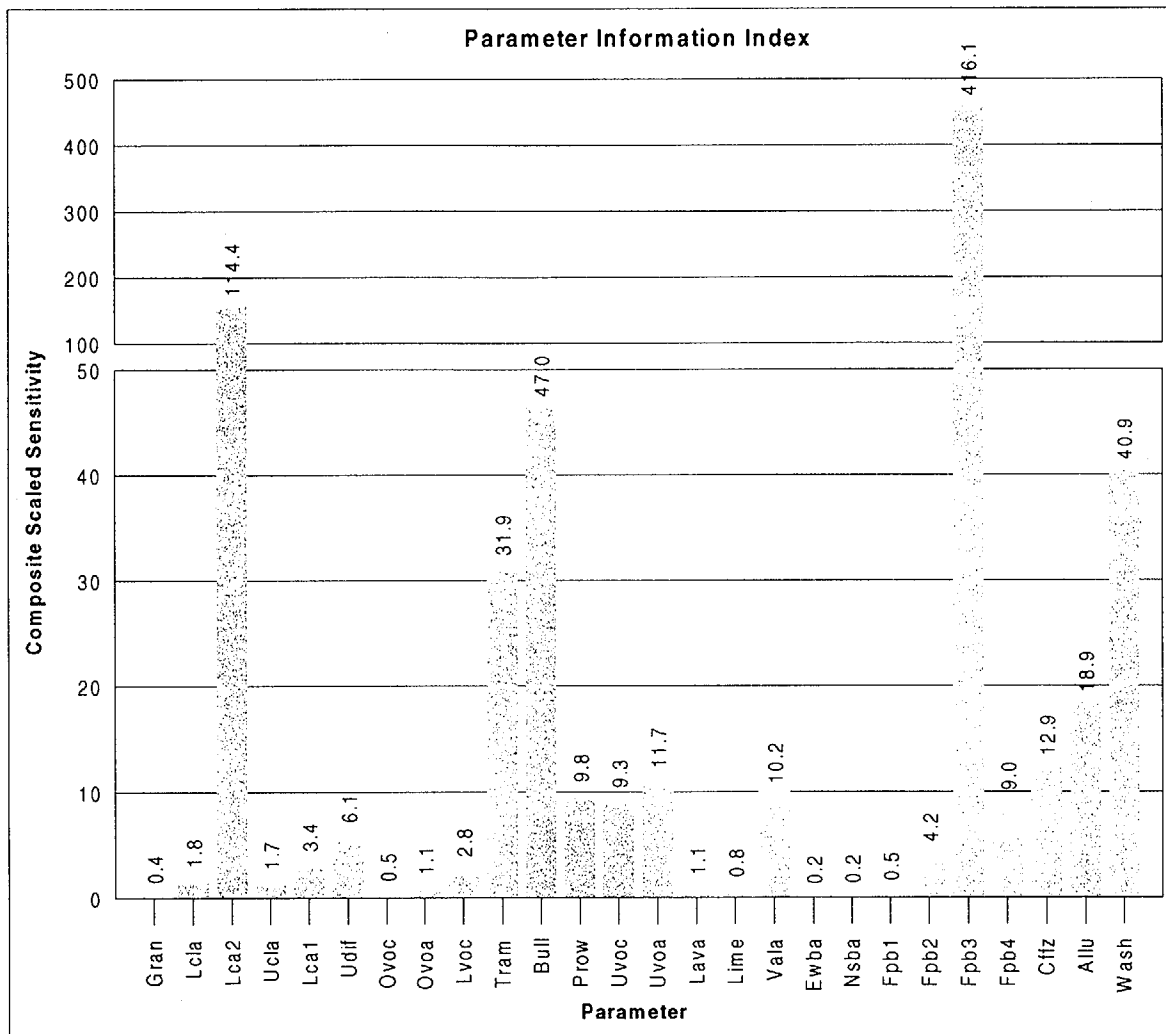
Figure 18 shows a bar chart of the largest absolute weighted sensitivity for each observation along with the corresponding parameter label. The raw sensitivities were taken directly from the PEST output and were then multiplied by the square root of the weight using an Excel spreadsheet. The observation sensitivities indicate that the parameters are more sensitive to some of the observations and less sensitive to others. The observations with the largest sensitivities generally correspond to the parameter representing the permeability of the Claim Canyon, Calico Hills, and Shoshone Mountain fault zones. Figure 19 shows a spatial plot of the parameter label corresponding to the largest absolute weighted sensitivity for each observation location. Locations with sensitivity larger than 200 are shown with a circle around the parameter name. It appears that the model is most sensitive to observations located close to Yucca Mountain. These were also the observations given the highest weight (Table 7).

Correlation between parameters indicates whether the parameter estimates are unique and depends on the sensitivity of the observations to the parameters as discussed above. Thus, parameter correlation also depends on how well the parameters are defined by the observations. If two parameters are correlated, then multiplying the parameter values by a common factor will result in the same head distribution, and the parameter estimation will not converge. Although there is debate over what correlation values are significant, parameters with correlations less than

Table 16. Estimated Values, Coefficients of Variation, and 95-Percent Confidence Intervals for the Parameters of the Final Calibrated Model

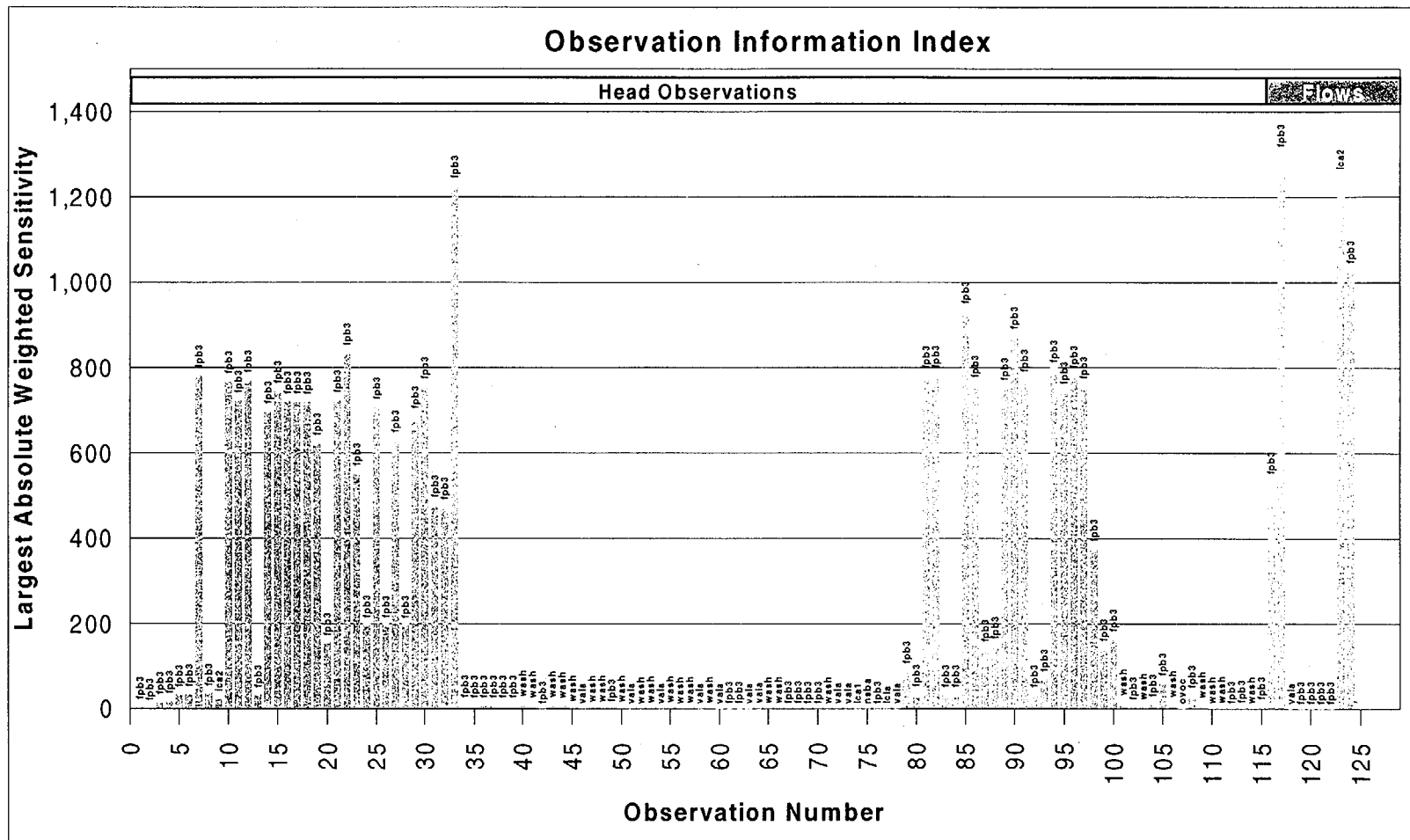
Parameter label	Parameter description	Units	Log-transformed for regression	Estimated value	Composite scaled sensitivity	Coefficient of variation	95-percent linear confidence intervals on the estimate.
Gran	Granites		Yes	1.96E-16	0.4	>50	3.87E-185 ; 9.92E+152
L.cla	Lower-elastic confining unit		Yes	1.00E-16	2	>50	2.61E-24 ; 3.84E-09
L.ca2	Lower-carbonate aquifer		Yes	5.00E-14	114	41	4.22E-18 ; 5.92E-10
U.cla	Upper-elastic confining unit		Yes	1.00E-16	2	>50	5.02E-88 ; 1.99E+55
L.ca1	Lower-carbonate aquifer thrust		Yes	1.00E-14	3	>50	1.92E-47 ; 5.22E+18
Udif	Undifferentiated valley fill		Yes	5.00E-15	6	>50	2.84E-20 ; 8.80E-10
Ovoc	Older-volcanic confining unit		Yes	2.00E-16	0.5	>50	1.235786-110 ; 3.24E+78
Ovoa	Older-volcanic aquifer unit		Yes	5.00E-16	1	>50	3.17E-33 ; 7.89E+01
L.voc	Lower-volcanic confining unit		Yes	2.00E-15	3	>50	7.43E-20 ; 5.38E-11
Tram	Tram unit		Yes	2.34E-13	32	2	1.31E-15 ; 4.18E-11
Bull	Bullfrog unit		Yes	1.57E-11	47	2	1.28E-13 ; 1.91E-09
Prow	Prowpass unit		Yes	8.02E-12	10	>50	1.16E-19 ; 5.53E-04
Uvoc	Upper-volcanic confining unit		Yes	4.98E-14	9	>50	6.98E-26 ; 3.56E-02
Uvoa	Upper-volcanic aquifer		Yes	8.00E-14	12	>50	3.15E-23 ; 2.03E-04
Lava	Lava-flow aquifer		Yes	1.00E-12	1	>50	7.56E-49 ; 1.32E+24
Lime	Limestone aquifer		Yes	1.00E-12	1	>50	6.86E-29 ; 1.46E+04
Vala	Valley-fill aquifer		Yes	5.02E-12	10	>50	3.45E-17 ; 7.30E-07
Ewba	East-west barrier zone		Yes	1.05E-18	0.2	>50	1.047933-318 ; 1.047933+28
Nsba	Solitario Canyon fault		Yes	1.00E-18	0.2	>50	2.51E-69 ; 3.98E+32
Fpb1	Fortymile Wash Zone (middle 1 & 2)		No	10.0	0.5	>50	-63.8 ; 83.8
Fpb2	Spotted Range-Mine Mountain zone (thrust_sc)		No	11.8	4	>50	-97.9 ; 121.4
Fpb3	Claim Canyon, Calico Hills, Shoshone Mtn zones		No	7.11E-03	416	1	-7.65E-01 ; 7.79E-01
Fpb4	Imbricate fault zone		Yes	1.0	9	>50	4.33E-05 ; 23200
Cffz	Crater Flat fault		Yes	4.98E-14	13	>50	6.82E-19 ; 3.63E-09
Allu	Alluvial uncertainty zone		Yes	3.22E-12	19	>50	4.96E-17 ; 2.09E-07
Wash	Lower Fortymile-Wash channel		Yes	5.08E-12	41	2	6.01E-14 ; 4.29E-10

DTN: TBD



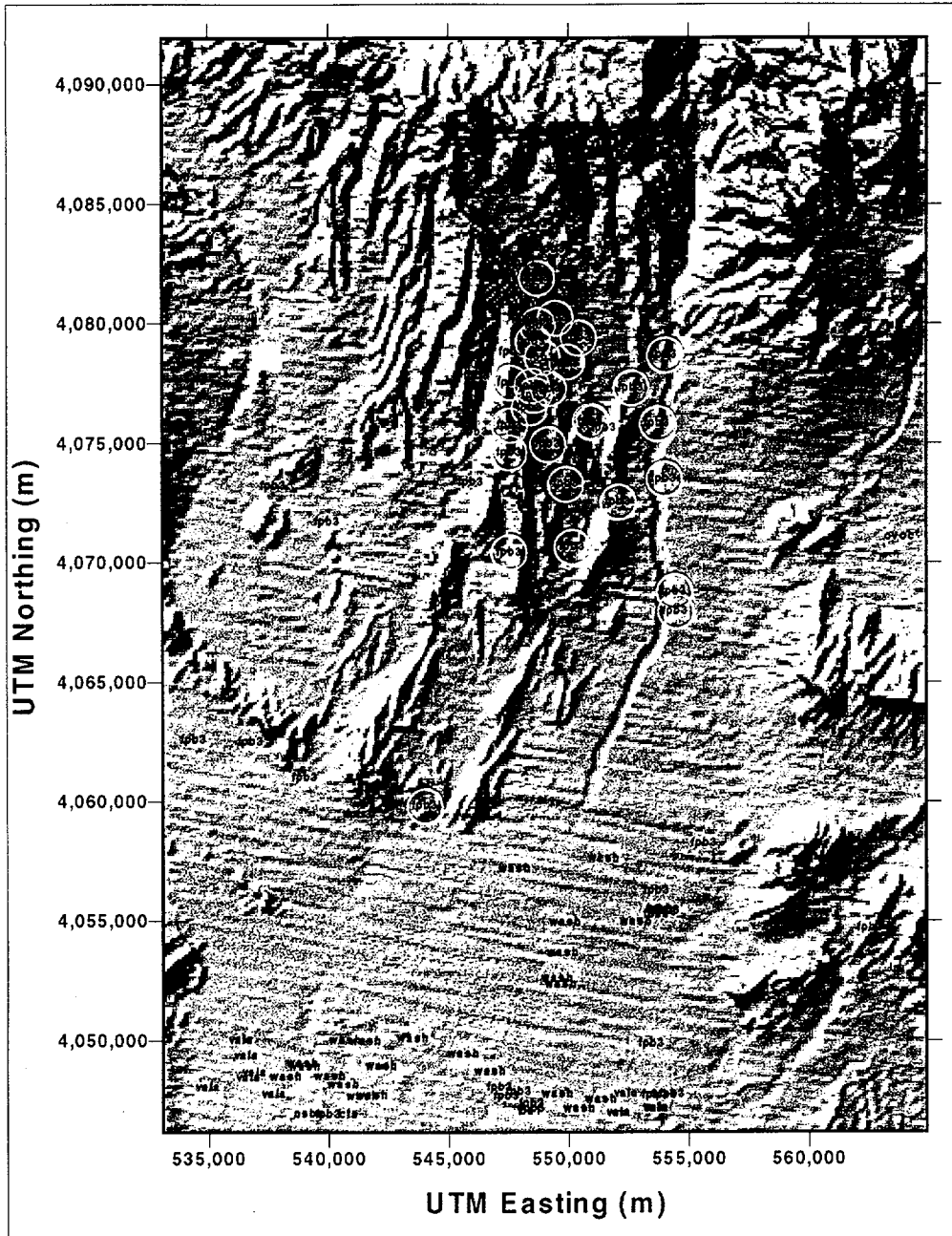
DTN: TBD

Figure 17. Composite Scaled Sensitivities for the Estimated Parameters for the Final Calibrated Model Listed in Table 16



DTN: TBD

Figure 18. Largest Absolute Weighted Sensitivity and Corresponding Parameter Label for the Final Calibrated Model



DTN: TBD

NOTE: Values larger than 200 indicated with circle

Figure 19. Largest Absolute Weighted Sensitivity for Each Observation Location

0.98 can generally be considered to be uncorrelated. For the site-scale SZ flow model the values were taken directly from the PEST output. There is only one correlation with an absolute value greater than 0.95. The correlation between the Lower-Carbonate Aquifer permeability and the Spotted Range-Mine Mountain fault zone permeability has a value of -1.0 , indicating that the two parameters cannot be estimated uniquely and that one should be set at a fixed value.

6.9.2 Analysis of Weighted Residuals

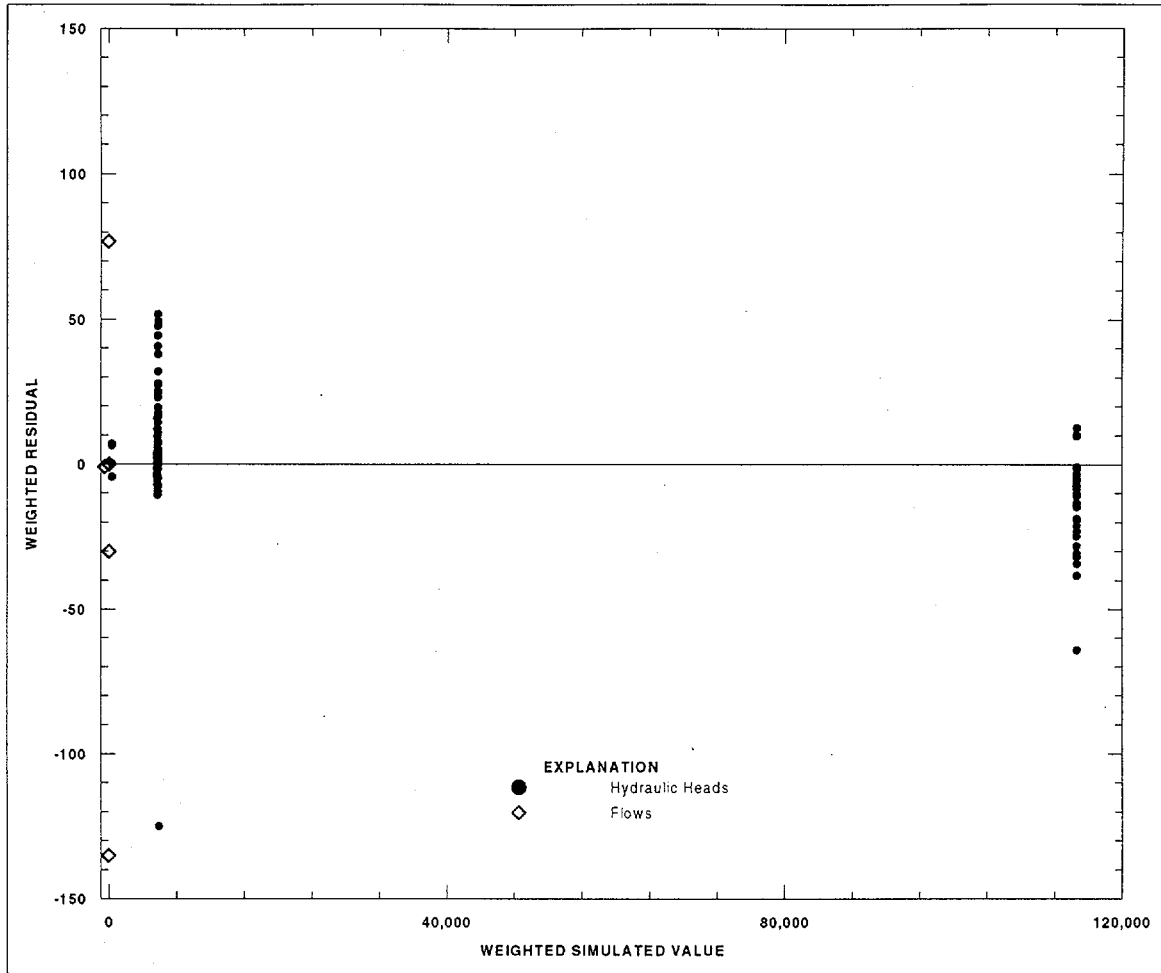
Groundwater flow model validity can be judged by evaluation of the lack of bias in the weighted residuals (Draper and Smith 1981; Cooley and Naff 1990). There are three plots that are useful in determining the randomness of the weighted residuals: 1) distribution of weighted residuals relative to weighted simulated values, 2) spatial distribution of weighted residuals, and 3) normal probability plot of weighted residuals. These plots for the site-scale SZ flow model are discussed in the following paragraphs.

A plot of the weighted residuals as a function of the weighted simulated values for the site-scale SZ flow model is shown in Figure 20. In PEST, the residuals are calculated as the simulated value minus the observed value, which is opposite of the convention used in MODFLOW in which the residuals equal the observed value minus the simulated value. The residuals were taken directly from the PEST output file and then multiplied by -1 and the square root of the weight to maintain a consistent convention with the Regional model's sensitivity analysis. Ideally, the weighted residuals vary randomly about zero for all weighted simulated values. The presence of any systematic trend in the distribution of the weighted residuals is indicative of some sort of bias present in the model. The grouping of the weighted simulated values reflects the discrete weights that were used in the parameter estimation. The group of points at a weighted simulated value of 5,700 correspond to a weight of 1 and appear to have more positive weighted residuals than negative. The group of points at a weighted simulated value of 114,000 correspond to a weight of 20 and appear to have more negative weighted residuals than positive. This result indicates that, at locations where there is more confidence in the observed value, the model overpredicts the head, and where there is less confidence in the observed value, the model underpredicts the head. This systematic trend indicates that there is some bias present in the model conceptualization.

A plot of the weighted residual as a function of observation location for the site-scale SZ flow model is shown in Figure 21 in which blue diamonds indicate a positive residual and red circles indicate a negative residual. The size of the circle is proportional to the size of the weighted residual, which varies from -135 to 77 . Ideally, the positive and negative weighted residuals are randomly distributed with observation location. The weighted residuals for this model are clearly grouped into regions of positive and negative values, indicating that some sort of bias is present in the model conceptualization.

A normal probability plot of the weighted residuals for the site-scale SZ flow model is shown in Figure 22. The standard normal statistic for each of the weighted residuals was calculated using the methodology of Hill (1994) with an Excel spreadsheet. As discussed by D'Agnesse and others (1997), the points would be expected to lie along a straight line if the weighted residuals were both independent and normal. The normality of the weighted residuals is important to the

use of measures of parameter and prediction uncertainty such as linear confidence intervals. The



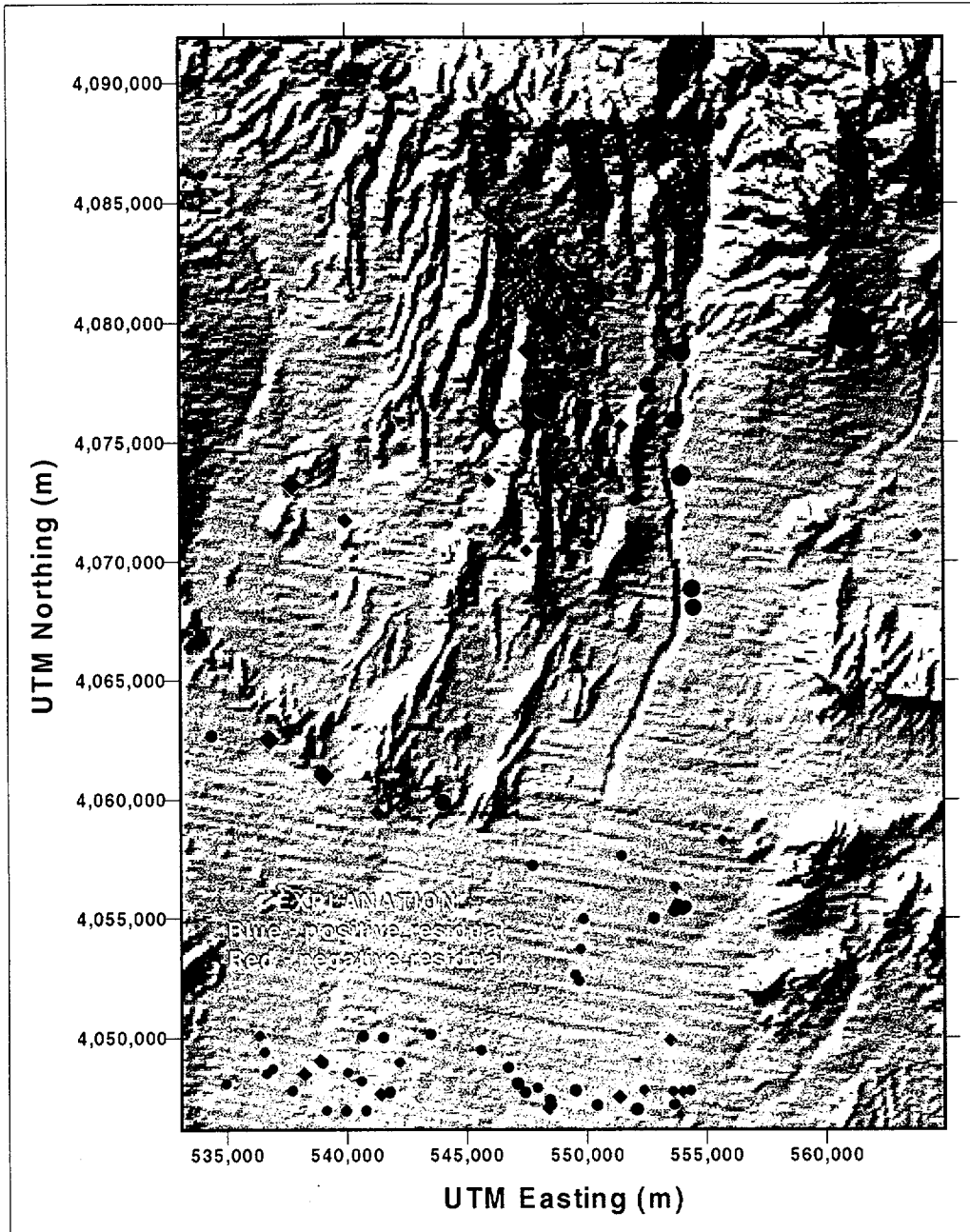
DTN: TBD

Figure 20. Weighted Residual as a Function of Weighted Simulated Value for the Final Calibrated Model

weighted residuals need to normally distributed and the model needs to be effectively linear for the parameter values to be normally distributed. The use of linear confidence intervals on the estimated parameters and predicted heads and flows assumes that the parameters are normally distributed (Hill 1994). Clearly the points in Figure 22 do not fall on a straight line. Figure 23 shows a normal probability plot of the weighted residuals along with four sets of random normal correlated deviates. The correlated deviates were calculated using the RESANP program of Cooley and Naff (1990). If the weighted residuals are random but correlated rather than independent, then the random normal correlated deviates should show similar curvilinearity to the weighted residuals. Most of the curvilinearity of the weighted residuals cannot be attributed to the regression-derived correlations, indicating that the weighted residuals are not normally distributed.

In summary, the SZ model sensitivity analysis shows that there are some unresolved issues that

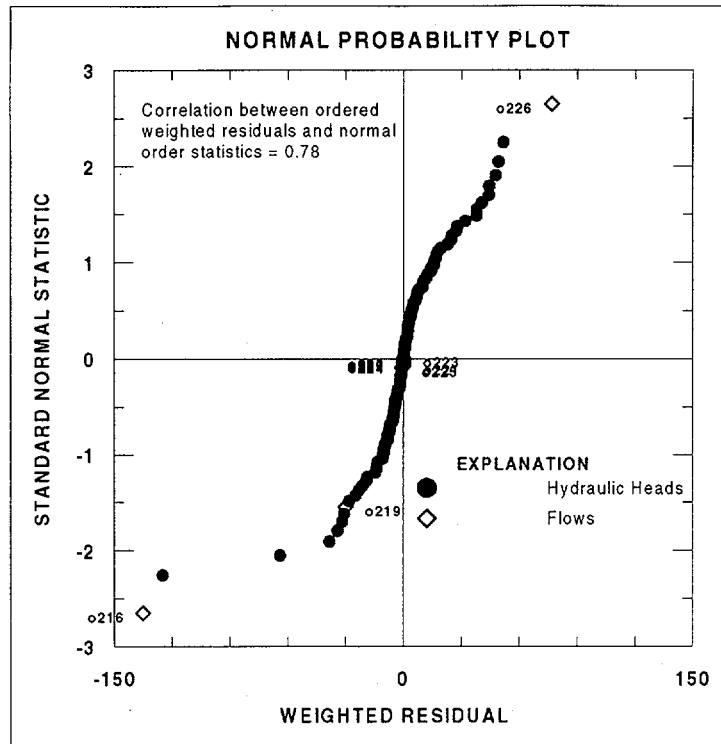
should to be addressed. These include some correlated residuals, notably in the low gradient area. While the residuals are small in the low gradient area, there is some excess water that need to be understood. There also are likely correlated parameters that should be separated. Guided by a more sophisticated sensitivity analysis, a better parameter distribution may be constructed in the future.



DTN: TBD

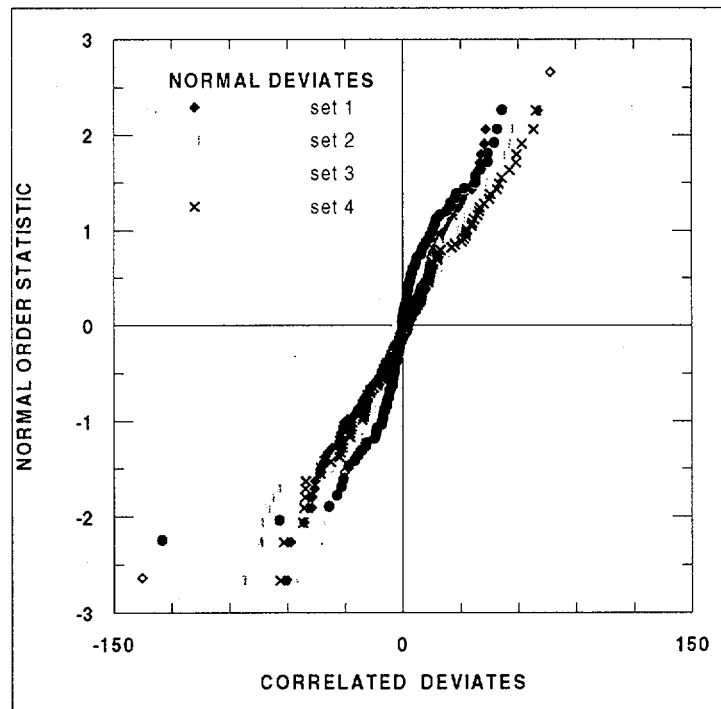
NOTE: Positive residuals are indicated with a blue diamond and negative residuals are indicated with a red circle. The size of the points is proportional to the magnitude of the residuals which vary from -135 to 77.

Figure 21. Weighted Residual as a Function of Observation Location



DTN: TBD

Figure 22. Normal Probability Plot of Weighted Residuals for the Final Calibrated Model



DTN: TBD

Figure 23. Normal Probability Plot of Weighted Residuals (red circles) and Correlated Normal Random Deviates

6.10 MODEL VALIDATION ISSUES AND RECOMMENDATIONS FOR THE SATURATED-ZONE FLOW

Though the use of the flow equations described in Section 6.5 is well established in both continuum and fractured rock applications, more confidence is need to insure that the integrated approach to calibration described herein can successfully reduce the uncertainty in the PA predictions. To this end we propose additional calibration studies at either Idaho National Engineering and Environmental Laboratory (INEEL) or Hanford. These studies would include flux-based and head- (or pressure) based calibration targets as well as evaluating the possibility of using transport pathways directly in the calibration process. Additional confidence in the SZ flow model at Yucca Mountain might also be achieved by incorporating temperature and transient analysis (where appropriate) in the calibration process. As discussed previously, the effect of temperature is already included in the fluid viscosity in the SZ model. What is meant here is the inclusion of the energy balance equation and calculating SZ temperatures. The computed temperatures could then be compared to borehole data. The transient analysis refers to modeling the C-Wells pump test. This modeling would provide confidence that the SZ model is accurately representing the volcanic aquifers in the vicinity of Yucca Mountain.

INTENTIONALLY LEFT BLANK

7. CONCLUSIONS

The calibration of a site-scale SZ flow model is a complex and difficult task. The model represented a compilation of data from many sources including geology, hydrologic testing, and geochemistry. The SZ model used a 500-m grid (areal) that grid convergence studies showed was adequate for representing the hydrogeologic framework while keeping the numerical error small. Though the calibration is not unique, several important data sets were matched. The low hydraulic gradient in the area to the south-southeast of Yucca Mountain was modeled accurately, although the heads themselves were 1 to 2 m high. Getting the gradient right was important because the fluid fluxes to the 5-km compliance boundary depends strongly on the hydraulic gradient. Besides reproducing observed head and regional model flux data, the model matches other data—some quantitatively and some qualitatively. These data include permeability values derived from single-well and multiple-well tests, fluxes derived from the regional model, hydrochemical data, and specific discharge values estimated by the expert elicitation panel. The permeabilities of the geologic units, though used as a calibration parameters, were monitored closely to insure that they remained in ranges derived from field tests. Sometimes these ranges were fairly tight (1–2 orders of magnitude) but sometimes had a range of 2 to 4 orders of magnitude. The calibration process was complicated by the existence of faults and other features that had calibration parameters associated with them. The fluxes from the regional model were used as targets because the regional model was a relatively complete water balance of the Death Valley hydrologic system with fluxes constrained by spring data as well as other sources. These fluxes could therefore help link the SZ flow model to these other more global water-balance data. The SZ model reasonably matched the flux data from the regional model (~21% on the southern boundary). The hydrochemical data were used as a quality check for pathline direction. The SZ model produced pathlines from the potential repository area that agree with those inferred from geochemistry.

The SZ model matches much of the existing SZ-related data, especially in the inferred pathway for fluid leaving the potential repository area. Time and manpower constraints precluded using all the data. Notable among these omitted data are the C-Wells transient data. Even though effort has been made to ensure that errors are on the conservative side, such as using multihole tests where available (to constrain permeabilities) and making sure that the SZ model has a specific discharge that is higher than that predicted by the expert elicitation committee, it is very difficult, because of the complexity of the model, to ensure that the model is conservative.

INTENTIONALLY LEFT BLANK

8. REFERENCES

8.1 DOCUMENTS CITED

Blankennagel, R.K. and Weir, J.E. 1973. *Geohydrology of the Eastern Part of Pahute Mesa, Nevada Test Site, Nye County, Nevada*. USGS Professional Paper 712-B. Denver, Colorado: U.S. Geological Survey. TIC: 219642. (Sec. 6.7.7.3; describe hydrogeologic controls on groundwater movement at the NTS; pp. 6, 11, Fig. 4, Table 2; Sec. 6.7.7.7; geology of Pahute Mesa and hydraulics of lava flows; Table 3; Sec. 6.7.7.7; data source for Table 13)

Bower, K.M., Gable, C.W., and Zivoloski, G.A., "Effect of Grid Resolution on Control Volume Finite Element Groundwater Modeling of Realistic Geology", LA-UR-001870. . Los Alamos, New Mexico: Los Alamos National Laboratory. TIC: TBD. (Sec. 6.2.2; study to determine grid resolution for flow and transport)

Bredehoeft, J.D.. 1997. "Fault Permeability Near Yucca Mountain." *Water Resources Research*, 33 (11), 2459-2463. Washington, D.C.: American Geophysical Union. TIC: 236570. (Sec. 6.7.2; evidence for the upward gradient of groundwater heads at YM)

Cooley, R.L. and Naff, R.L.. 1990. "Regression Modeling of Ground-Water Flow." *USGS Techniques in Water Resources Investigations*, Chapter B4, Book 3. Denver, Colorado: U.S. Geological Survey. (Sec. 6.9.2; evaluation of the lack of bias in weighted residuals. RESANP program used to calculate correlated deviates)

CRWMS M&O (Civilian Radioactive Waste Management System Management and Operating Contractor). 1998. *Saturated Zone Flow and Transport Expert Elicitation Project*. Yucca Mountain Project Deliverable SL5X4AM3. Las Vegas, Nevada: CRWMS M&O. ACC: MOL.19980825.0008. (Table 3-2; Sec. 5, Assumption 5, Sec. 6.1.6; justification of a vertical to horizontal anisotropy ratio of 0.1; Sec. 6.4; estimates of discharge within 5-km compliance boundary; Sec. 6.7.9; suggested comparing SZ flow model with numerical model of the larger regional system; Fig. 3-2e; Sec. 6.8; estimate of specific discharge at 5-km compliance boundary)

CRWMS M&O 1999a. *Calibrated Saturated Zone Flow and Transport Model Development Plan*. Las Vegas, Nevada: CRWMS M&O. ACC: TBD. (Sec. 1; development plan governing this analysis)

CRWMS M&O 1999c. *Water-level data Analysis for the Saturated Zone Site-Scale Flow and Transport*. Analysis and Modeling Report ????. Las Vegas, Nevada: CRWMS M&O. ACC: TBD (Sec. 6.1.2; description of boundary conditions represented as current water levels)

CRWMS M&O 1999e. *Activity Evaluation—M&O Site Investigations*. Las Vegas, Nevada: CRWMS M&O. ACC: MOL.19990317.0330.

CRWMS M&O 1999f. *Recharge And Lateral Groundwater Flow Boundary Conditions Of The SZ Site-Scale Model*. ANL-NBS-MD-000010. Las Vegas, Nevada: CRWMS M&O. ACC: In Progress. (Sec. 6.1.4: recharge map used (with some modifications) in analysis)

CRWMS M&O 2000a. *Particle Tracking Model and Abstraction of Transport Processes*. ANL-NBS-HS-000026, Rev 00C. Las Vegas, Nevada: CRWMS M&O. ACC: Draft AMR. (Sec. 3.4: verification of particle-tracking portion of FEHM; Sec. 6.7.9:)

CRWMS M&O 2000b. *Statamodel surfaces for the SZ Site-Scale Model*. ANL-NBS-MD-???. Las Vegas, Nevada: CRWMS M&O. ACC: In Progress (Claudia Faunt).

CRWMS M&O 2000c. *Geochemical and Isotopic Constraints on Groundwater Flow Directions, Mixing, and Recharge at Yucca Mountain*. ANL-NBS-HS-000021, Rev. 00D. Las Vegas, Nevada: CRWMS M&O. ACC: In Progress.

Czarnecki, J.B., Faunt, C.C., Gable, C.W., and Zyzoloski, G.A. 1997. *Hydrogeology and Preliminary Three-Dimensional Finite-Element Ground-Water Flow Model of the Site Saturated Zone, Yucca Mountain, Nevada*. USGS, Yucca Mountain Project Milestone Report SP23NM3. Denver, Colorado: U.S. Geological Survey. ACC: MOL.19980204.0519. (Sec. 6.7.1: **approach taken to calibrate code similar to that used in this AMR for the SZ site-scale model**)

D'Agnese, F.A., Faunt, C.C., Turner, A.K., and Hill, M.C. 1997. *Hydrogeologic Evaluation and Numerical Simulation of the Death Valley Regional Ground Water Flow System*. USGS Water Resources Investigations Report 96-4300. Denver, Colorado: U.S. Geological Survey. ACC: MOL.19980306.0253. (Sec. 6.7.9: data from spring discharges to help fix water flux through system and hydrogeologic model; Sec. 6.7.10: **volcanic units, clastic confining units, and the carbonate aquifer, play a major role in the performance of regional SZ model**)

Dash, Z.V., Robinson, B.A., and Zyzoloski, G.A., 1997. *Software Requirements, Design, and Verification and Validation for the FEHM Application—A Finite-Element Heat- and Mass-Transfer Code*. LANL Report LA-13305-MS. Los Alamos, New Mexico: Los Alamos National Laboratory. TIC: TBD. (Sec. 3.3: documentation of FEHM code used in flow modeling; Sec. 6.5: verification of use of separation of nonlinear and geometric parts in FEHM)

Day, W.C.; Dickerson, R.P.; Potter, C.J.; Sweetkind, D.S.; San Juan, C.A.; Drake, R.M., II; and Fridrich, C.J. 1998. *Bedrock Geologic Map of the Yucca Mountain Area, Nye County, Nevada*. Geologic Investigations Series I-2627. Denver, Colorado: U.S. Geological Survey. ACC: MOL.19981014.0301. (pp. 6–7, **USGS MAP I-2601**; Sec. 6: **description of Solitario Canyon Fault orientation**; Sec. 6.3: :YM area geologic map: basis of Fig. 3)

Draper, N.R. and Smith, H. 1981. *Applied Regression Analysis*. New York, New York: John Wiley & Sons. (Sec. 6.9.2: evaluation of the lack of bias in weighted residuals)

Faunt, C.C. 1997. *Effect of Faulting on Ground-Water Movement in the Death Valley Region, Nevada and California*. Water-Resources Investigations Report 95-4132. Denver, Colorado: U.S. Geological Survey. ACC: MOL.19980429.0119. (p. 30; Sec. 6.7.7.11: transmissivity of faults in Death Valley region; pp. 34–35, Table 4-4; Sec. 6.7.7.11.1: **mean orientation of the**

minimum horizontal stress in vicinity of YM; Fig. 16; Sec. 6.7.7.11.3; reasons local head gradient can increase across a fault)

Forsyth, P.A. 1989. "A Control Volume Finite Element Method for Local Mesh Refinement. SPE 18415." *10th Reservoir Simulation Symposium, Houston, Texas, February 6-8, 1989*, pp. 85-96. Houston, Texas: Society of Petroleum Engineers. ACC: TIC: TBD.. (Ref. only: Sec. 6.5: description of CVFE method as used in petroleum reservoir engineering)

Geldon, A.L.; Umari, A.M.A.; Fahy, M.F.; Earle, J.D.; Gemmell, J.M.; and Darnell, J. 1997. *Results of Hydraulic and Conservative Tracer Tests in Miocene Tuffaceous Rocks at the C-Hole Complex, 1995 to 1997, Yucca Mountain, Nye County, Nevada*. USGS Milestone Report SP23PM3. Denver, Colorado: U.S. Geological Survey. ACC: MOL.19980122.0412. (Fig. 3: Secs. 6.7.7.2, 6.7.8: reasons for differences in permeability values between single- and cross-hole tests)

Hill, M.C. 1992. *A Computer Program (MODFLOWP) for Estimating Parameters of a Transient, Three-Dimensional, Ground-Water Flow Model Using Nonlinear Regression*. USGS Open-File Report 91-484. Denver, Colorado: U.S. Geological Survey. (Ref. only: Secs. 6.9.1, 6.9.2: scaled sensitivities compared to values produced by this software)

Hill, M.C. 1994. *Five Computer Programs for Testing Weighted Residuals and Calculating Linear Confidence and Prediction Intervals on Results From the Ground-Water Parameter-Estimation Computer Program MODFLOWP*. USGS Open-File Report 93-481. Denver, Colorado: U.S. Geological Survey. (6.9.2: use of linear confidence intervals assumes they are normally distributed)

Laczniaik, R.J.; Cole, J.C.; Sawyer, D.A.; and Trudeau, D.A. 1996. *Summary of Hydrogeologic Controls on Groundwater Flow at the Nevada Test Site, Nye County, Nevada*. USGS Water-Resources Investigations Report 96-4109. Denver, Colorado: U.S. Geological Survey. TIC: 226157. (Sec. 6.7.7.3: describe hydrogeologic controls on groundwater movement at the NTS: p. 36; Sec. 6.7.7.7: geology of Silent Canyon caldera complex)

Luckey, R.R.; Tucci, P.; Faunt, C.C.; Ervin, E.M.; Steinkampf, W.C.; D'Agnese, F.A.; and Patterson, G.L. 1996. *Status of Understanding of the Saturated-Zone Groundwater Flow System at Yucca Mountain, Nevada, as of 1995*. USGS Water Resources Investigations Report 96-4077. Denver, Colorado: U.S. Geological Survey. TIC: 227084; 242049. ACC: MOL.19980429.0133. (p. 13; Sec. 6: hydrogeologic setting of the SZ flow system in the vicinity of Yucca Mountain and recharge from precipitation in the region; Fig. 7; Sec. 6.7.7.1: definitions of stratigraphic units).

MINITAB 1998. *Minitab Statistical Software, User's Guide 2: Data Analysis and Quality Tools*. Release 12. State College, Pennsylvania: Minitab, Inc. TIC: TBD. (Sec. 6.7.7.1: software used in statistical analysis of permeabilities)

Oatfield, W.J.; and Czarnecki, J.B.. "Hydrogeologic Inferences from Drillers' Logs and from Gravity and Resistivity Surveys in the Amargosa Desert, Southern Nevada." *Journal of Hydrology*, 124, 131-158. Amsterdam, Netherlands: Elsevier. TIC: TBD. (Sec. 6.3: field observations of channelization and alluvial material)

Plummer, L.N., Prestemon, E.C., and Parkhurst, D.L. 1994. *An Interactive Code (NETPATH) for Modeling Net Geochemical Reactions along a Flow Path, Version 2.0*. USGS Water Investigations Report 94-4169. Denver, Colorado: U.S. Geological Survey. TIC: 234831. (pp. 1–30; Sec. 6.7.5.3: geochemical software used to correct carbon-14 ages for the effects of chemical reactions)

Press, W.H.; Teukolsky, S.A.; Vetterling, W.T.; and Flannery, B.P. 1992. *Numerical Recipes in FORTRAN 77, The Art of Scientific Computing, Volume 1 of Fortran Numerical Recipes*. 2nd edition. Cambridge, United Kingdom: Cambridge University Press. TIC: 243606. (pp. 678–683; Sec. 6.4: the LM-based optimization algorithm; pp. 436–448; Sec. 6.4: description of simulated annealing process with PEST)

Sass, J.H.; Lachenbruch, A.H.; Dudley, W.W. Jr.; Priest, S.S.; and Munroe, R.J. 1988. *Temperature, Thermal Conductivity, and Heat Flow Near Yucca Mountain, Nevada: Some Tectonic and Hydrologic Implications*. USGS Open-File Report 87-649. Denver, Colorado: U.S. Geological Survey. TIC: 203195. ACC: NNA.19890123.0010. (p. 2, Figs. 4–8, 10; Sec. 6.1.5, 6.5: temperature profiles in wells and temperature variability)

Sawyer, D.A., Fleck, R.J., Lanphere, M.A., Warren, R.G., Broxton, D.E., and Hudson, M.R. 1994. "Episodic Caldera Volcanism in the Miocene Southwestern Nevada Volcanic Field—Revised Stratigraphic Framework, $^{40}\text{Ar}/^{39}\text{Ar}$ Geochronology, and Implications for Magmatism and Extension." *Geological Society of America Bulletin*, 106(10), 1304–1318. Denver, Colorado: U.S. Geological Society. TIC: 222523. (Fig. 1; Sec. 6: history of Yucca Mountain lava deposits)

[NOT CITED IN TEXT] Scott, R.B. and Bonk, J. 1984. *Preliminary Geologic Map of Yucca Mountain, Nye County, Nevada, with Geologic Sections*. U.S. Geological Survey Report OFR 84-494. Denver, Colorado: U.S. Geological Survey. ACC: HQS.19980517.1443.

Simonds, F.W.; Whitney, J.W.; Fox, K.F.; Ramelli, A.R.; Yount, J.C.; Carr, M.D.; Menges, C.M.; Dickerson, R.P.; and Scott, R.B. 1995. *Map Showing Fault Activity in the Yucca Mountain Area, Nye County, Nevada*. USGS Miscellaneous Investigations Series. Denver, Colorado: U.S. Geological Survey. TIC: 232483. ACC: MOL.19980618.0033. (Sec. 6.7.7.11.4: faults or fault segments near Yucca Mountain that have undergone recent movement)

Streeter, V.L. and Wylie, E.B. 1985. *Fluid Mechanics*. Eighth Edition. New York, New York: McGraw-Hill Book Company. TIC: TBD. (p.559; Sec. 6.1.5: viscosity of water as a function of temperature)

Verma, S., and Aziz, K., 1997. "A Control Volume Scheme for Flexible Grids in Reservoir Simulation. SPE 37999." *SPE Reservoir Simulation Symposium, Dallas, Texas, June 8-11, 1997*, 215-228. Richardson, Texas: Society of Petroleum Engineers. ACC: TIC: TBD. (Sec. 6.5: control-volume aspect in CVFE approach allows local mass conservation and upstream weighting)

Viswanathan, H.S.; Robinson, B.A.; Valocchi, A.J.; and Triay, I.R. 1998. "A Reactive Transport Model of Neptunium Migration from the Potential Repository at Yucca Mountain."

Journal of Hydrology, 209, 251-280. Amsterdam, Netherlands: Elsevier. TIC: TBD. (Ref. only; Sec. 6.5; description of reactive-transport module of FEHM)

Waddell, R.K. 1982. *Two-Dimensional, Steady-State Model of Ground-Water Flow, Nevada Test Site and Vicinity, Nevada-California*. USGS Water-Resources Investigations Report 82-4085. Denver, Colorado: U.S. Geological Survey. TIC: 203212. (pp. 15-16; Sec. 6; YM part of Alkali Flat-Furnace Creek subbasin of the Death Valley groundwater basin)

Winograd, I.J. and Pearson, F.J., Jr. 1976. "Major Carbon-14 Anomaly in a Regional Carbonate Aquifer: Possible Evidence for Megascala Channeling, South Central Great Basin." *Water Resources Research*, 12, 1125-1143. TIC: 217731. ACC: HQS.19880517.1875. (Sec. 6.7.7.4; existence of a "mega channel" between southern Frenchman Flat and the discharge area at Ash Meadows; p. c37; Sec. 6.7.7.5; definition of Valley Fill Aquifer; Sec. 6.7.7.11.1: **relatively young carbon-14 ages of groundwater discharging from springs at the distal end of megachannel**)

Winograd, I.J. and Thordarson, W. 1975. *Hydrogeologic and Hydrochemical Framework, South-Central Great Basin, Nevada-California with Special Reference to the Nevada Test Site*. USGS Professional Paper 712-C. Denver, Colorado: U.S. Geological Survey. TIC: 206787. ACC: NNA.19870406.0201; HQS.19880517.2908. (p. C112; Secs. 6.7.5.4, 6.7.5.7; proposed that **groundwater in alluvial aquifer near Skeleton Hills may have originated by upward leakage from carbonate aquifer near Gravity Fault**; Sec. 6.7.7.3; describe hydrogeologic controls on groundwater movement at the NTS; pp. c19, c20, c25, c28, c103, c116, Table 3; Secs. 6.7.7.4, 6.7.7.5, 6.7.7.6; transmissivities from hydraulic tests in Lower Carbonate Aquifer; pp. c84-c85; Sec. 6.7.7.5; **hydraulic head contours south of Lathrop Wells probably reflect effects of upward leakage from the lower carbonate aquifer into poorly permeable valley fill**; Table 3; Secs. 6.7.7.4, 6.7.7.5, 6.7.7.6; transmissivities used as data source for Tables 10, 11, 12; Tables 1, 4, pp. c42-c43, c53, c71, Plate 1; Secs. 6.7.7.9; **qualitative evaluations of the relative magnitude of permeability of Lower Clastic Aquitard**; Table 1, pp. c 43, c118; Sec. 6.7.7.10; **qualitative evaluations of the relative magnitude of permeability of Upper Clastic Aquitard**; pp. c67-68, c82; Sec. 6.7.7.11.3; interpretations of regional hydraulic data in terms of barriers and faults)

Zienkiewicz, O.C. 1977. *The Finite Element Method*. Third Edition. New York, New York: McGraw-Hill Company. (UK) Ltd. TIC: 224157. ACC: NNA.19910327.0066. (Ref. only; Sec. 6.5; complete description of finite-element method)

Zyvoloski, G. 1983. "Finite Element Methods for Geothermal Reservoir Simulation." *International Journal of Numerical Analysis Methods Geomech.* 7, 75-86. TIC: 224068. (Sec. 6.5; **separation of the nonlinear and purely geometric parts in FEHM**)

Zyvoloski, G.A., Robinson, B.A., Dash, Z.V., and Trease, L.L. 1997a. User's Manual for the *FEHM Application—A Finite-Element Heat- and Mass-Transfer Code*. LANL Report LA-13306-M. Los Alamos, New Mexico: Los Alamos National Laboratory. TIC: TBD. (all: Sec. 6.4; description of FEHM code)

Zyvoloski, G.A., Robinson, B.A., Dash, Z.V., and Trease, L.L. 1997b. *Summary of the Models and Methods for the FEHM Application—A Finite-Element Heat- and Mass-Transfer Code*. LANL Report LA-13307-MS. Los Alamos, New Mexico: Los Alamos National Laboratory.

TIC: 235587. (Sec. 6.5: description of FEHM and numerical model used in flow and transport calculations)

8.2 CODES, STANDARDS, REGULATIONS, AND PROCEDURES

AP-3.10Q, Rev.2, ICN 0. *Analysis and Models*. Washington, D.C.: U.S. Department of Energy, Office of Civilian Radioactive Waste Management. ACC: MOL.20000217.0246.

AP-SI.1Q, Rev. 2, ICN 4. *Software Management*. Washington, D.C.: U.S. Department of Energy, Office of Civilian Radioactive Waste Management. ACC: MOL.20000223.0508.

CRWMS M&O (Civilian Radioactive Waste Management System Management and Operating Contractor). 1999a. *Geochemical and Isotopic Constraints on Groundwater Flow Directions, Mixing, and Recharge at Yucca Mountain, Nevada*, Rev 00. Analysis and Modeling Report Development Plan: B2010. TDP-NBS-HS-000019. Las Vegas, Nevada: CRWMS M&O. TBD.

CRWMS M&O (Civilian Radioactive Waste Management System Management and Operating Contractor). 1999b. *Activity Evaluation-M&O Site Investigations*. Las Vegas, Nevada: CRWMS M&O. ACC: MOL.19990317.0330.

CRWMS M&O (Civilian Radioactive Waste Management System Management and Operating Contractor). 1999c. *Activity Evaluation for M&O Site Investigations-(Q)*. Las Vegas, Nevada: CRWMS M&O. ACC: MOL.19990928.0224.

DOE (Department of Energy). 2000. *Quality Assurance and Requirements Description*. DOE/RW-0333P, Rev. 9. Washington, DC.: DOE OCRWM. ACC: MOL.19991028.0012.

Dyer, J.R. 1999. "Revised Interim Guidance Pending Issuance of New U.S. Nuclear Regulatory Commission (NRC) Regulations (Revision 01, July 22, 1999), for Yucca Mountain, Nevada." Letter from J.R. Dyer (DOE) to D. R. Wilkins (CRWMS M&O), September 9, 1999, OL&RC:SB-1714, with enclosure, "Interim Guidance Pending Issuance of New U.S. Nuclear Regulatory Commission (NRC) Regulations (Revision 01)." ACC: 19990910.0079.

QAP-2-0, Rev. 5. *Conduct of Activities*. Las Vegas, Nevada: CRWMS M&O. ACC: MOL.19980826.0209.

Wemheuer, R.F. 1999. "First Issue of FY00 NEPO QAP-2-0 Activity Evaluations." Interoffice correspondence from R.F. Wemheuer (CRWMS M&O) to R.A. Morgan (CRWMS M&O), October 1, 1999, LV.NEPO.RTPS.TAG.10/99-155 with attachments, Activity Evaluations. ACC: MOL.19991028.0162.

8.3 SOFTWARE

8.4 SOURCE DATA, LISTED BY DATA TRACKING NUMBER

GS930208318523.001. *Temperature and Thermal Conductivity in Wells Near Yucca Mountain*. Submittal date: 02/16/93. (Sec. 6.6: temperature profiles in wells)

GS960808314222.003? Water level and head distributions

LA9911GZ12213S.001. (Sec. 6.7.3; includes description of small computer routine used to convert FEHM output to a TECPLOT readable form)

MO9901MWDGFM031.000. (Sec. 6.2.2; Geologic Framework Model; Ref. only?)

GS000308312322.003

GS000308312322.004

GS920408312321.001

GS920408312321.003

GS920508312321.004

GS930108315213.002

GS930308312323.001

GS930508312322.001

GS930908312323.003

GS931100121347.007

GS940308312322.001

GS950808312322.001

GS971900012847.004

GS980908312322.008

GS991299992271.001 (data set 9902----2272.001)

GS990608312133.001

DTN?? Surface defining hydrogeologic units

SN9907T0571599.001 TBV-1214? Feature and fault distributions

DTN?? Boundary conditions

SN9908T(or 7?)0581999.001. Title? (Secs. 6.2.1, 6.2.3; Infiltration Map or distribution of recharge flux)

SNT05082597001.003, Title? (Sec. 6.7.7. Table 9: permeability distributions analyzed statistically in this AMR)

ATTACHMENT I. CONVERT FEHM OUTPUT TO TECPLOT INPUT

program readpaths

C

c modified from bill arnold 7-23-99

C

```
implicit real*8(a-h,o-z)
character*80 file_name
integer maxstep,maxpart
parameter (maxstep=400000,maxpart=100)
real*8 x(maxpart,maxstep), y(maxpart,maxstep)
&      , z(maxpart,maxstep)
integer nstep(maxstep)
```

C

c if you add z coordinate the memory usage might exceed limit

```
write(*,*)
& 'Enter file for particle paths( usually *.sptr2) NOW'
read*,'(a80)' file_name
open(file=file_name,unit=10,status='old')
open(file='paths.plt',unit=12,status='unknown')
write(*,*)
& 'Enter number of particles NOW'
read*,'*' npart

if(npart.gt.maxpart) then
  write(*,*)
  & '>>>> Stopping, number of particles exceeds max of ',maxpart
  stop
endif
do i=1,npart
  nstep(i) = 0
enddo

do 20 i=1,maxstep
  read(10,* ,end=50) np,x1,y1,z1,t1
  if(np.le.maxpart) then
    nstep(np)=nstep(np)+1
    x(np,nstep(np))=x1
    y(np,nstep(np))=y1
    z(np,nstep(np))=z1
  endif
20 continue
  write(*,*) '>>> maxstep lines read, some lines not read'

50 continue
```

```
write(12,*) 'TITLE = "Particle Plots"'  
write(12,*) 'VARIABLES = X,Y,Z'  
c write(12,*) 'VARIABLES = X,Y'  
do 100 i=1,npart  
  write(12,*) 'ZONE I=',nstep(i)  
  do 100 j=1,nstep(i)  
    write(12,*) x(i,j),y(i,j),z(i,j)  
c    write(12,*) x(i,j),y(i,j)  
100 continue
```

```
C  
close(10)  
close(12)  
end
```